Coordination Chemistry Reviews 255 (2011) 1055–1084

Contents lists available at ScienceDirect

Coordination Chemistry Reviews

journal homepage: www.elsevier.com/locate/ccr

Review

Spectroscopic studies of molybdenum and tungsten enzymes

M. Jake Pushie, Graham N. George*

Department of Geological Sciences, 114 Science Place, University of Saskatchewan, Saskatoon, Saskatchewan S7N 5E2, Canada

Contents

Abbreviations: AOR, aldehyde oxidoreductase; AH, acetylene hydratase; DFT, density functional theory; DMSO, dimethylsulfoxide; ENDOR, electron nuclear double resonance; EPR, electron paramagnetic resonance; ESEEM, electron spin echo envelope modulation; EXAFS, extended X-ray absorption fine structure; FDH, formate dehydrogenase; Fdh-N, anaerobic respiratory formate dehydrogenase; Fdh-O, fermentative formate dehydrogenase; FOR, formaldehyde ferredoxin oxidoreductase; Moco, molybdenum cofactor; MPT, eukaryotic molybdopterin lacking any nucleotide-modification; MDG, prokaryotic molybdopterin with guanidine modification; MCD, prokaryotic molybdopterin with cytosine modification; MOP, molybdenum protein; Nar, membrane-associated respiratory nitrate reductases; Nap, periplasmic dissimilatory nitrate reductases; Nas, cytoplasmic assimilatory nitrate reductases; PCMB, p-chloro-mercuribenzoate; SO, sulfite oxidase SO; TMAO, trimethylamine N-oxide; XAS, X-ray absorption spectroscopy; XO, xanthine oxidase.

* Corresponding author.
E-mail address: g.george@usask.ca (G.N. George).

doi:10.1016/j.ccr.2011.01.056

ARTICLE INFO

Article history:
Received 14 November 2010
Accepted 31 January 2011

Keywords:
Molybdenum enzymes
Tungsten enzymes
Spectroscopic characterization
X-ray absorption spectroscopy
Electron paramagnetic resonance spectroscopy
Coordination structure
Sulfite oxidase family
DMSO reductase family
Xanthine oxidase family

ABSTRACT

Molybdenum and tungsten are the only second and third-row transition elements with a known function in living systems. Molybdenum fulfills functional roles in enzyme systems in almost all living creatures, from bacteria through plants to invertebrates and mammals, while tungsten takes the place of molybdenum in some prokaryotes, especially the hyperthermophilic archaea. The enzymes contain the metal bound by an unusual sulfur-containing cofactor. Despite possessing common structural elements, the enzymes are remarkable in the range of different chemical reactions that are catalyzed, although almost all are two-electron oxidation–reduction reactions in which an oxygen atom is transferred to or from the molybdenum. The functional roles filled by molybdenum enzymes are equally diverse; for example, they play essential roles in microbial respiration, in the uptake of nitrogen in green plants, in controlling insect eye color, and in human health. Spectroscopic studies, in particular electron paramagnetic resonance and X-ray absorption spectroscopy, have played an essential role in our understanding of the active site structures and catalytic mechanisms of the molybdenum and tungsten enzymes. This review summarizes the role spectroscopy has played in the state of our knowledge of the molybdenum and tungsten enzymes, with particular regard to structural information on the molybdenum sites.

1. Introduction

Transition metal ions play innumerable and varied essential roles in the chemistry of living systems, in particular at the active sites of metalloenzymes [1]. Most of these systems contain first row transition ions, but remarkably molybdenum and tungsten are the only known second and third row transition ions that have well-defined roles in biology [2]. With the exception of nitrogenase and related proteins [3] and some proteins of unknown function [4,5], all molybdenum enzymes that have been described to date contain a novel pyranopterin-dithiolene cofactor in which the Mo atom is coordinated by the dithiolene moiety (Fig. 1) [6]. The molybdenum cofactor is often abbreviated as Moco and the organic moiety is commonly called molybdopterin. The latter term was coined prior to the discovery of the tungsten enzymes, and refers to the cofactor without any molybdenum bound to it. Thus, as a slightly confusing consequence, the tungsten enzymes all contain molybdopterin but not molybdenum. Eukaryotic Mo-enzymes generally contain molybdopterin lacking the nucleotide group (often abbreviated MPT, Fig. 1) while prokaryotic molybdopterins often contain a dinucleotide moiety (abbreviated MGD with guanidine, or MCD with cytosine, Fig. 1). Interestingly, many of the tungsten enzymes possess an unmodified molybdopterin. The enzymes have been divided into families [7,8], named for their prototypical members and categorized by the structures of the oxidized Mo^{VI} forms.

With some notable exceptions [9,10] all of the enzymes catalyze oxygen transfer between water and a substrate molecule, with the molybdenum changing between Mo^{VI} and Mo^{IV} during the process:

$$\text{Enzyme-Mo}^{IV} + \text{R(O)} + 2\text{H}^+ \leftrightarrow \text{Enzyme-Mo}^{VI} + \text{R} + \text{H}_2\text{O}$$

Many of the enzymes are thought to have an oxygen atom transfer mechanism where the oxygen transferred to or from substrate is covalently bound to Mo at some point in the catalytic cycle. The electrons required or generated during the catalytic cycle are moved by either intermolecular or intramolecular electron transfer, and many of the enzymes have redox-active sites in addition to molybdenum such as FAD, iron–sulfur clusters or heme moieties. Characteristic structures for each of the three families of enzymes are shown in Fig. 2.

The dimethylsulfoxide (DMSO) reductase family (Fig. 2a) is the largest and most diverse of the three families and contains enzymes with two molybdopterins bound to the molybdenum. Some members have Mo coordination from an amino acid side chain (*e.g.* [11,12]), while other members do not (*e.g.* [13]). Members of this family are found only in the bacteria and archaea, and include diverse enzymes such as DMSO reductase and trimethylamine N-oxide (TMAO) reductase, formate dehydrogenases, dissimilatory nitrate reductases and the tungsten containing enzymes, which have a diverse membership in their own right. Many enzymes of the DMSO reductase family also have a single oxo ligand in their oxidized states (Mo=O), but some of the more recently characterized members may not. The family can be further divided, depending on the coordinated amino acid residue and sequence homologies. In the *Type I enzymes*, the coordinating amino acid ligand is usually a cysteine or selenocysteine, *e.g. Escherichia coli* formate dehydrogenase [11,14] and *Desulfovibrio* dissimilatory nitrate reductases [15]. In the *Type II enzymes* the coordinated residue is an aspartate such as in *E. coli* nitrate reductase [16,17] and ethylbenzene dehydrogenase [18]. In the *Type III enzymes* the coordinated residue is serine, and this group includes the DMSO reductases themselves [12,19] and dimethylsulfide dehydrogenase [20], which catalyzes the reverse reaction to DMSO reductase. The nature of the enzyme mechanism depends on the individual enzyme. The tungsten enzymes are found in both bacteria and archaea, being especially abundant in the latter where molybdenum enzymes do not appear to occur.

The sulfite oxidase family is characterized by Mo coordination with a single cofactor dithiolene, plus one cysteinyl sulfur bound to Mo and two terminal oxygen ligands (Mo=O) in the oxidized enzyme [21]. The family includes the bacterial sulfite dehydrogenases [22], both the plant [23,24] and the animal sulfite oxidases [21,25], and the assimilatory nitrate reductases [26]. The most intensively studied members of this family are the animal sulfite oxidases, in part because of their clinical importance.

The xanthine oxidase family is another well studied family, predominantly through extensive work on its prototypical member xanthine oxidase [27]. The family is characterized by Mo coordination by one cofactor dithiolene, a single Mo=O group, and a sulfide group, Mo=S or a derivative thereof. It includes the bacterial and plant xanthine dehydrogenases [28], and various animal enzymes such as xanthine oxidase and aldehyde oxidase [29–31]. An exotic family member is the bacterial enzyme carbon monoxide dehydrogenase, which has a sulfide bridge between Mo and Cu, forming a novel binuclear site [32].

The first crystal structure of a molybdopterin-containing enzyme was actually that of a tungsten-containing aldehyde ferredoxin oxidoreductase from the hyperthermophilic archaeon *Pyrococcus furiosus* in 1995 [33]. This was rapidly followed by the first structure of the molybdenum-containing enzyme, an aldehyde oxidoreductase from *Desulfovibrio gigas* [34] and then by the first of several DMSO reductase structures in 1996 [12]. At the time of writing, some 15 years after the first structure, a very large

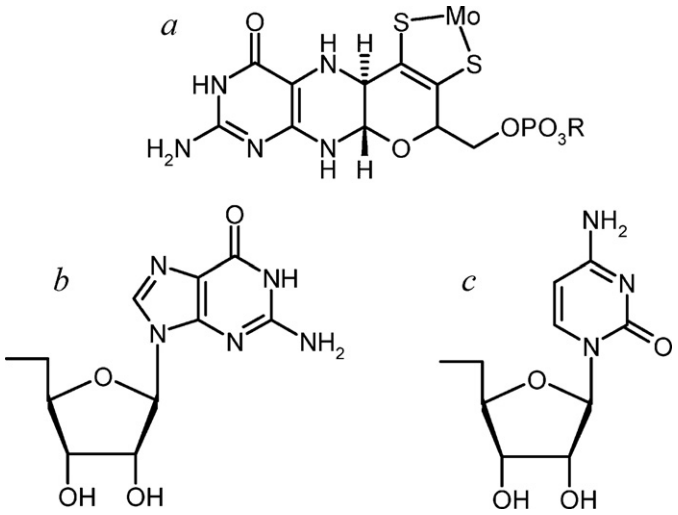

Fig. 1. (a) Structure of the molybdopterin cofactor, the group R can be H (molybdopterin or MPT), (b) guanosine (molybdopterin guanine dinucleotide or MGD), or (c) cystosine (molybdopterin cytidine dinucleotide or MCD).

number of molybdenum enzyme crystal structures have now been reported, with detailed structural information for every major category and type of Mo enzyme. This wealth of structural information has revolutionized and considerably stimulated the field, but many open questions remain, particularly concerning the detailed structures of the molybdenum sites, and the nature of the catalytic mechanisms.

Spectroscopic methods have played important roles in both our understanding of active site structure and catalytic function of the molybdenum enzymes. This review will focus on the contribution that these techniques have made to our understanding of these systems, with an emphasis on structure and catalytic mechanism at the molybdenum and tungsten sites within the enzymes. This is not intended to be an exhaustive review of all of the spectroscopic literature on all molybdenum and tungsten enzymes, but rather a perspective on the most important developments.

2. Spectroscopic techniques

2.1. Electron paramagnetic resonance spectroscopy

Electron paramagnetic resonance (EPR) spectroscopy [35] has been very extensively employed in the study of the molybdenum enzymes [36]. Most reports of EPR experiments on molybdenum enzymes are continuous wave EPR (CW EPR) although vital contributions have recently been made using pulsed techniques (discussed below). The discussion presented here only includes aspects relevant to the Mo enzymes and for a more complete discussion the reader is referred to more specialized texts [37]. CW EPR utilizes the absorption of electromagnetic radiation in the microwave region by paramagnetic systems, with transitions having $\Delta M_s = \pm 1$ and $\Delta M_I = 0$ observed under ordinary circumstances. In the molybdenum enzymes the metal cycles between Mo^{VI} and Mo^{IV} formal oxidation states, and in many cases the paramagnetic formally $4d^1$ Mo^V oxidation state can be generated, either using a redox titration or via intramolecular electron transfer between other redox-active sites within the enzyme (*e.g.* the cytochrome b_5 moiety in sulfite oxidase or [2Fe–2S] clusters and FAD in xanthine oxidase). Spectroscopically, Mo^V is a typical d^1 second transition ion, and has the advantage that the CW EPR linewidths are often sharper than for other transition metals in proteins. The sharp linewidths mean that weak nuclear hyperfine interactions from nearby atoms can often be resolved. Observation of such ligand hyperfine interactions has been extensively used to probe the structures of Mo^V sites within enzymes, often through substitution with enriched stable magnetic nuclei such as ^2H, ^{13}C, ^{15}N, ^{17}O, and ^{33}S. Fig. 3 shows a schematic energy level diagram illustrating hyperfine interaction from a single $I = 1/2$ nucleus. Hyperfine splitting from the naturally abundant $I = 5/2$ ^{95}Mo and ^{97}Mo isotopes is generally clearly visible as satellite features in EPR spectra. These isotopes are present at abundances of 15.9% and 9.6% for ^{95}Mo and ^{97}Mo, respectively. They have very similar magnetic moments, although ^{97}Mo has an 11.5-fold larger nuclear electric quadrupole moment than ^{95}Mo, and enrichment of both of these stable isotopes has been used to derive accurate spin Hamiltonian parameters and structural conclusions on enzyme active sites [38,39]. EPR is also quantitative in that it can be double-integrated and the concentration of paramagnetic species estimated with reference to double-integration of the EPR spectrum of a standard solution. EPR is often used in combination with other methods, such as redox-titrations to determine electrochemical parameters, or rapid freezing (freeze quench) to determine reaction kinetics.

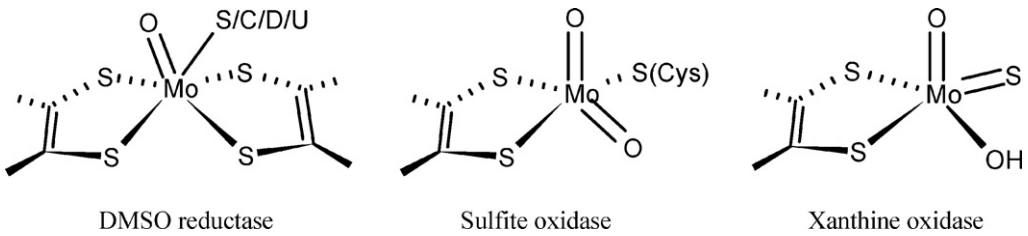

Fig. 2. Families of molybdenum enzymes based on the oxidized Mo^{VI} structure. The DMSO reductase family has an amino acid ligand which is either serine (S), cysteine (C), aspartate (D) or selenocysteine (U). Some members of the family appear may lack the Mo=O group.

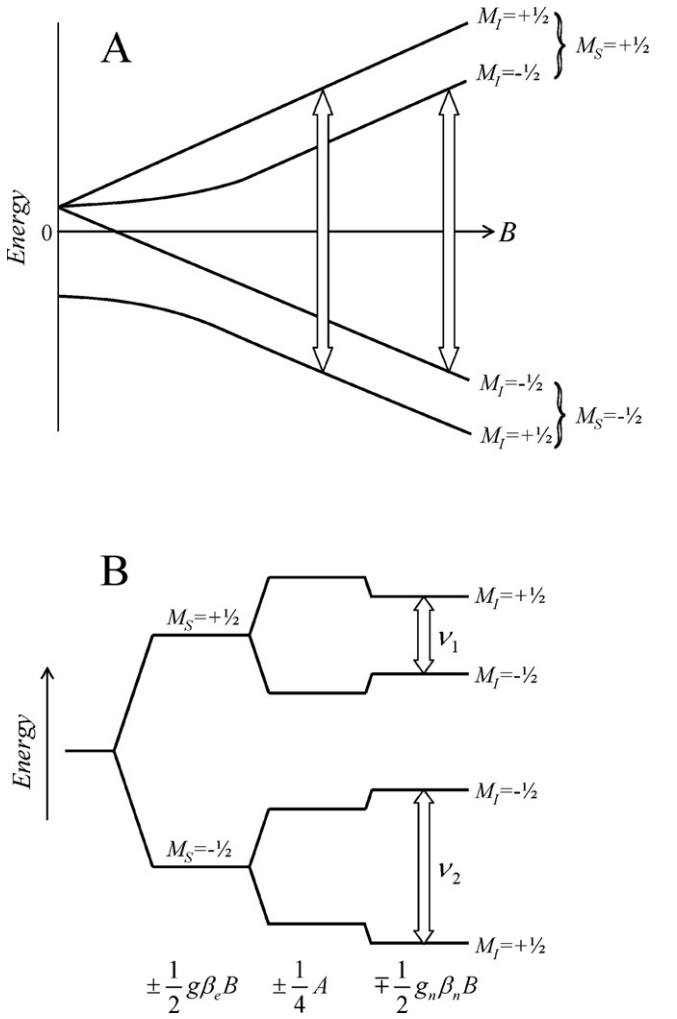

Fig. 3. EPR and ENDOR. (a) The Schematic energy levels appropriate for a field swept experiment on a system with $S = 1/2$ and $I = 1/2$. Only the electronic Zeeman and hyperfine interactions are included. The EPR transitions are marked as the vertical arrows. (b) A schematic of the energy levels for a frequency-swept ENDOR experiment for a system with $S = 1/2$ and $I = 1/2$ and with a hyperfine interaction larger than the nuclear Zeeman interaction.

2.1.1. The spin Hamiltonian formalism

The beauty of the spin Hamiltonian formalism is that equations can be cast in terms of electron spin, with orbital contributions being external to the calculation as spectroscopic parameters. We will briefly review this for $S = 1/2$ systems (Fig. 3). We can use the generalized Hamiltonian:

$$\mathcal{H} = \beta_e \mathbf{B}\cdot\mathbf{g}\cdot\mathbf{S} + h\mathbf{I}\cdot\mathbf{A}\cdot\mathbf{S} + h\mathbf{I}\cdot\mathbf{P}\cdot\mathbf{I} - \beta_n g_n \mathbf{B}\cdot\mathbf{I}$$

where β_e and β_n are the Bohr magneton and the nuclear magneton, respectively, and h is Plank's constant. The first term (the electronic Zeeman term, $\beta_e\mathbf{B}\cdot\mathbf{g}\cdot\mathbf{S}$) couples the magnetic field vector **B** with the electron spin **S** and **g** interaction matrix (sometimes called the *g*-tensor). The second term, $h\mathbf{I}\cdot\mathbf{A}\cdot\mathbf{S}$ includes the hyperfine interaction **A**, and couples the effects of nuclear spin **I** with electron spin **S**. Biological systems are generally measured as frozen solutions, and the spectra are thus an average of all possible molecular orientations with respect to the applied magnetic field, giving what is usually referred to as a powder lineshape. Normally the electronic Zeeman term is by far the largest and is characterized by an anisotropic **g** that has its origins in spin–orbit coupling to excited state orbitals. The hyperfine interaction will split the resonance due to the electronic Zeeman into $(2I + 1)$ approximately equally spaced transitions. The size of the hyperfine interaction has a number of different contributions including point-dipole, the spin electron density in orbitals involving the magnetic atom, and spin exchange interactions with both isotropic and anisotropic components. The third term in the generalized Hamiltonian above ($h\mathbf{I}\cdot\mathbf{P}\cdot\mathbf{I}$) is the nuclear electric quadrupole coupling interaction, where **P** is the quadrupole coupling tensor. Nuclei with $I = 1/2$ have no nuclear electric quadrupole moment, and quadrupole coupling thus occurs only for nuclei with $I > 1/2$. The nuclear electric quadrupole coupling depends upon the electric field gradient at the magnetic nucleus which means that it is directly related to chemical environment. In CW EPR the quadrupole coupling is usually weaker than the hyperfine and effectively competes with the applied magnetic field for orientation of the axis of nuclear spin. This results in M_I becoming a poor quantum number and shifted hyperfine features with additional $\Delta M_I = \pm 1, \pm 2$ (up to $\pm 2I$) transitions. Finally, the last term, $\beta_N g_n \mathbf{B}\cdot\mathbf{I}$, is the nuclear Zeeman interaction, which, for hyperfine coupling that is visible with ordinary EPR, is generally the smallest in magnitude. For most CW EPR analyses only the first two terms need to be included, but all four are needed for electron nuclear double resonance (ENDOR) and electron spin echo envelope modulation (ESEEM).

Substitution with stable magnetic isotopes has been used extensively in the molybdenum enzymes. The most common of these is exchange into ^2H_2O to detect water-exchangeable protons. Other isotopes that have been employed with the Mo enzymes include ^{13}C, ^{17}O, ^{33}S, ^{95}Mo, ^{97}Mo, ^{199}Hg and ^{201}Hg. In instances such as ^1H and ^2H, where both isotopes are magnetic with $I = 1/2$ and 1, respectively, the hyperfine coupling can be calculated from the ratio of the nuclear *g*-values, g_n. For the isotopes of hydrogen ^1H and ^2H, g_n has the value of 5.5857 and 0.8574, respectively.

$$A(^2\mathrm{H}) = A(^1\mathrm{H})\left(\frac{g_n(^2\mathrm{H})}{g_n(^1\mathrm{H})}\right) = A(^1\mathrm{H})\frac{0.8574}{5.5857}$$

Hyperfine splitting from ^2H will thus only be about 15% of that from ^1H, and in most cases this means that it will not be observable by CW EPR, although with ENDOR and ESEEM it has been useful, as we will discuss below.

Mo^V is $4d^1$ so that in the absence of any contributions due to ligand covalency all *g*-values should be less than the free electron value. Covalent ligands such as sulfur or selenium tend to raise the *g*-values, and because of the sulfur-rich coordination environment in the molybdenum enzymes this is quite frequently observed. Spin–orbit coupling is much stronger for tungsten than for molybdenum, and thus W^V *g*-values are both lower and more anisotropic. The CW EPR linewidths also tend to be broader for W^V (relative to Mo^V) which can obscure important structure such as proton hyperfine splitting. EPR has excellent sensitivity so that excellent signal to noise can be obtained with samples containing 30 μM Mo^V, and it can readily be used to monitor the active site of enzyme preparations. A major disadvantage of EPR and related methods is that they probe only the paramagnetic Mo^V oxidation state and that the Mo^{IV} and Mo^{VI} are thus unobservable. A second major disadvantage of CW EPR is that weak coupling often cannot be observed. This has been partly overcome by ENDOR and ESEEM which provide more sensitivity to weakly coupled nuclei, and can sometimes by used to assign signs. Finally, spin Hamiltonian parameters can often be difficult to accurately and unambiguously associate with structure, although for the molybdenum enzymes structures deduced from CW EPR, ENDOR and ESEEM have often turned out to be remarkably accurate.

2.1.2. Electron nuclear double resonance

Electron nuclear double resonance spectroscopy observes nuclear transitions (Fig. 3) and can be used to observe weak hyper-

fine coupling [40]. Pulsed EPR methods such as electron spin echo envelope modulation (ESEEM) overlap in their sensitivity, and both provide access to weak couplings that CW EPR cannot access [41]. Both CW ENDOR and pulsed ENDOR have been extensively used in recent years for the Mo enzymes [42]. ENDOR stimulates transitions between nuclear levels by application of radio frequency (RF) radiation and is detected by changes in the EPR absorption. The CW ENDOR experiment is conducted at a fixed magnetic field within the EPR absorption envelope by sweeping the RF frequency. The ENDOR frequencies (Fig. 3) are given by:

$$\nu_{ENDOR} = \left| \nu_n \pm \frac{A}{2} \right|, \quad \nu_n = \frac{g_n \beta_n B_0}{h}$$

where h is Plank's constant, ν_n is the nuclear Larmor frequency, and other symbols are defined above. A number of different ENDOR methods are available [43], and a detailed explanation is outside the scope of this review. When the coupling is weak and $\nu_n > |A/2|$ then the ENDOR lines are centred symmetrically around ν_n with a spacing A, but if $\nu_n < |A/2|$ then the ENDOR lines are centred around $|A/2|$ with a spacing of $2\nu_n$ (Fig. 3). Like all techniques, ENDOR has its weaknesses. Strongly coupled nuclei often cannot be detected, and identically coupled nuclei cannot be explicitly counted. Moreover, with complex spectra, interpretation may not always be simple, for example, ^{95}Mo hyperfine coupling in nitrogenase was overestimated by a factor of almost three [44].

2.1.3. Electron spin echo envelope modulation

Electron spin echo envelope modulation (ESEEM) is a pulsed EPR technique that can give similar information to ENDOR. In an ESSEM experiment the magnetic field is set to a fixed position within the EPR absorption envelope and short, intense microwave pulses are applied. The method is perhaps best thought of in terms of Larmor precession of the classical magnetic moments of electrons and nuclei. The microwave pulses are typically π or $\pi/2$ pulses lasting for 1/2 or 1/4 of the Larmor precession time, tipping the magnetization through 180° or 90°, respectively. The microwave pulses are applied in specially chosen sequences that are usually tailored to obtain a specific signal, and the time between two of the pulses is varied. The variation of electron spin orientation under the influence of these pulses leads to simultaneous reorientation of the nuclear spins and the microwave signals thus generated are measured – effectively a spin echo of the applied pulses. The echo decays exponentially with modulations from weak nuclear hyperfine and quadrupole coupling interactions. These modulations are observed when the probability of the formally forbidden $\Delta M_I = \pm 1$ EPR transitions is non-zero, which in practice means that either the hyperfine interactions are anisotropic or there is quadrupole coupling present. Data reduction requires background subtraction and the use of Fourier transforms to give peaks corresponding to coupling frequencies. Pulsed ENDOR is experimentally related to ESEEM with an additional RF pulse being used to stimulate nuclear transitions and change the electron spin echo. Plotting the echo intensity against the RF frequency gives the ENDOR spectrum. Again, various pulse sequences have been described and the reader is referred to the literature for a more in-depth description (*e.g.* [45]).

2.2. Vibrational spectroscopy

Vibrational spectroscopy can provide information on geometrical deformations of metal sites. Resonance Raman has been used to probe the active site structure of a number of molybdenum enzymes. The technique depends on the enhancement in Raman emission at wavelengths close to an electronic absorption band [46]. The method can potentially identify such features as *cis*-dioxo Mo^{VI} sites from observation of *sym* and *anti* modes. Badger's rule [47] is a useful empirical relationship that can relate bond-length data from other techniques such as extended X-ray absorption fine structure (EXAFS) with vibrational frequency:

$$R = \frac{C_{ij}}{\nu_e^{2/3}} + d_{ij}$$

where R is the equilibrium inter-nuclear distance, ν_e is the vibrational frequency, and C_{ij} and d_{ij} are the empirical constants that are determined for a pair of atoms by fitting the relation to a series of different R and ν_e although in practice obtaining useful values of C_{ij} and d_{ij} requires some effort [48].

Substitution with stable isotopes will shift the frequency of bands and exchange with $H_2{}^{18}O$ has been used effectively to identify modes from exchangeable oxygen (*e.g.* Mo=O stretch). Overall, resonance Raman spectroscopy can provide a wealth of information on active site structure. Its major disadvantage is that fluorescent groups and other chromophores interfere. It is thus well suited to enzymes such *Rhodobacter* DMSO reductase which has only the Mo active site and no other chromophores, but more difficult to use with enzymes such as xanthine dehydrogenase which tend to be fluorescent and possess a number of different chromophores (iron–sulfur clusters, flavin, *etc.*). Finally, it is difficult to apply when more than one species is present, as there is always the risk that observed spectra correspond to minority species. We note in passing that Fourier transform infra red (FT-IR) spectroscopy can in principal be used to study the Mo enzymes, but to date it has been little used.

2.3. X-ray absorption spectroscopy

X-ray absorption spectroscopy (XAS) provides a powerful probe of both local molecular and electronic structure, and because of the special contributions that this technique have made to the study of molybdenum enzymes we will discuss it in detail. As spectroscopic methods go it is a relatively new technique, originating in the early 1970s, but in recent years it has become increasingly applied and it has been essential in development of our understanding of the molybdenum enzymes active site structure. X-ray absorption spectra arise from core-level excitation by absorption of X-rays (Fig. 4), and are thus associated with an absorption edge. They are usually separated into two different regions: the extended X-ray absorption fine structure or EXAFS, which occurs at energies higher than the absorption edge; and the near-edge region which consists of features before the major inflection, and any after the inflection which are not part of the analyzable EXAFS. XAS is element-specific and can be used to investigate solids, liquids (including solutions), gaseous materials, and any mixtures thereof. It probes all of an element within a sample with moderate sensitivity, and is applicable to a very wide range of elements. XAS theory is well developed, and the methods of analysis of the EXAFS part of the spectrum to give a local radial structure for the absorbing atom, are also well established. We will discuss the different information available from these different regions below. This content included in this review is not intended to be comprehensive, but instead seeks to illustrate the capabilities of the method relevant to the molybdenum enzymes.

2.3.1. Near-edge spectroscopy

We noted above that XAS provides a probe of both electronic and of physical structure. The features observed in near-edge spectra arise from predominantly dipole-allowed (*i.e.* $\Delta l = \pm 1$) transitions to bound state molecular orbitals, and analysis of near-edge spectra can thus yield information on electronic structure (*i.e.* oxidation state, and in some cases geometry). The near-edge spectrum shifts to higher energies with increasing metal oxidation state, although equally large changes can be observed from changes in the ligand

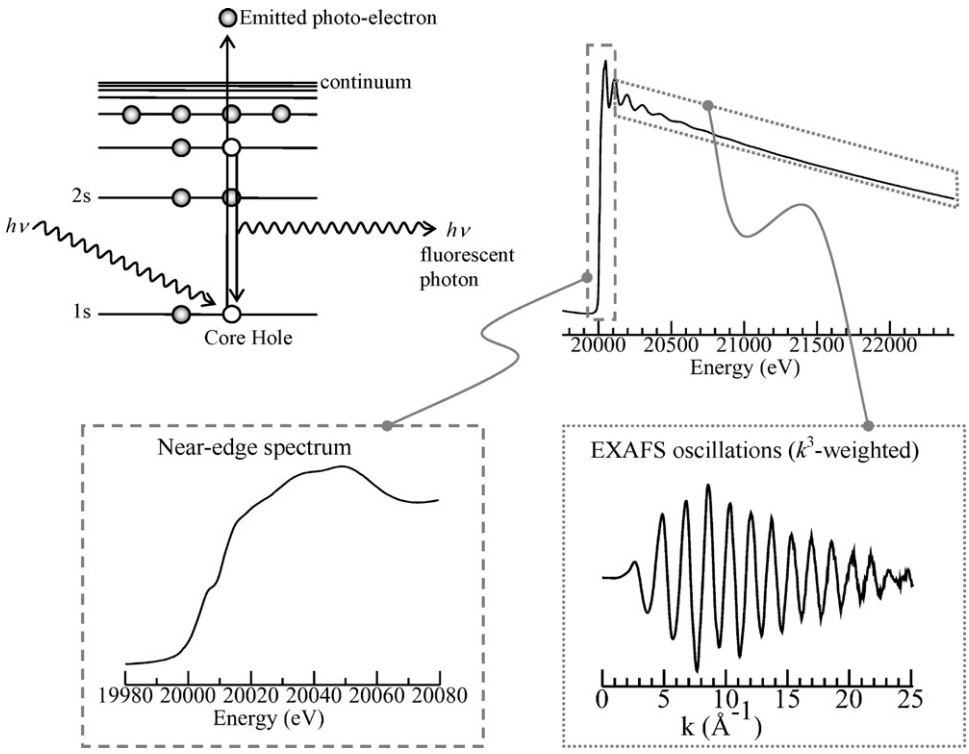

Fig. 4. Schematic of the underlying physical process (a) and of the different spectral regions of X-ray absorption spectroscopy (b) showing the near-edge (c) and EXAFS (d) regions of the spectrum.

environment. In general increased sulfur coordination would shift the near-edge to lower energy while increased oxygen coordination would shift to high. Broadening due to the short lifetime of the core hole can be limiting for measurements at the Mo K-edge, whereas for K-edges of ligand atoms such as sulfur the much longer core-hole lifetime translates to sharper near-edge spectra with a correspondingly richer spectroscopy.

Relative orbital energies measured by separation of features in the near-edge spectra correspond to excited states, and the so-called $Z+1$ approximation states that, because of the presence of a core-hole, the various transition energies correspond more closely to those of the element in the next group (*i.e.* atomic number increased by one; Tc in the case of Mo). With the molybdenum enzymes a prominent feature is the so-called oxo-edge peak at *ca.* 20,009 eV which is observed in species with Mo=O coordination, and is often used as an indicator of this type of bonding in enzymes. This feature arises from formally dipole forbidden $1s \rightarrow 4d$ transitions into π^* orbitals oriented along the Mo=O bond vectors [49], and its intensity is approximately related to the number of Mo=O ligands present [50]. With Mo L_{III} and L_{II} near-edge spectra, which arise from 2p excitation, the dipole selection rules mean that transitions to the 4d-manifold are intense and estimates of the ligand field splitting of the 4d-manifold have been obtained [51] (Fig. 5). Investigations of L-edge X-ray magnetic circular dichroism also provide promise for this related technique as a novel probe of electronic structure of the paramagnetic Mo^V oxidation state, but are presently unexplored for the molybdenum enzymes.

2.3.2. Extended X-ray absorption fine structure spectroscopy

At X-ray energies below an X-ray absorption edge, the incident X-rays have insufficient energy to eject a core electron, and above the edge the electron leaves the atom possessing a kinetic energy which is a function of the difference in the X-ray energy E above the absorption edge threshold energy E_0. For a photoelectron of de Broglie wavelength $\lambda_e = h/m_e v$ (where h is Planck's constant, m_e the electron rest mass, and v the electron velocity), we can define the wave-vector $k = 2\pi/\lambda_e$. The photoelectron kinetic energy is $(E - E_0) = m_e v^2/2$, and k is thus given by:

$$k = \sqrt{\frac{2m_e}{\hbar^2}(E - E_0)}$$

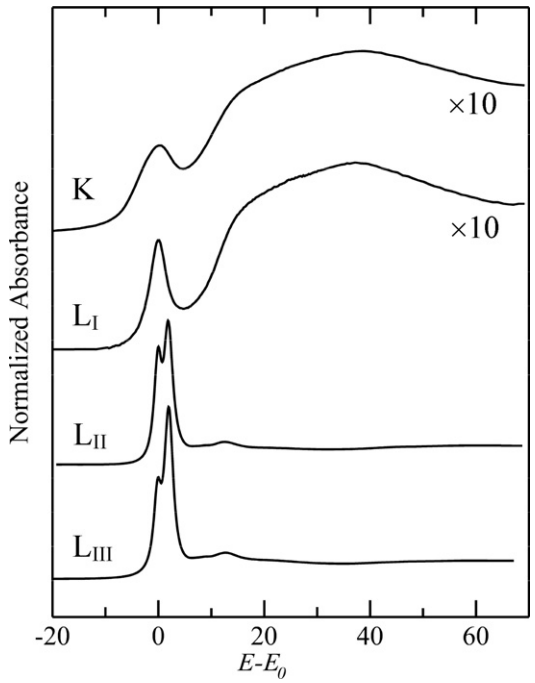

Fig. 5. Comparison of the Mo near-edge spectra at the K, L_I, L_{II} and L_{III} edges of an aqueous solution of Na_2MoO_4. With the L_{III} and L_{II} edges the $2p \rightarrow 4d$ transition are dipole allowed which gives rise to the intense absorption, whereas with K and L_I edges these transitions are formally forbidden. The difference in the L_{III} and L_{II} spectra has its roots in electron spin.

We now consider the emitted photoelectron leaving the absorber atom as a photoelectron wave, for a K-edge (*i.e.* 1s excitation) this will have *p*-symmetry, which will confer polarization sensitivity to the EXAFS. This photoelectron wave will be scattered by any neighboring atoms. Because the initial state wave function (1s for a Mo K-edge) is very compact (almost a delta function) and centred at the absorber atom nucleus, the absorption depends to a good approximation upon the final state wave-function at the nucleus of the absorber atom (*i.e.* Mo). Quantum mechanical analysis thus tells us that the X-ray absorption coefficient will be at a maximum when the backscattered wave is in phase with the outgoing wave at the nucleus of the absorber, and at a minimum when it is out of phase. This can be considered conceptually as being due to constructive and destructive interference, respectively. Thus, as we increase the X-ray energy E above the edge E_0, λ_e will decrease, and as it does so the absorption will go through successive minima and maxima. It is this oscillatory modulation of the absorption which is known as the EXAFS. The frequency of the EXAFS depends upon the atomic separation, and the amplitude of the EXAFS, which is a reflection of the effectiveness of the backscatterer atoms, upon the size (atomic number) and the number of backscatterer atoms. Because the backscatterer atom modulates the phase of the photoelectron, the phase of the EXAFS will also depend upon the nature of the backscatterer. Thus, both phase and amplitude of the EXAFS depend on the backscatterer and this allows identification of the backscatterer. In general it is not possible to discriminate atoms with similar atomic number (*e.g.* Mo–S and Mo–Cl give nearly identical EXAFS, while that from Mo–S and Mo–O is quite different).

The EXAFS $\chi(k)$ is described by the simple equation which is summed over all EXAFS absorber–backscatterer pairs i:

$$\chi(k) = \sum_i \frac{N_i S_0^2 \,\mathrm{Im}\{\delta_i^c(k)\} f_{eff}(\pi, k, R)}{kR_i^2} e^{-2\sigma_i^2 k^2} e^{-2R_i/\lambda(k)} \times \sin[2kR_i + 2\,\mathrm{Re}\{\delta_i^c(k)\} + \Phi_{eff}(k)]$$

in which N is the coordination number, R is the absorber–backscatterer distance, the term $e^{-2\sigma^2 k^2}$ is the Debye–Waller factor where σ^2 is the mean-square deviation in R, δ^c the central-atom phase shift, Φ_{eff} the backscatterer phase-shift, f_{eff} the effective curved-wave backscattering amplitude, $\lambda(k)$ is the photoelectron mean free path, and S_0^2 is a many-body amplitude reduction factor. It has become common practice to incorrectly refer to σ^2 as the Debye–Waller factor.

The simple formalism given above is applicable to multiple scattering by simply considering i as the index of a scattering path, in which case N is then the degeneracy of each multiple scattering path. We can simplify the expression further by combining variables into a total amplitude function $A(k,R)$ and a total phase function $\varphi(k)$:

$$\chi(k) = \sum_i \frac{N_i A_i(k, R)}{kR_i^2} e^{-2\sigma_i^2 k^2} e^{-2R_i/\lambda(k)} \sin[2kR_i + \varphi_i(k)]$$

The EXAFS spectra are extracted from the raw XAS spectra by what are now standard techniques. It is common practice to weight the EXAFS by k^3 in order to counteract the damping of the spectra caused by thermal vibrations, and from the fall-off in scattering amplitude. In addition, the theory used to analyze the spectra is more accurate at higher k, increasing approximately as k^1, and the k-weighting emphasizes the part of the spectrum that can be most accurately analyzed. EXAFS spectra are usually Fourier transformed in order to visualize the frequency contributions to the EXAFS corresponding to individual interactions as peaks:

$$\rho(R) = \frac{1}{4\pi^{1/2}} \int_{k_{\min}}^{k_{\max}} \chi(k) k^3 e^{i2kR}\,\mathrm{d}k$$

The results of the Fourier transform are usually displayed as the transform magnitude, $|\rho(R)|$ versus R:

$$|\rho(R)| = \sqrt{\mathrm{Re}\{\rho(R)\}^2 + \mathrm{Im}\{\rho(R)\}^2}$$

The Fourier transform shows peaks with positions corresponding to the interatomic distances plus half the average phase-shift slope (usually this is about −0.3 Å). It is common practice to phase-correct Fourier transforms. This is done using an EXAFS phase function, typically a theoretical one, for the dominant absorber–backscatterer interaction in the EXAFS:

$$\rho(R) = \frac{1}{4\pi^{1/2}} \int_{k_{\min}}^{k_{\max}} \chi(k) k^3\, e^{i2kR + i\varphi(k)}\,\mathrm{d}k$$

The effect of phase-correcting the transform is to move the peaks to values close to the actual absorber–backscatterer distances (R_i), in the absence of any phase correction the peaks will be at positions $R + \Delta$, where Δ is approximately half the average phase-shift slope over the k range of the transform for a given interaction. Moreover, without phase-correction peak shapes are often asymmetric due to structure in the phase-shift function, and with heavy backscatterers multiple peaks can arise in the transform for a single absorber–backscatterer distance. Fig. 6 illustrates the effects of phase-correction on the Fourier transform of molybdate. Strictly speaking, phase-correction is only valid in systems that have just one kind of backscatterer, such as the molybdate $[MoO_4]^{2-}$ example of Fig. 6. This is because only a single $\varphi(k)$ can be used (typically for the EXAFS with the largest backscattering amplitude), and thus the other interactions will be mismatched. In practice, the use of phase-correction still generally yields much clearer looking transforms in these cases, although in general it is good practice to label the abscissa $R + \Delta$ to indicate the presence of a partial mismatch.

While some analysis packages do analyze data in Fourier space, in most cases the EXAFS Fourier transform is not usually interpreted directly and instead a radial structural model is fit to the extracted experimental k-space EXAFS oscillations. Typically *ab initio* theory is used to approximate the model, employing what is

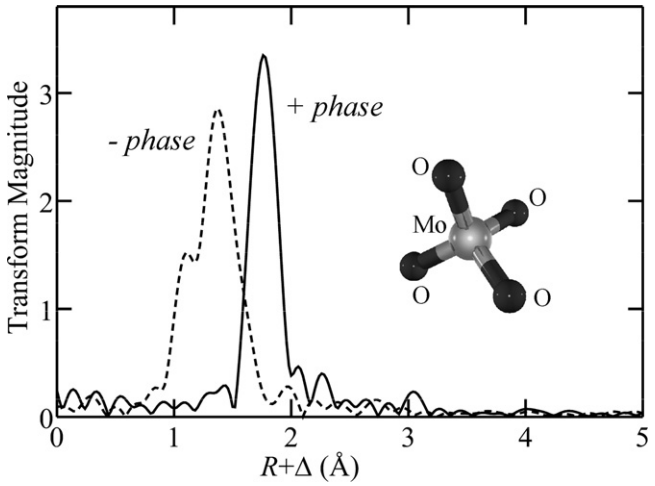

Fig. 6. Effects of neglecting phase-correction in the EXAFS Fourier transform. EXAFS Fourier transforms of solid Na_2MoO_4 which contains an approximately tetrahedral anion with four essentially equivalent Mo–O bonds. The solid line shows the transform when phase-correction for Mo–O backscattering is used, while the broken line shows the transform when no phase-correction is applied.

commonly called EXAFS curve-fitting analysis to determine values for N, R and σ^2. N and σ^2 are typically highly correlated in the refinement, and because of this determination of these is only to an accuracy of around ±20%. Similarly, while ligand identity can to an extent be established from the characteristic $A(k,R)$ and $\varphi(k)$, with data of limited k-range miss-assignment of ligands is quite possible and occasionally occurs. A common value for a shift in E_0 (or ΔE_0) between computed and experimentally measured EXAFS is also often refined. With modern theory such as FEFF [52] a common ΔE_0 value for all components can be co-refined, but the wise experimenter will be guided by values from model compounds, particularly if data with only limited k-range are available [53]. An example of an EXAFS analysis of the coordination compound $[MoO_2(dtc)_2]$ [54] is illustrated in Fig. 7. This example includes EXAFS which nearly cancel. Of the four Mo–S bonds present two are approximately *trans* to Mo=O groups and two are approximately

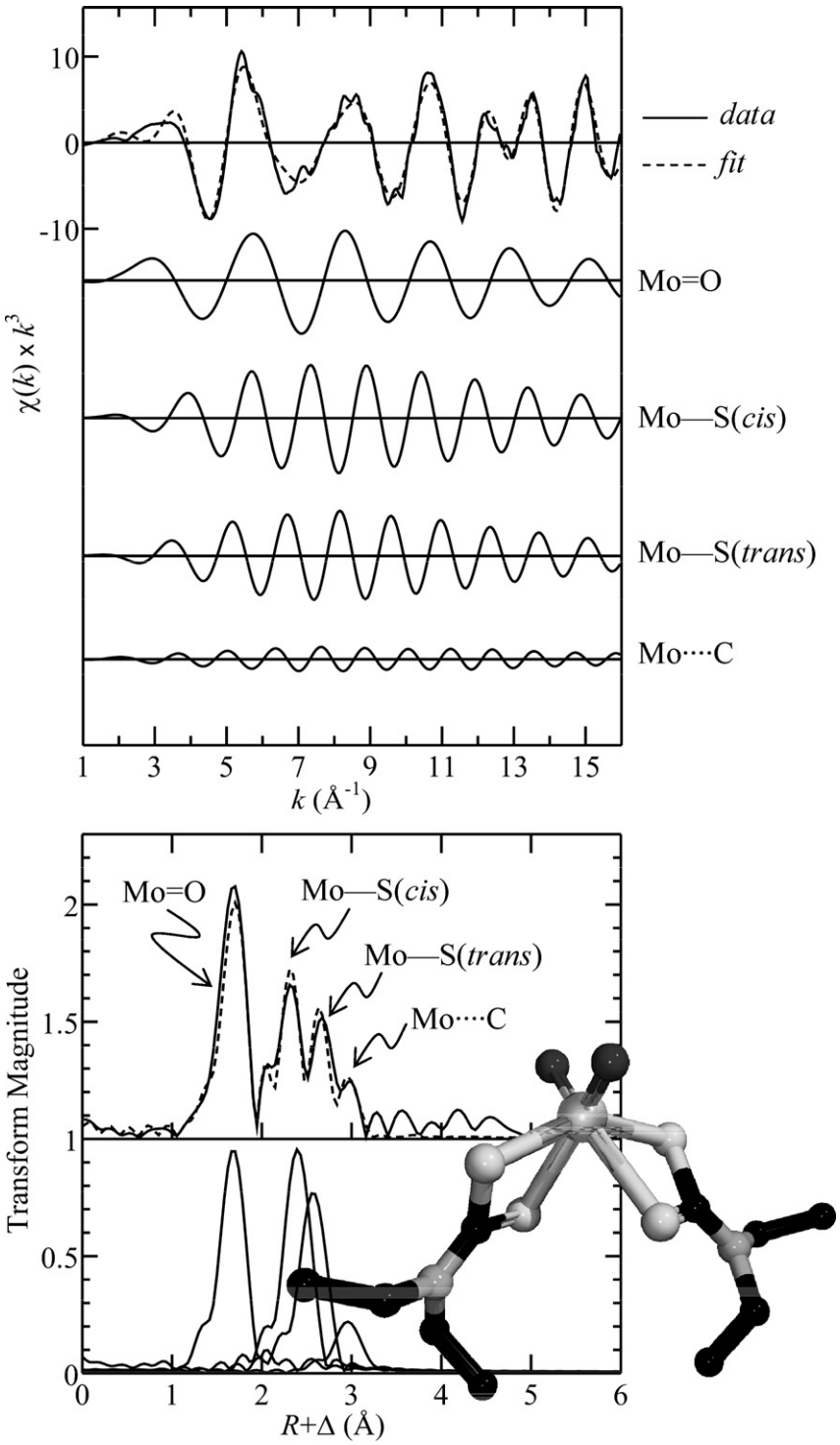

Fig. 7. Summary of EXAFS analysis methodology for the coordination compound $MoO_2(dtc)_2$. The EXAFS is modeled by inclusion of successively important backscatterers, with refinement of structural parameters at each stage. The final fit includes Mo=O, two different Mo–S (*cis* and *trans* to the Mo=O groups) and a long-range Mo···C interaction. The final refined bond-lengths were Mo=O 1.707(1) Å, Mo–S (*cis*) 2.470(2) Å, Mo–S (*trans*) 2.650(2) Å, Mo···C 3.02(1) Å. These values are within 0.01 Å of the values determined by X-ray crystallography [54].

cis. The former Mo–S bonds are significantly longer than the latter due to *trans* effects from the oxo groups.

A major strength of EXAFS is the accuracy with which it can determine R, the average inter-atomic distance for a given type; for directly coordinated ligands this is approximately ±0.02 Å. We note that the precision is generally an order of magnitude better than this, so that relative changes in similar species can be very well defined. The EXAFS resolution is the minimum distance between similar ligands that can be discerned, and this is directly related to the extent of the data and is approximately given by $\Delta R \approx \pi/2k$. For typical data ranges ΔR is rather poor at around 0.15 Å, and this is one major limitation of EXAFS analysis.

Multiple scattering occurs when the photo-electron is scattered by more than just one atom before returning to the absorber atom. Appropriate analysis can in some cases give information on geometry, particularly when linear or close to linear arrangements of atoms are present. Multiple scattering paths are usually referred by the number of legs in the multiple scattering pathway, and it is important to include all relevant multiple scattering paths for a given atomic arrangement (*e.g.* [55,56]). For an arrangement of three atoms multiple scattering with up to four legs is important, while for four atoms multiple scattering with up to six legs is important. For linear arrangements of two backscatterer atoms with similar size the multiple scattering EXAFS from the three-leg path will be approximately 90° out of phase with the single scattering (two-leg) path, and the EXAFS from the four-leg path will be approximately 180° out of phase with the single scattering path. With some notable exceptions [4,5], multiple scattering is not important in molybdenum enzyme EXAFS.

The Debye–Waller factor, formally the term $e^{-2\sigma_i^2 k^2}$ in the EXAFS expression, is often used to refer to σ_i^2, the mean-square deviation from the average absorber–backscatterer distance R_i. Each σ^2 has both vibrational and static components, such that $\sigma^2 = \sigma_{vib}^2 + \sigma_{stat}^2$. EXAFS measurements are typically carried out at liquid helium temperatures, in part to cryo-protect the sample against X-ray related damage (photo-reduction or photo-oxidation) but also to minimize the σ_{vib}^2 which results in stronger EXAFS. Moreover, the simple Gaussian model $e^{-2\sigma^2 k^2}$ for the pair distribution function is only valid at low temperature, and at higher temperatures it becomes asymmetric, or anharmonic, and cumulant expansion is needed for analysis. This introduces both more complexity and more uncertainty in the analysis, and the wise experimenter will always employ low temperatures for EXAFS measurements. To a first approximation σ_{vib}^2 for a single absorber–backscatterer pair can be estimated using the expression for a diatomic harmonic oscillator:

$$\sigma_{vib}^2 = \left(\frac{h}{8\pi^2 \mu \upsilon}\right) \coth\left(\frac{h\upsilon}{2kT}\right)$$

where υ is the vibrational frequency of the bond-stretch vibration, μ is the reduced mass, k is Boltzmann's constant (not to be confused with the photo-electron wave vector k) and T is the temperature. The contribution σ_{stat}^2 arises from structural disorder in the bond-lengths differing by less than the EXAFS resolution ΔR, discussed below. For N backscatterer atoms separated from the absorber atom by an average distance R and individually by R_i, the static component is given by:

$$\sigma_{stat}^2 \approx \frac{1}{N}\sum (R_i - R)^2, \quad \text{where} \quad |R_i - R| \leq \frac{\pi}{2k}$$

Credible EXAFS analyses must employ chemically reasonable bounds for σ^2 values. When multiple bonds are present, an upper bound for σ^2 is not trivial to define, because of uncertainty the value of σ_{stat}^2, however, the use of an overly large σ^2 value will effectively remove the contribution from the EXAFS by damping all but the lowest k oscillations. Minimum values for σ^2 are simple to define as they cannot be less than σ_{vib}^2. Using υ for known compounds and the above relationships, we have previously estimated values for σ_{vib}^2 of 0.0020 Å^2 for Mo–S bonds and 0.0015 Å^2 for Mo=O bonds at 10 K [57] which is a typical temperature for EXAFS measurement.

As we have discussed, the primary strength of EXAFS analysis for metallo-proteins is in the accuracy of determination of inter-atomic distances, which is typically better than 0.02 Å for directly coordinated atoms. If more than one neighbor atom of a given type is present (*e.g.* a site with four Mo–S ligands, all with similar bond-lengths) then an important point is that the EXAFS determines an average inter-atomic separation within the resolution of the data. To a reasonable approximation the resolution ΔR, which is the smallest difference in similar inter-atomic distances that can be detected is given by $\Delta R \approx \pi/2k$ (where k is extent of the data in Å^{-1}). Thus, a weakness of EXAFS is that it typically has a rather limited bond-length resolution when used with conventional data ranges, so that with data extending to $k = 12$ Å^{-1}, the resolution will be at best 0.13 Å. It is interesting to note that early EXAFS analysis of xanthine oxidase claimed [58] to be able to discriminate different sulfur coordinations; a short one at 2.25 Å attributed to a Mo=S moiety already suspected from previous EPR studies, plus two Mo–S at 2.46 Å. Given that these early data were analyzed between $k = 4.6$ and 11.5 Å, and were very noisy above $k \approx 9$ Å^{-1} we expect a resolution of at best 0.23 Å; suggesting that the proposed different sulfur coordinations cannot possibly have been resolved in this early analysis.

One major weakness of EXAFS spectroscopy is therefore its limited bond-length resolution, which in most cases will approach 0.15 Å. Recently, Harris et al. [59] have shown that for molybdenum it is possible to overcome this by significantly extending the k-range of the data. We note that for first transition metal ions this is not particularly practical as the K-edges of transition metals with higher atomic number truncate the k-range of the data. Thus, Cu K-edge measurements are typically truncated to $k \approx 13$ Å^{-1} by traces of zinc in samples or in the beamline. Harris et al. [59] collected sulfite oxidase EXAFS data up to $k = 25$ Å^{-1}, resulting in an approximate bond-length resolution of 0.065 Å, and allowing observation of new details in the active site.

Another limitation in EXAFS analysis relates to the number of independent degrees of freedom of the spectrum. If δk is the k-range of being analyzed $\delta k = (k_{max} - k_{min})$, and δR is the region in R-space over which the fit is made then the information content of a spectrum can be specified by the number of independent relevant points, N_I. The number of independent variables N_{var} that can be determined by EXAFS curve-fitting must be less than or equal to N_I [60]:

$$N_I = \left(\frac{2\delta k \delta R}{\pi}\right) + 2$$

This limitation is obviously also helped by increasing the k-range, but for conventional data which might range from $k = 2$ to 14 Å^{-1}, $\delta k = 12$ Å^{-1}, and for analysis that extends in total between 1.6 and 2.6 Å in R-space, $\delta R = 1$ Å, then $N_I = 9.6$, so that 9 variables are the most that can be extracted from the data. Of the lamentably numerous published erroneous EXAFS analyses many have either approached or seriously exceeded this limit, and care must be taken not to do so. Another frequent issue with published Mo enzyme EXAFS data is that they are often collected to insufficient signal to noise. Noise in EXAFS spectra is very frequently close to "white" in that a broad range of frequencies are represented. When undesirable practices such as Fourier filtering are used the noise in the low-R frequency range is obscured, and erroneous conclusions can result. The careful experimenter will use k-weighting of the count

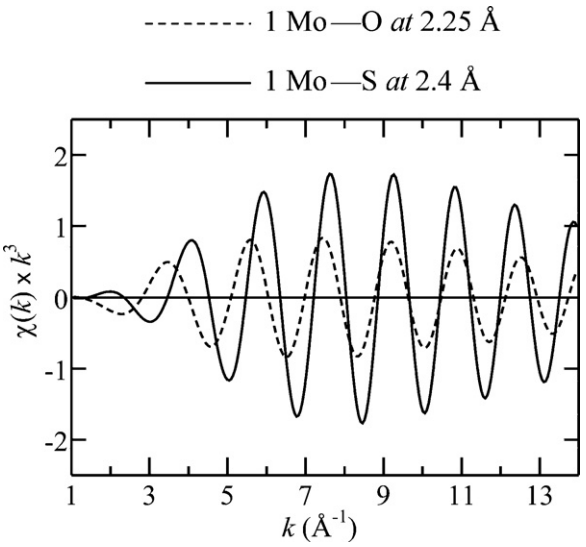

Fig. 8. Phase overlap of Mo–O and Mo–S EXAFS in a hypothetical analysis. Computed EXAFS for one Mo–S and one Mo–O is compared and can be seen to overlap in phase at high *k*.

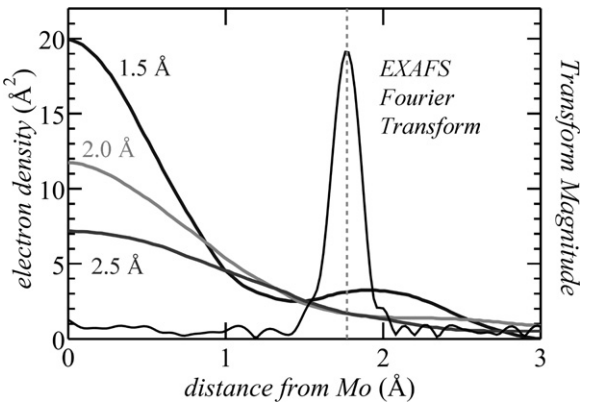

Fig. 9. EXAFS *vs.* crystallography regarding accuracy of determined bond-lengths. The figure shows computed electron densities for $[MoO_4]^{2-}$ along one Mo–O vector calculated for different crystallographic resolutions. A defined peak in electron density is only observed at the highest resolution, and this is subject to possible confusion due to Fourier ringing. This is compared with the Mo–O phase corrected EXAFS Fourier transform of $[MoO_4]^{2-}$ (experimental data), emphasizing the relative accuracy of bond-length determination of the two methods.

times, both because the data are k^3-weighted and because the high-k end of the spectrum is simpler to analyze. The common practice is to use k^2-weighting of count times, because with k^3-weighting scan times begin to become impractical. Moreover, in photon statistics the standard deviation of the photon noise is equal to the square root of the average number of photons. The signal-to-noise for k^3-weighted data would thus indicate the use of k^6 weighted count times for equal noise across the whole spectrum, which is even more impractical.

Finally, we consider interactions that overlap in phase. With the Mo enzymes the most common of these are Mo–O and Mo–S interactions. This is because the different bond-lengths R and phase-functions $\varphi(k)$ can conspire to make the Mo–O and Mo–S hard to discriminate (Fig. 8). Detection of Mo–O is thus often particularly difficult in the case of the Mo enzymes of the DMSO reductase family, where the intense EXAFS from sulfur backscatterers can mask the presence of Mo–O interactions. Moreover, it is also possible for EXAFS to cancel, thus the $\varphi(k)$ for oxygen and sulfur approximately differ by about 180°, and if Mo–O and Mo–S are present with the similar bond-lengths then their EXAFS will cancel and detection will be problematic.

2.3.3. Comparison of XAS and crystallography

Protein crystallography provides a wealth of information on large macromolecules that is unrivalled by any other technique. For large molecules at low resolutions the method is, strictly speaking, underdetermined, and restraints and to a lesser extent constraints are essential for solving the structure [61]. For example, inter-atomic distances in the amino acids are taken from small molecule crystal structures and treated as fixed quantities. Moreover, because of the limited resolution, and as discussed by Rees and co-workers [62] Fourier series termination artifacts can cause problems in determining the positions of light atoms in the vicinity of a heavy atom such as a metal ion. XAS can make definite contributions mainly due to three considerations. (i) Accuracy of determination of bond-lengths, as illustrated in Fig. 9 the strongest structural capability is the determination of bond-lengths. (ii) The lower radiation dose to the sample means that there is typically less photo-reduction with XAS [63]. This is particularly true of the molybdenum enzymes because the photoabsorption cross sec-

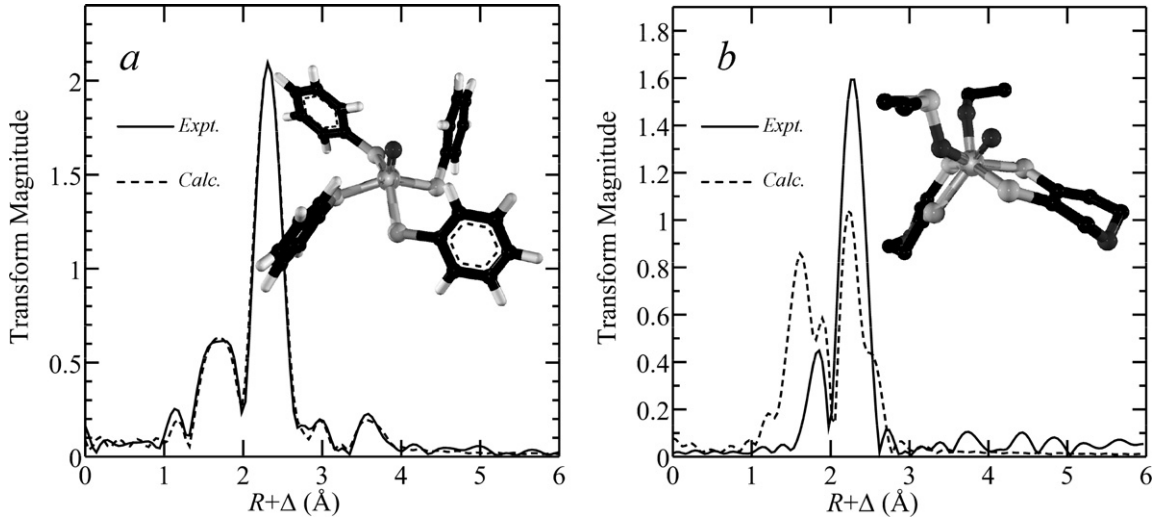

Fig. 10. EXAFS *vs.* crystallography for small and large molecules. In both (a) and (b) EXAFS spectra were computed using structural details from crystallography and employing chemically reasonable Debye–Waller factors. In the small molecule (a) the simulated EXAFS accurately reproduces the experimental data, whereas with the protein (b) the simulation and experimental data are significantly different. This shows that EXAFS can add structural information to that obtained from crystallography.

tion at the Mo K-edge (*ca.* 20 keV) is substantially lower than at the photon-energies commonly used for macromolecular crystallography (usually 10–12 keV). In the case of XAS changes in the near-edge spectrum will in any case betray the presence of photoreduction. (iii) Examination of solutions (usually frozen) is simple and no artifacts of crystallization are possible.

Fig. 10 compares the experimental and computed EXAFS Fourier transforms for a low molecular weight compound and for a protein. In both cases the inter-atomic distances and coordination numbers from crystallography are used without adjustment, and Debye–Waller factors are constrained within chemically reasonable bounds. For the small molecule structure, the agreement between the experimental transform and the transform derived from the crystal structure can be seen to be excellent, but for the protein this is not the case. This clearly illustrates both that EXAFS works well, and that it can add information to the more difficult protein crystal structure.

2.3.4. X-ray fluorescence spectroscopy

High resolution X-ray fluorescence spectroscopy can be used as a probe of electronic and local molecular structure, for example, ligation such as Mo–OH_2 and Mo–OH might be discriminated by examining the Kβ″ emission which arises from a formally forbidden O → Mo(1s) ligand to metal charge transfer transition and is very sensitive to bond-length. Details of electronic structure might also be revealed by examining the $K\beta_4$ emission (also formally dipole forbidden) which arises from Mo(4d) → Mo(1s) emission [64]. This technique has promise but the measurements are technically demanding and may only be feasible on a few beamlines world-wide.

3. The DMSO reductase family of molybdenum enzymes

The dimethylsulfoxide (DMSO) reductase family is the largest and most diverse of the three families of molybdenum enzymes. It contains enzymes with two molybdopterins bound to the molybdenum. This family also includes the only enzymes that natively contain tungsten. Spectroscopic studies have provided a major impact upon our overall knowledge of this group. We will consider the DMSO reductases and their close relatives, the dissimilatory nitrate reductases, the formate dehydrogenases and the tungsten enzymes.

3.1. The active site structure of Rhodobacter DMSO reductases

These enzymes are of the so-called type III DMSO family members. The active site structures of the DMSO reductase from *Rhodobacter sphaeroides* and *Rhodobacter capsulatus* were previously the subject of some controversy. These enzymes fulfill identical physiological functions in the species in which they are found, and have nearly identical amino acid sequences. As DMSO reductase is the prototypical member of this family, and because spectroscopy proved important in understanding the active site, we will describe this in some detail. The enzyme catalyzes the reduction of dimethylsulfoxide to dimethylsulfide:

$$\text{Enzyme-Mo}^{IV} + (CH_3)_2S{=}O + 2H^+ \rightarrow \text{Enzyme-Mo}^{VI} + (CH_3)_2S + H_2O$$

DMSO reductase is unusual in having the molybdenum active site as the sole chromophore, which means that it is accessible by various spectroscopic methods such as UV–vis and resonance Raman spectroscopy in an uncomplicated manner. DMSO reductase was only the second molybdenum-containing enzyme to have its crystal structure solved, and crystallographic studies by three different groups were published in rapid succession [12,65,66]. These indicated essentially identical polypeptide folds, although the active site structures were significantly different. The original structure first reported by Rees and co-workers of the *R. sphaeroides* enzyme suggested a five-coordinate active site for the oxidized Mo^{VI} enzyme with one Mo=O, coordination by the Oγ of Ser147, and three sulfur donors from two dithiolenes [12]. The reduced Mo^{IV} enzyme showed a novel three-coordinate site with two sulfurs from one dithiolene and the other dissociated, plus coordination by Ser147 Oγ [12]. A novel catalytic mechanism was proposed based upon dissociation and re-association of one of the cofactor dithiolenes together with oxo atom transfer [12]. The second structure reported was that of the *R. capsulatus* enzyme by Huber and co-workers [65], and while the polypeptide fold was nearly identical, the active site structure was different; a Mo^{VI} *cis*-dioxo molybdenum coordination with two Mo=O groups, one cofactor providing two sulfur ligands and the other dissociated, plus coordination by Oγ from Ser147 [65]. A third structure, again of the *R. capsulatus* enzyme by Baily and co-workers [66] suggested a novel seven-coordinate active site with a *cis*-dioxo Mo^{VI} plus four sulfur donors from the two dithiolenes, and Ser147 Oγ. The reduced Mo^{IV} enzyme was reported to be a five-coordinate mono-oxo site, with three sulfur donors from two dithiolenes and Ser147 Oγ. A remarkable and important finding was subsequently reported by the same group, which is that adding the product of catalytic turnover, dimethylsulfide (DMS), to oxidized DMSO reductase resulted in a substrate-bound form of the reduced enzyme with a color change from brown-green to a vivid pink-purple [67]. The crystal structure of this substrate-bound enzyme was reported as a seven-coordinate mono-oxo molybdenum site, with four sulfurs from two dithiolenes an oxygen from Ser147 Oγ, plus DMSO covalently bound via its oxygen [67]. The bound DMSO was reported to have an unusually long S=O bond length of 1.7 Å, which can be compared with low-molecular weight complexes that have S=O of about 1.5 Å [68]. The crystal structure of the related enzyme TMAO reductase from *Shewanella massilia* was also reported to have an unusual seven-coordinate molybdenum site [69] and was very similar to the structure of Bailey and co-workers of the *R. capsulatus* DMSO reductase [66].

The crystallographic conclusions (Fig. 11) were inconsistent with previous EXAFS spectroscopy [70], and with subsequent resonance Raman spectroscopy [71]. A further EXAFS study by a Garner and co-workers [72] concluded that EXAFS fully supported the Bailey structures [66,67]. All of these papers postulated somewhat different catalytic mechanisms, and there was little consensus about the nature of the active site or any clear idea of the catalytic mechanism.

A third EXAFS study by George et al. [57] (Fig. 12) critically examined the published structures and showed that the active site structures proposed from crystallography were all substantially chemically unreasonable [57]. For example, atoms that were supposedly non-bonded had overlapping van der Waals radii, and structures contained impossibly small bond-angles, such as the O=Mo=O angle or improbably large bond-angles such as the (Ser147)Cβ–Oγ–Mo angle [57]. This study concluded that the crystallographic analyses were all in error, and that the correct active site resembled that suggested by the original EXAFS study [70]. These workers also criticized the EXAFS study by Garner and co-workers [72] and showed that their analysis was flawed due to their use of chemically impossible Debye–Waller factors [57]. George et al. also exchanged the enzyme into $H_2{}^{17}O$ and showed that Mo^V EPR was consistent with a single coupled oxygen [57]. A subsequent EXAFS study of the related enzyme biotin sulfoxide reductase [73] indicated an active site structure that closely resembled that postulated from the original EXAFS study of DMSO reductase [70]. The data from resonance Raman spectroscopy [71] completely supported the EXAFS analyses [57,70] and showed unambiguously

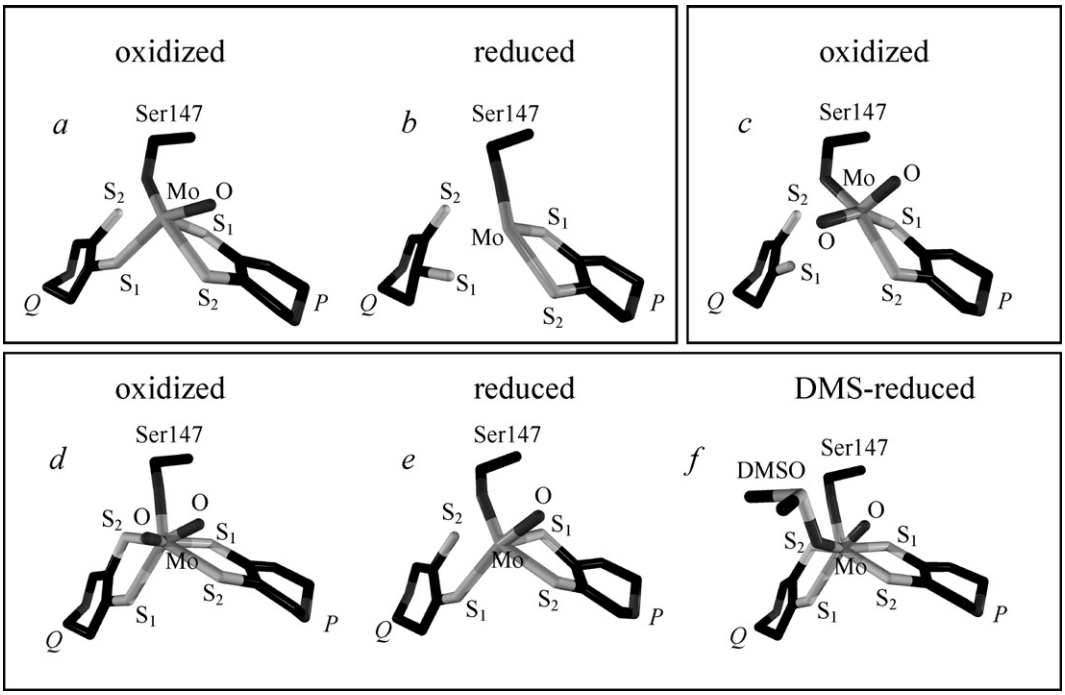

Fig. 11. Initial DMSO reductase active site structures proposed from X-ray crystallographic studies of *R. sphaeroides* and *R. capsulatus* enzymes. Coordinates were taken from the protein data bank using entries 1CXS, 1CXT, 1DMS, 1DMR, 2DMR and 4DMR for structures (a)–(f), respectively. For (a) and (b) see [12], (c) see [65], (d) and (e) see [66], and (f) see [67].

that the active site of oxidized enzyme contained a single Mo=O group, that the reduced enzyme was a *des*-oxo species and these workers suggested a catalytic mechanism based on oxo transfer from Mo [71]. Despite the weight of spectroscopic evidence, the suggestion that the crystal structures were erroneous remained highly controversial until a high-resolution crystallographic study [19] showed co-crystallization of two different active site structures – one resembling the structure suggested by EXAFS [57], and the other resembling one of the earlier crystal structures (Fig. 13), which was attributed to inactive enzyme in which one of the two molybdopterins is dissociated from Mo [19]. The use of HEPES buffer in the crystallization media was implicated in the conversion from the native to the (putatively) inactive form [19]. This study directly confirmed the presence of multiple structures of the active

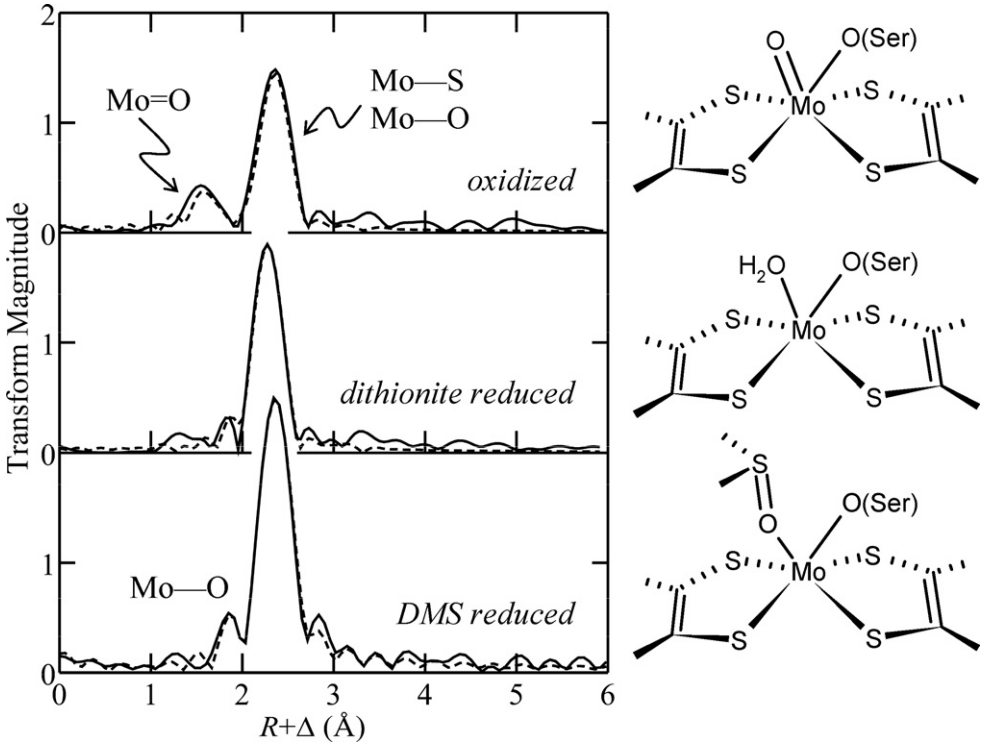

Fig. 12. Mo K-edge EXAFS Fourier transforms (solid lines) plus best fits (broken lines) together with likely structures (right) for different forms of *R. sphaeroides* DMSO reductase. Data are re-plotted from Ref. [57]. Transforms are phase-corrected for Mo–S backscattering.

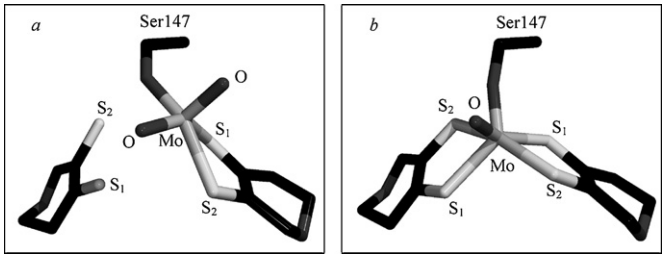

Fig. 13. Crystallography of DMSO reductase showing the two different active sites which co-crystallized [19]. Coordinates were taken from the protein data bank entry 1EU1. The structure (a) resembles that of Huber and co-workers [65], while (b) resembles that suggested from spectroscopic studies and is attributed to the active enzyme.

site, which had previously been demonstrated by EPR spectroscopy [74], and that one of the two molybdopterins might dissociate in some forms of the enzyme had already been suggested in the first EXAFS study [70]. The most likely explanation for the earlier confusion is that co-crystallization of multiple species confused the analyses and resulted in impossibly crowded active site structures. Further EXAFS of TMAO reductase indicated that these enzyme active sites could exist in multiple forms, like DMSO reductase, and that the active site structure closely resembled that of DMSO reductase [75]. In general the phenomenon of altered molybdenum active sites, often with *cis*-dioxo Mo^{VI} cores, appears quite common and a cycle of oxidation and reduction is required to restore the site to the fully active structure [75]. Finally, recent *in situ* EXAFS experiments on the *E. coli* DMSO reductase, still contained within its native membranes (and thus more likely to be in a physiologically relevant form), indicated an active site structure similar to that proposed from the original EXAFS experiments [76].

The substrate-bound form of the enzyme [67] is of considerable interest because it is thought to be analogous to an intermediate of catalytic turnover. Both resonance Raman and XAS indicate that the molybdenum atom is a *des*-oxo Mo^{IV} species [57,71], but subsequent electronic spectra of both the dimethylsulfide bound enzyme and the analogous species formed using dimethylselenide were interpreted as supporting a $Mo^{V}\cdots OS^{\bullet}$ pair [77]. Because of the core-hole lifetime broadening of the Mo K-edge, near-edge spectra were not unambiguous in assigning oxidation state, although resonance Raman data could only be reconciled with a formal oxidation state of Mo^{IV} for the DMS-treated enzyme [71]. EXAFS of the DMSO-bound species [57] failed to detect any long-range interactions from the distant DMSO sulfur in the Mo–O=S$(CH_3)_2$ coordination assigned by crystallography, presumably because the amplitude of this is below detection limits and within the noise of the data [57]. Analogous complexes to the DMS complex can be formed with dimethylselenide $(CH_3)_2Se$ [74,78] and trimethylarsine $(CH_3)_3As$ [78]. These complexes have very similar electronic spectra to that of the DMS complex, and show strong outer shell EXAFS from the Se and As with well-defined peaks in the Mo K-edge EXAFS Fourier transforms at about 3.4 Å [78]. Moreover, the $(CH_3)_3As$ complex forms quantitatively at stoichiometric levels [78] and analysis of both As and Mo EXAFS and near-edge spectra conclusively demonstrated that the Mo site was formally Mo^{VI} bound to $(CH_3)_3As{=}O$, with very little distortion from the free ligand (Fig. 14). At the time of writing the active site structure and overall catalytic mechanisms of DMSO reductase and its close relatives seem reasonably clear, probably being oxo-transfer in nature [57].

3.2. Prokaryotic nitrate reductases

Nitrate reductases catalyze the two-electron reduction of nitrates to nitrites:

$$NO_3^- + 2H^+ + 2e^- \rightarrow NO_2^- + H_2O$$

In this section we consider the prokaryotic nitrate reductases, which are distinct from the assimilatory nitrate reductases of higher organisms, which belong to the sulfite oxidase family. The dissimilatory nitrate reductases can be divided into two broad categories – the respiratory membrane-bound nitrate reductases (Nar), the periplasmic dissimilatory enzymes (Nap) and the cytoplasmic assimilatory enzymes (Nas).

3.2.1. The respiratory nitrate reductase enzymes

The respiratory nitrate reductase enzymes are closely related to the DMSO reductase family. Whereas the Mo centre in DMSO reductase is bound by a Ser side chain, the nitrate reductases are divergent and utilize different amino acids. The structure of the NarG enzymes has been studied by two independent groups [79,17]. The crystal structures provide a wealth of detailed information at the whole-enzyme level and for understanding the route of electron transfer, but they differ in the coordination deduced for Mo. Both crystal structures depict *bis*-dithiolene coordination, with Asp222 coordinating Mo providing the sole coordinate covalent bond to the enzyme complex. The nature of the Asp222 coordination, however, differs between the two. The structure from Strynadka and coworkers [79] depicts bidentate coordination through the δ_1 and δ_2 O-atoms of the Asp222 carboxylate side chain, whereas the same residue in Iwata and coworkers structure is monodentate [17]. A similar monodentate aspartate coordination has been observed for the related ethylbenzene dehydrogenase [18]. Both structures display highly distorted Mo coordinations, with a vacant face at the Mo centre and crowded face opposite with apparent bond angles between ~90° and 70° between the Asp and one of the dithiolenes. These are likely the result of averaged structures arising from photoreduction of the Mo centre during diffraction data collection.

Previous structural investigations of *E. coli* nitrate reductases by EXAFS and Mo^{V} EPR have been reported. Mo^{V} EPR shows characteristic Low-pH and High-pH signals, [80], with both High-pH and Low-pH signals showing a coupled solvent-exchangeable proton, and the Low-pH signal predominates in the presence of anions. Similar properties have been reported for the enzyme from *Pseudomonas aeruginosa* [81]. A large number of anion complexes of the *E. coli* enzyme were characterized by George et al. [80] including nitrate, nitrite, chloride and fluoride. The latter showed resolved hyperfine coupling to a single ^{19}F indicating that the anion is located in the vicinity of the Mo. Subsequent EXAFS studies [82] showed the presence of approximately four Mo–S, together with a single Mo=O group in the oxidized enzyme, indicating a mono-oxo Mo^{VI} site [82]. These workers also suggested the presence of a *des*-oxo Mo^{IV} site, although sample inhomogeneity was observed to be a problem [82]. The effects of exchange into $H_2{}^{17}O$ enriched water clearly indicated a broadening due to ^{17}O hyperfine interaction in the High-pH signal, but no such effects were observed with the Low-pH signal, even when ^{17}O-enriched nitrate ($N^{17}O_3^-$) was used to generate the nitrate complex, or following turnover with enriched nitrate [82]. The small size of the ^{17}O hyperfine coupling in the High-pH signal might be cause to anticipate a similarly small coupling for the Low-pH signal which could easily have been missed with ordinary EPR [82], and experiments using more sophisticated methods such as ENDOR are required. Based on a recent re-investigation of the oxidized form of NarGHI from *E. coli* using EXAFS it appears that there are no contributions from oxo type coordination to the Mo centre, instead there are 2 Mo–O interactions at slightly longer (and inequivalent) distances, in addition to the expected 4 Mo–S donors expected from *bis*-dithiolene coordination [83]. Site directed mutagenesis of residues proposed to interfere with Asp222 coordination gives rise to significantly disrupted coordination environments which confirm the importance of Asp222.

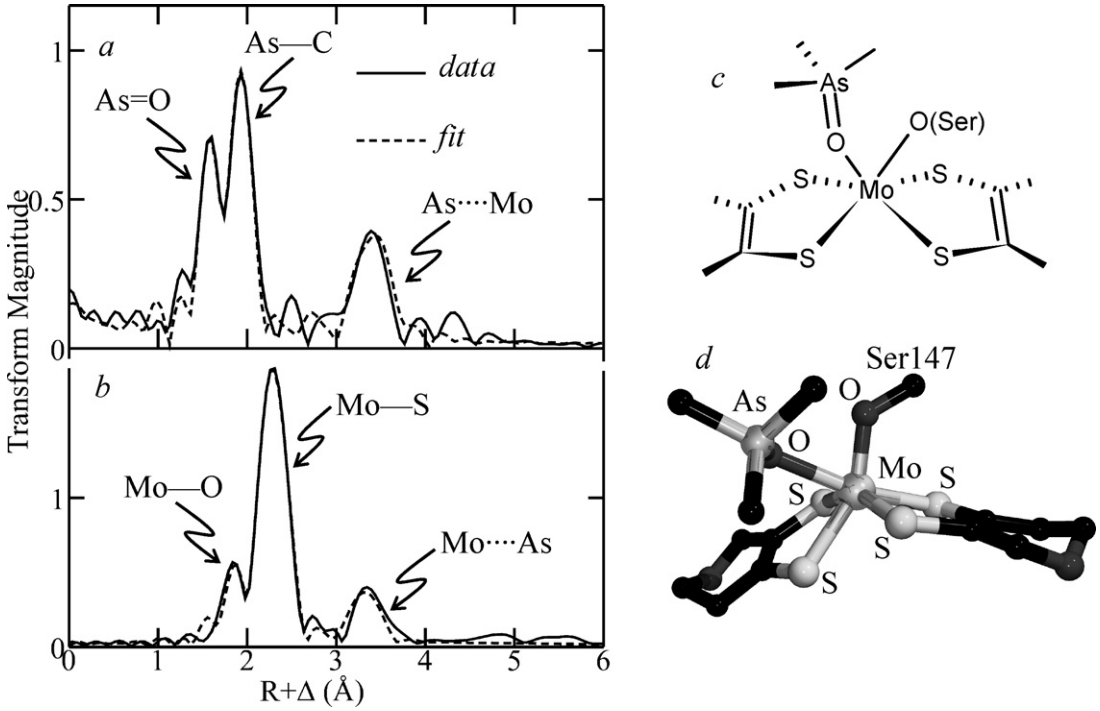

Fig. 14. EXAFS Fourier transforms (solid lines) plus best fits (broken lines) of the complex formed between *R. sphaeroides* DMSO reductase and trimethylarsine. Complimentary data measured at the As K-edge (a) and the Mo K-edge (b) are shown, phase-corrected for As–C and Mo–S backscattering, respectively. Data are re-plotted from Ref. [78]. The structural conclusions are illustrated in (c) and compared well with the energy-minimized density functional theory structure (d).

The possibility exists for a dynamic role for Asp222 where the ligand may change from bidentate to monodentate during the catalytic cycle – lending tacit support for coordination geometries that follow the spirit of the two published crystal structures. Because of multiple additional chromophores in nitrate reductase the applicability of other spectroscopic techniques such as resonance Raman is limited to other regions of the enzyme than the Mo-containing active site. Another relative of this family is the selenate reductase from *Thauera selenatis*, which has been studied by EXAFS [84] and which showed a mono-oxo Mo^{VI} site and a *des*-oxo Mo^{IV} site with approximately four Mo–S ligands in both. This study also detected a hitherto undetected low-valent selenium coordinated to an unknown metal ion (possibly iron) in the enzyme, although its role is unknown [84].

3.2.2. The periplasmic nitrate reductase enzymes

Several crystal structures of the periplasmic nitrate reductases (Nap) have been published to-date [15,85–88] and have confirmed much of the previous structural characterization using spectroscopic techniques. The Mo centre is coordinated by two molybdopterin dithiolenes and a sulfur atom from a Cys residue. The initial crystal structure had suggested that the sixth ligand to Mo was OH or H_2O [15]. This conclusion was overturned by convincing evidence from two high-resolution crystal structures [85,86] which indicated that the additional ligand was a sixth S atom, and this has recently been confirmed in a high resolution (1.5 Å) crystal structure of NapAB from *Cupriavidus necator* [88]. The reduced form of the enzyme contains a *des*-oxo Mo site with 6 Mo–S ligands, while the oxidized form contains an additional Mo–O ligand and probably 5 Mo–S ligands. Aside from coordination by the two molybdopterin dithiolenes (which seems very likely) it remains unclear whether the fifth ligand is a terminal sulfur of some type or coordinated cysteinate.

Bennett et al. investigated Nap from *Thiosphaera pantotrophica* by EPR and identified multiple EPR signals and concluded that the Nas and Nap enzymes were similar, whereas the membrane-bound Nar from *E. coli* was significantly different [89]. Subsequent examination using EPR, ENDOR and EXAFS produced a complex spectroscopic picture of the enzyme [90,91]. A number of different Mo^{V} EPR signals were observed, and these were called High-*g* resting, High-*g* nitrate, Low-*g* split, Low-*g* un-split and Very high-*g*. We will not describe the spectroscopy of all of these in depth here, as all integrate to quite low levels, and may (or may not) be due to minority inactive species. We note that the Very high-*g* EPR signal is similar to signals from *Azotobacter vinelandii* assimilatory nitrate reductase [92]. The High-*g* resting corresponds to between 2.5% and 10% of Mo present [91] and shows weak coupling to two $I = 1/2$ nuclei that are not exchangeable with solvent. These have been attributed to the methylene protons of a coordinating Cys residue [90,91], and there is no evidence from CW EPR or ENDOR of a Mo–OH coordination similar to that observed in other molybdenum enzymes [91]. For cysteine methylenes to give such large coupling as that observed (19 and 8.4 MHz for A_z) significant spin-density must be present on the cysteine, which might argue for electronic similarities of the signal-giving species with the selenocysteine of *E. coli* formate dehydrogenase (see below) which has extensive spin-density on selenium.

The EXAFS spectra that have been reported to date are of close-to inadequate signal-to-noise, but do indicate the presence of significant Mo=O coordination in the as-isolated enzyme, which is reduced on redox-cycling [91]. This suggests that some molybdopterin dissociation of the type observed with *Rhodobacter* DMSO reductases (discussed above) is present in the preparations used [91]. Structures for the Nap active site proposed by Najmudin et al. [85] are shown in Fig. 15. Clarification of the crystal structure can be expected to have its usual galvanizing effect on the field, but at the time of writing it seems clear that much work remains to be done in the spectroscopic characterization of the Nap enzymes.

3.2.3. The prokaryotic assimilatory nitrate reductase enzymes

The prokaryotic cytoplasmic assimilatory nitrate reductases (Nas) are the least well characterized of the nitrate reductases,

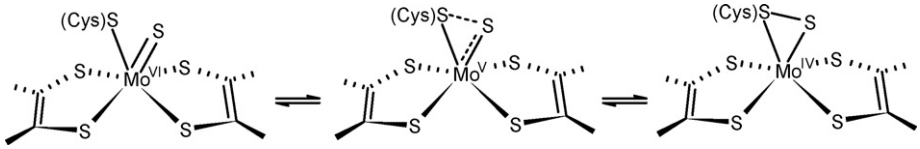

Fig. 15. Postulated active site structures for the Nap nitrate reductases according to Najmudin et al. [85].

in particular in regard to the structure and properties of the Mo active site. Recently Jepson et al. [93] carried out the first structural characterization a prokaryote Nas, named NarB (not to be confused with the membrane-associated respiratory nitrate reductases, Nar), from the cyanobacterium *Synechococcus* sp. PCC 7942. Mo^V EPR reveals that this enzyme is more closely related to the Nap group of enzymes than it is to Nar [93], but that NarB is fine-tuned to operate at the lower potentials accessible in the cytoplasm compared to the periplasmic Nap enzymes. Mo^V EPR of NarB reveals similarities with the Very high-*g* signal from *Paracoccus pantotrophus* Nap and the High-*g* signal from *A. vinelandii* Nas [89–91]. The coordinating Cys residue from the Nap enzymes is also conserved in the bacterial Nas enzymes [93]. The similarities in the Mo^V EPR spectra of NarB and Nap combined with the conservation of the aforementioned Cys residue is strong evidence for the importance of Cys coordination to Mo in bacterial Nas enzymes. Aside from the presence of *bis*-molybdopterin-dithiolene and cysteinate coordination of Mo in Nas, clearer structural and mechanistic insight awaits further investigation of this under-represented class of enzymes.

3.3. Formate dehydrogenases

E. coli contains two related but differently expressed formate dehydrogenases (FDHs). One is the anaerobic respiratory FDH (Fdh-N) and is expressed in cells using nitrate or other electron acceptors. The other fermentative FDH (Fdh-O) is linked to hydrogenase, being part of a formate hydrogen-lyase complex, and is expressed in the absence of alternative electron acceptors. Much work has been done on FDH_H, the catalytic component of fermentative Fdh-O. Formate dehydrogenases catalyze the conversion of formate to carbon dioxide or carbonate:

$$HC(O)O^- \rightarrow CO_2 + H^+ + 2e^-$$

E. coli FDH_H has long been known to include a selenocysteine moiety [94,95]. The Mo^V EPR signal shows clear hyperfine coupling to the $I = 1/2$ ^{77}Se on enrichment [96]. *E. coli* FDH_H has been characterized by crystallography which indicated an active site with two dithiolene cofactors, plus a ligand to molybdenum from selenocysteine [11]. This study was followed by an EXAFS study [14] at both the Mo and Se K-edges which, although in substantial agreement with the crystallography, indicated four or five Mo–S at 2.36 Å, plus one Mo–Se at 2.62 Å. In contrast to the crystallographic analysis, the EXAFS indicated the presence of an additional Se–S coordination from the Se K-edge data, with a bond-length of 2.19 Å. A Se–Mo at 2.62 Å and Se–C at 1.99 Å were also observed [14]. Interestingly, the active site had no Mo=O ligands [11,14], and both EXAFS and crystallographic analysis suggested that the active site might possibly contain an additional long Mo–O bond [11,14], constituting a novel coordination – a *des*-oxo Mo^{VI}, coordinated with a selenylsulfide. A very similar active site coordination was suggested from crystallography of the respiratory *E. coli* enzyme [97]. On mutation of the coordinating SeCys140 to Cys the active site adopted a mono-oxo Mo^{VI} coordination [14]. A very similar selenium coordination was observed by EXAFS for *D. gigas* formate dehydrogenase [98], although this enzyme additionally possessed Mo=O ligation in the fully oxidized form. The nature of the Se–S coordination was initially something of a conundrum, and the sulfur was initially suggested to be one of the cofactor ditholene sulfurs (Fig. 16). Later crystallographic studies of the *D. gigas* tungsten containing formate dehydrogenase (considered below) [99] suggested an additional sulfur coordination to Mo from sulfide. Moreover, subsequent re-evaluation of the original *E. coli* FDH_H crystallography suggested that the original analysis had been partly in error, with a loop in the active site having been miss-traced [100] and this study concluded that the Se ligand from selenocysteine was dissociated from Mo in the formate-reduced enzyme, and is displaced by some 12 Å. This conclusion is not consistent with the Mo^V EPR of formate-reduced enzyme, which shows a remarkably large and anisotropic ^{77}Se hyperfine interaction [96] (Fig. 17) almost five times larger than low-molecular weight Mo^V compounds with Se coordination [101]. We note that the presence of well-resolved $^{95,97}Mo$ hyperfine structure with coupling approximately in the normal range [96] excludes the possibility that the EPR signal arises from a selenium-centred free radical. Thus, Khangulov et al. estimate a spin density on Se that could be as large as 0.27 electrons and integration of the Mo^V EPR signal indicated that a significant fraction of the Mo was present as Mo^V [96]. Thus, either the crystallography is again somehow in error, or the Mo^V EPR bears no relation to the species crystallographically characterized. As pointed out by George et al. [98] the presence of Se–S coordination constitutes an extra redox capability of the Mo site – with both the Mo and the Se–S capable of being reduced by two electrons, although whether or not

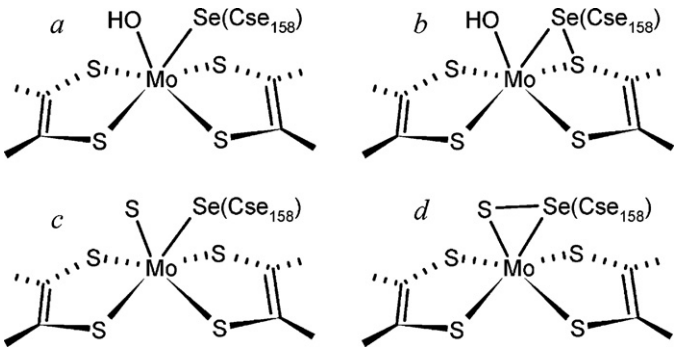

Fig. 16. Active site structures postulated for oxidized *E. coli* FDH_H. (a) The active site originally suggested from X-ray crystallography [11], (b) that from EXAFS spectroscopy [14], and (c) and (d) from further crystallographic analysis [99,100].

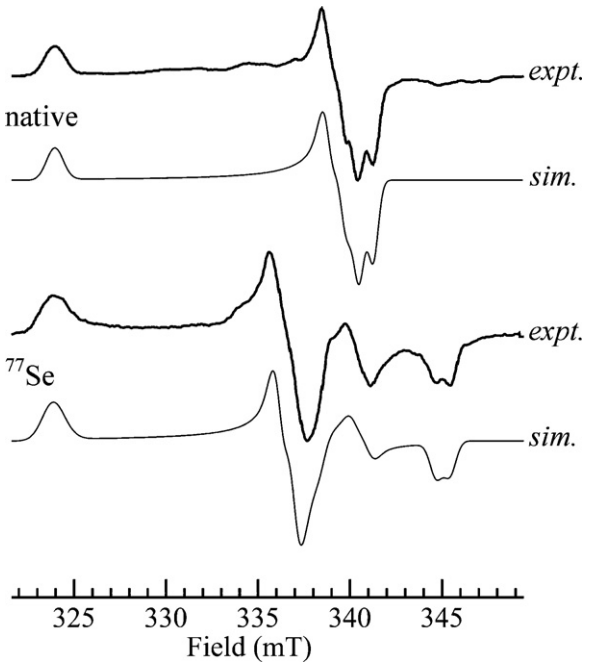

Fig. 17. *E. coli* formate dehydrogenase Mo^{V} EPR signals. Experimental spectra are redrawn from Ref. [96] and simulations were calculated using the spin Hamiltonian parameters given by Khangulov et al. [96], and show the remarkably large $A(^{77}Se)_{xyz}$ of ~13, 75 and 240 MHz.

this is important in the context of catalysis remains unclear. The Se–S distance observed by EXAFS at 2.19 Å is much shorter than the crystallographically determined distance in the tungsten FDH of about 3.3 Å [99], and it seems likely that photoreduction may have occurred in the X-ray crystallographic experiments, especially as the Se–S EXAFS interaction is a very intense and well determined structural parameter. At the time of writing, doubts remain as to whether formate reduction actually causes large changes to the active site, or whether the X-ray crystallography suffered from artifacts due to photoreduction, and the catalytic mechanisms that have been suggested also seem less than certain [102]. Irrespective of the exact catalytic mechanism, the lack of oxygen at the active site is supported by experiments using ^{13}C-labeled formate in ^{18}O-enriched water which produced $^{13}CO_2$ containing no ^{18}O-label [96]. The same study also used $^{2}HCO_2^-$ to show that the coupled proton in the Mo^{V} EPR signal derives from formate [96]. This work conclusively established that FDH is perhaps unique among the molybdenum enzymes in not catalyzing the incorporation of oxygen from water into product [96]. Many open questions remain about this intriguing group of molybdenum and tungsten enzymes, and it seems clear that more experimental work is required to provide the answers.

3.4. Arsenite oxidase

The soil pseudomonad *Alcaligenes faecalis* produces an arsenite-inducible periplasmic enzyme that catalyzes the two-electron oxidation of arsenite to arsenate utilizing either azurin or a *c*-type cytochrome as an electron acceptor:

$$As(OH)_3 + H_2O \rightarrow As(OH)_2O_2^- + 3H^+ + 2e^-$$

Arsenite oxidase is a member of the DMSO-reductase class of molybdenum enzymes, and its crystal structure has been reported [13]. It is unusual in that it contains no amino acid ligand to Mo. The enzyme is also unusual in that it gives no Mo^{V} EPR signals, but has been studied by a combination of XAS and

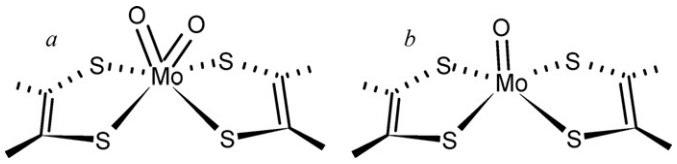

Fig. 18. Proposed structure of the *Alcaligenes faecalis* arsenite oxidase active site in the oxidized Mo^{VI} form (a) and in the arsenite-reduced Mo^{IV} form (b) [103,104].

resonance Raman spectroscopy [103]. The Mo K-edge EXAFS indicated four Mo–S interactions at 2.47 and 2.37 Å for oxidized and arsenite-reduced enzyme, respectively [103], confirming the *bis*-dithiolene coordination observed crystallographically [13]. The data for arsenite-reduced enzyme indicated a single Mo=O ligand at 1.70 Å, also consistent with the crystallography [13]. Interestingly, the Mo K-edge EXAFS site indicated could be interpreted as a $[MoO_2]^{2+}$ site with a bond-length of 1.78 Å, which is a chemically unlikely bond-length [68], or an asymmetric coordination with one Mo=O at 1.70 Å, plus one short Mo–O at 1.83 Å [103]. The observation of two oxygen ligands to the oxidized active site suggests that the crystallographic sample [13] may have been photo-reduced. This suggestion of a novel asymmetric oxygen coordination was consistent with the resonance Raman [103] which did not indicate a symmetric Mo^{VI} *cis*-dioxo site. The longer Mo–O could be formulated as either Mo–OH or as an unusually although not implausibly long Mo=O [103]. Electrochemical studies suggested that the oxidized active site is best characterized as a $[MoO_2]^{2+}$ site rather than $[MoO(OH)]^{3+}$ [104] (Fig. 18). Taken together, these results suggest that the long Mo=O is the atom transferred to arsenite and that the second shorter Mo=O acts as facilitator via the "spectator oxo" effect [105,106].

3.5. Tungsten enzymes

We have noted above that tungsten is the only third transition ion with a biological function. It is also the heaviest element known to have a function in biology, the second heaviest being cadmium [107]. Tungsten-containing enzymes are found only in prokaryotes, and particularly in hyperthermophilic archaea, methanogens, and acetogens. The hyperthermophilic archaea are obligately tungsten-dependent and cannot produce molybdenum-containing homologs of key tungstoenzymes. The first tungsten enzyme to be described was a formate dehydrogenase from *Clostridium thermoaceticum* [108], and this remained the only example and thus something of an anomaly for a number of years until work on hyperthermophilic archaea in the 1990s revealed that tungsten played a major role in these organisms. Probably the best-studied of these organisms is *P. furiosus*, a hyperthermophilic organism that grows optimally at around 100 °C, which contains five different tungsten enzymes [109], several of which have been extensively characterized. The best-studied of these is the aldehyde oxidoreductase (AOR). Early work observed an EPR signal characteristic of an $S = 3/2$ system reminiscent of that of the MoFe cluster nitrogenase, and so the enzyme was speculated to contain a similar cluster. In the absence of a known function it was called "red tungsten protein" [110]. Following the discovery of the enzyme function [110], early XAS showed that the enzyme should be categorized alongside the molybdenum enzymes [111], and indicated a mixed W=O and W–S coordination, with two W=O at 1.74 Å, approximately three W–S ligands at 2.41 Å, and possibly a W–O ligand at 2.1 Å. Subsequent crystallography, at the time the first of any Mo or W enzyme, indicated two molybdopterins coordinated to the metal [33]. Koehler et al. [112] have demonstrated that preparations of AOR from both *P. furiosus* and *Pyrococcus* strain ES-4, contain at least two forms of the tungsten active site. One form cycles between W^{IV} and W^{VI}

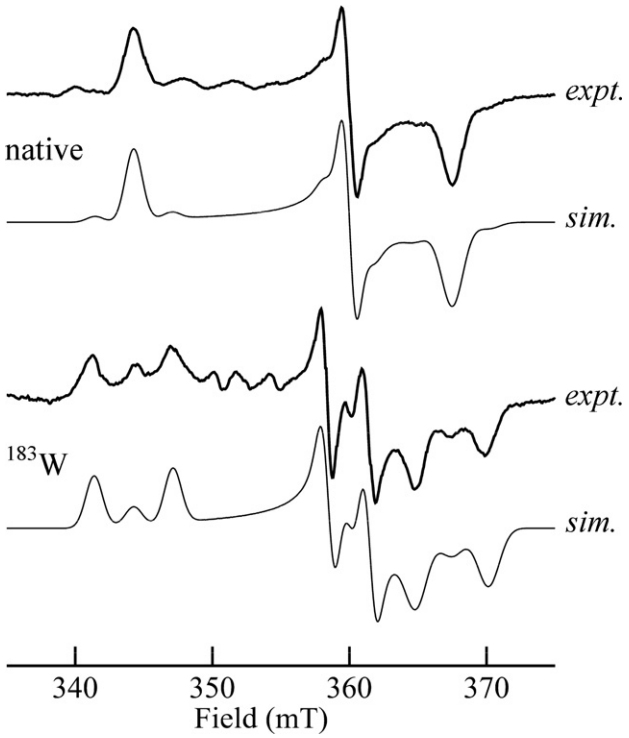

Fig. 19. Pf AOR EPR low-potential W^V EPR signals. Experimental spectra are redrawn from Ref. [112], and simulations using previously reported spin Hamiltonian parameters [112]; g_{xyz} = 1.863, 1.902, 1.989, and $A(^{183}W)_{xyz}$ = 138, 81, 160 MHz and employing the isotopic enrichments reported by these workers [112].

under physiological conditions via a low-potential W^V intermediate which has g_{xyz} = 1.863, 1.901, 1.989 (Fig. 19), while the other form appears to only cycle between the W^V and W^{VI} states, where the W^V EPR signal is only observed at high potentials. Koehler et al. [112] also indicate that the low-potential form is most likely associated with active enzyme, used variable temperature magnetic circular dichroism spectroscopy to show that both the low- and high-potential forms of AOR are probably bound through two dithiolenes [112]. A third additional minor "mid-potential" W^V EPR signal was observed between −345 mV to ∼100 mV, with significantly higher *g*-values (g_{xyz} = 1.940, 1.961, 1.988) although the origin of this species is unclear as it corresponded to less that 3% of the W present. In light of the evidence for mixed forms of the enzymes the crystallographic and XAS data are also likely derived from mixed active site forms. The EXAFS Fourier transforms of oxidized and reduced *P. furiosus* AOR are shown in Fig. 20. The data are consistent with the crystal structure indicating four Mo–S ligands, plus two or more oxygen donors. Similar tungsten coordination has been observed by crystallography of *P. furiosus* formaldehyde ferredoxin oxidoreductase (FOR) [113] and similar active sites seem likely for related enzymes such as glyceraldehyde-3-phosphate ferredoxin oxidoreductase [114], for which W^V EPR similar to that of AOR has been reported [115].

Other tungsten-containing enzymes include the tungsten-containing formate dehydrogenases, which are considered above together with the molybdenum-containing enzymes. Acetylene hydratase (AH) from the anaerobic bacterium *Pleobacter acetylenicus* [9] catalyzes a net hydration reaction with no apparent redox role:

$$HC{\equiv}CH + H_2O \rightarrow CH_3C(O)H$$

Protein crystallography shows that AH is structurally similar to other W-enzymes [10], although unlike other W-enzymes AH is not inactivated by air oxidation. In part because of its non-redox role, no spectroscopic studies have been reported to date for this novel enzyme. Finally, it has recently been reported that the archaeon *Pyrobaculum aerophilium* produces a tungsten-containing nitrate reductase that is functionally related to the Nar proteins [116] and this enzyme has W^V EPR that seems related to that of Mo^V nitrate reductase.

Given that the hyperthermophilic archaea are the most primitive organisms known, it seems plausible that tungsten enzymes

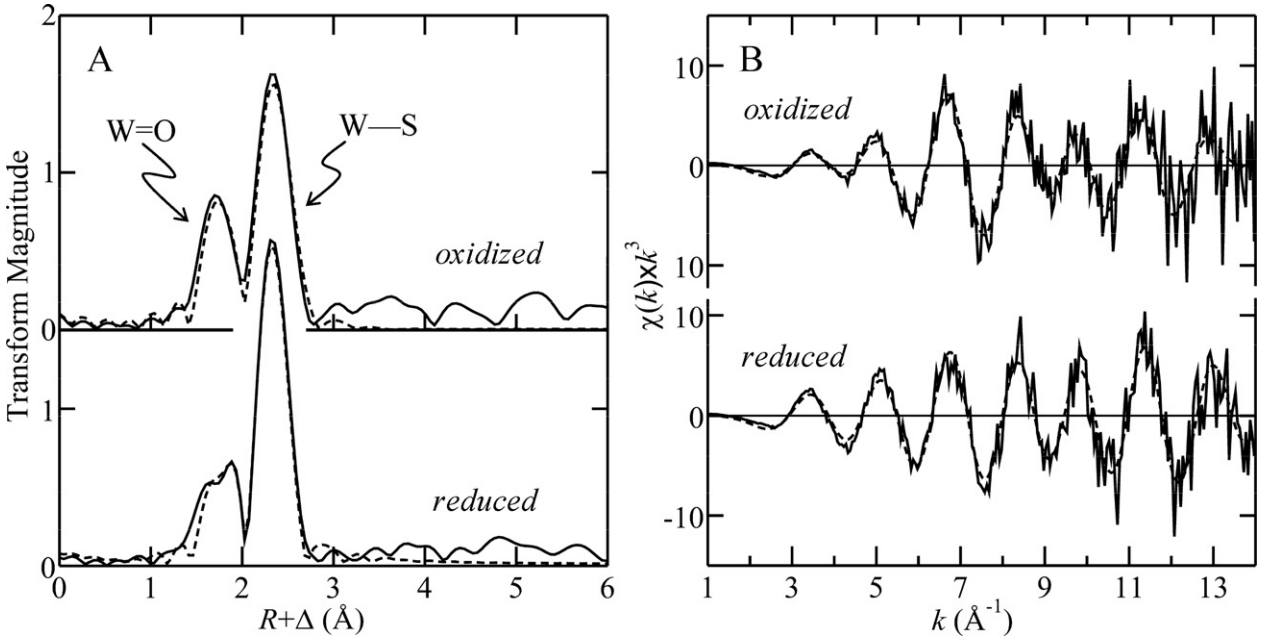

Fig. 20. W L_{III} EXAFS Fourier transforms of *Pyrococcus furiosus* AOR, phase-corrected for W–S backscattering (a) together with the EXAFS data (b). In both (a) and (b) solid lines show the experimental data and broken lines the best fits. Oxidized enzyme was fitted with ∼1.6 W=O at 1.75 Å, ∼3.4 W–S at 2.40 Å, and ∼0.6 W–O at 2.06 Å. The fractional coordination numbers strongly suggest that a mixture of species is present. Reduced enzyme appears more homogenous and is fitted by 1 W–O at 1.75 Å, 4 W–S at 2.39 Å, and 1 W–O at 1.97 Å.

might have been the evolutionary predecessors of the molybdenum enzymes. Their study may thus shed light on the chemical origins of the molybdenum enzymes, in addition to being of interest in their own right.

4. The sulfite oxidase family of molybdenum enzymes

The sulfite oxidase (SO) family comprises possibly the smallest of the three, but these enzymes are none the less interesting. They have been identified in mammals [117], insects [25], plants [23,24] and in a variety of prokaryotic microorganisms [22]. In animals the enzyme functions as the final step in the catabolism of sulfur-containing amino acids. In plants, sulfite oxidase is localized in the peroxisome, and functions in either sulfite detoxification or regulating the sulfate pool [118]. Sulfite oxidases are thus widespread in nature, and to date, all reported enzymes of this type contain what appears to be a closely related molybdenum at their active site. Also important are the nitrate reductases, these play essential roles in the global nitrogen cycle. The prokaryotic nitrate reductases have already been discussed above. Eukaryotic nitrate reductases are found in green photosynthetic plants, and are essential to these organisms. We will first consider sulfite oxidase, and then green plant nitrate reductases.

4.1. Sulfite oxidase

The prototypical members of the family are the animal sulfite oxidases, of which the best studied is the chicken enzyme, with human SO a close second. For this reason this review will focus primarily on these sulfite oxidases, and will not discuss the others in detail. The enzyme is responsible for the physiologically vital oxidation of sulfite to sulfate, residing in the mitochondrial inter-membrane space, it is dimeric with a subunit mass of about 52,000. Each monomer contains molybdenum associated with a single molybdopterin, and a cytochrome b_5 type heme. The two-electron oxidation of sulfite to sulfate occurs at the molybdenum site, which is reduced from Mo^{VI} to Mo^{IV} in the process. The catalytic cycle is completed with re-oxidation of the molybdenum first to Mo^{V}, and then to Mo^{VI}, by intramolecular electron transfer to the cytochrome b_5 site, with cytochrome *c* serving as the external electron acceptor [119]:

$$\text{Enzyme-Mo}^{VI} + {SO_3}^{2-} + H_2O \rightarrow \text{Enzyme-Mo}^{IV} + {SO_4}^{2-} + 2H^+$$

Protein crystallography of chicken SO showed a five coordinate molybdenum site, with an arginine-rich substrate binding pocket some 5 Å from molybdenum that contained a sulfate in the crystal [21]. Eukaryotic nitrate reductases are closely related to SO, and the crystal structure of the yeast enzyme showed a very similar active site to that of SO, but with one less arginine in the nearby basic pocket [26]. Since the first SO crystal structure study [21] a number of additional structures have been reported (discussed below), and all but one indicated a photo-reduced Mo site [63].

A number of mutations of human SO are known that have very serious pathological consequences [120]. When enzyme activity is affected the result is impaired central nervous system development, mental retardation and other severe symptoms including increased mortality [121]. A sulfite oxidase mutation was recently implicated in a Nevada Leukemia cluster [122]. This mutation, G628A, is in the un-translated 5'-region of the gene, which may somehow lead to decreased sulfite oxidase expression. The occurrence of leukemia is also linked to the environmental presence of tungsten [122], and we can conjecture that the mutation decreases gene expression, which combined with molybdenum antagonism by tungsten significantly lower sulfite oxidase levels. Further work is clearly needed to establish the mechanism.

Early work using XAS, showed sulfite oxidase to possess a dioxo Mo^{VI} active site [123], and this was confirmed by subsequent high-resolution EXAFS [59]. Crystallography showed two sulfur ligands from molybdopterin, one sulfur ligand from Cys185 (equivalent to Cys207 in the human enzyme), a single Mo=O and an additional long Mo–O in an approximate square-based pyramidal geometry. This differed with the spectroscopic conclusions only in the nature of the second Mo–O, and this fact led to the conclusion, formed in the crystal structure paper, that the active site was photo-reduced [21]. Resonance Raman studies of the human sulfite oxidase molybdenum domain, with the heme domain proteolytically removed to prevent interference by the cytochrome *b* moiety, confirmed the presence of *cis*-dioxo site in wild-type enzyme [124]. Plant sulfite oxidase lacks the heme domain that is present in the otherwise homologous animal enzymes. CW EPR studies of the *Arabidopsis thaliana* sulfite oxidase showed similar Mo^{V} EPR properties to the animal enzymes, and resonance Raman spectroscopic studies again confirmed a *cis*-dioxo active site [125]. As expected from the reported geometry of the active site the two Mo=O ligands were slightly inequivalent [125]. Sulfite oxidase is by far the best studied member of this family and the other members are probably very similar. We will therefore confine our discussion predominantly to the sulfite oxidases.

4.1.1. The active site structures of wild-type sulfite oxidase

Wild-type SO gives Mo^{V} EPR signals that can be divided into three different categories (Fig. 21). The High-pH signal occurs at low anion concentrations and at high pH values, while the Low-pH signal occurs at low-pH and at high chloride concentrations [126]. The third category of signals are those from oxy-anion complexes, which tend to form at low pH and high oxy-anion concentrations. Sulfite oxidase Mo^{V} EPR signals arising from anion complexes have been described for wild-type enzyme with phosphate [127–129], arsenate [130], and sulfite or sulfate [131–133]. Analysis of the ^{31}P hyperfine interaction of the phosphate signal [128,129], and structural analysis of the arsenate signal using EXAFS, together with observation of ^{75}As hyperfine in the Mo^{V} EPR [130], indicates that

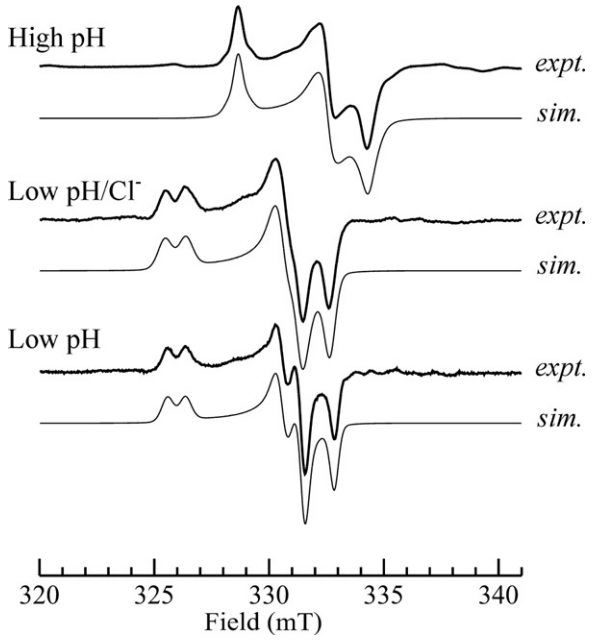

Fig. 21. Sulfite oxidase EPR signals. The Low-pH signal is developed by adding with stoichiometric sulfite, either in the presence of Cl^- or in the rigorous absence of chloride. Simulations were computed using spin Hamiltonian values taken from the literature [134,139].

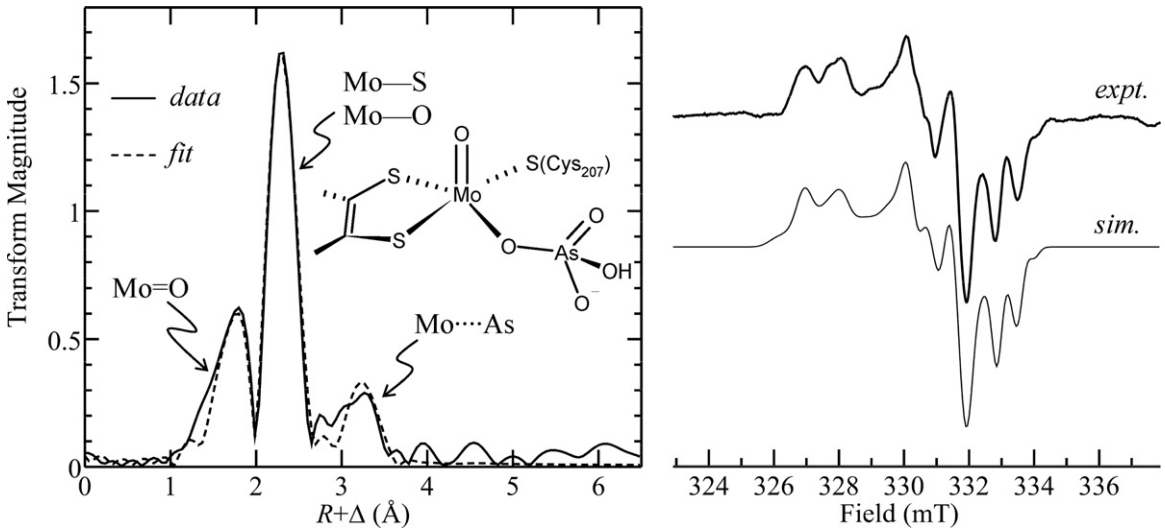

Fig. 22. Sulfite oxidase arsenate complex EXAFS Fourier transforms and Mo^{V} EPR. The EXAFS analysis indicated 3 Mo–S at 2.36 Å, 1 Mo=O at 1.70 Å, 1 Mo–O at 2.26 Å, and ~1 Mo···As at 3.20 Å. The EPR simulation was computed using the reported spin Hamiltonian parameters [130].

in both cases the anion is coordinated to molybdenum via one of its oxygen ligands (Fig. 22).

Both the Low-pH and High-pH Mo^{V} EPR signals have a solvent-exchangeable strongly coupled proton thought to originate from Mo–OH coordination, but a well-resolved splitting is only seen for the Low-pH CW EPR signal. The splitting is not directly observed in CW EPR of the High-pH signal, but its presence is betrayed by formally forbidden $\Delta M_I = \pm 1$ satellites separated by the proton frequency (the so-called proton spin-flip lines) [134]. The coupling to the exchangeable proton was subsequently directly observed using ESEEM spectroscopy [135,136]. Two different explanations have been suggested for the lack of observed proton hyperfine splitting in the High-pH signal; both assume a proton coordinated as Mo–OH with a small isotropic coupling and postulate different explanations as to why the anisotropic splitting is not directly observed in the CW EPR spectrum. The first hypothesizes that the anisotropic proton hyperfine tensor and the *g*-tensor are coincidentally oriented close to the so-called tri-magic angle. This results in close to zero hyperfine splitting at each of the principal *g*-values (g_x, g_y and g_z), although the $\Delta M_I = \pm 1$ satellites will have maximal intensity, and thus readily observed [134]. Computer simulations showed that this suggestion could account for the powder lineshapes of the High-pH CW EPR signals of sulfite oxidase [134] and sulfite dehydrogenase [137]. The second suggestion followed confirmation of the presence of proton hyperfine by pulsed EPR spectroscopy [135,136], and hypothesized that multiple static conformations with rotations about the Mo–O bond caused averaging of the CW EPR splitting yielding a featureless broadening of the spectrum [135,136]. At the time of writing both of these two explanations seem plausible, and which more accurately explains the lack of proton splitting in the SO High-pH CW EPR signal remains unclear.

Aspects of structure giving rise to the Low-pH signal have also been controversial. The broad line-widths of the Low-pH chloride signal have previously been speculated to be due to unresolved hyperfine interaction with $I = 3/2$ ^{35}Cl and ^{37}Cl nuclei [126], and early EXAFS data were rationalized as supporting Mo–Cl coordination (Fig. 23). However, Mo–Cl and Mo–S are essentially impossible to distinguish by EXAFS, and repeating these early experiments gave data of significantly better signal to noise that that did not support the original conclusions [138]. Doonan et al. reported that the Low-pH EPR signal was much sharper in the absence of chloride, and observed differential broadening of the Mo^{V} EPR signal at both X and S band microwave frequencies with ^{35}Cl and ^{37}Cl. These isotopes both have $I = 3/2$ but with only slightly different g_n values 0.548 and 0.456, respectively, giving rise to weak hyperfine interactions [139]. From the observed broadening Doonan et al. estimated ^{35}Cl and ^{37}Cl hyperfine coupling of the order of 4 MHz and concluded that the coupling is likely due to a Mo–Cl *trans* to the Mo=O group of the signal-giving species [139], and suggested that such a long Mo–Cl (expected to be ~2.65 Å) might easily be missed by EXAFS analysis [126]. Enemark and co-workers also detected chlorine using ESEEM spectroscopy [140] and the two groups initially concurred that chloride was likely to be coordinated to Mo, probably in a location *trans* to the single Mo=O group of the Low-pH form. Doonan et al. also reported that bromide and iodide gave related Mo^{V} EPR signals, but with large and resolved hyperfine structure due to the naturally abundant $I = 3/2$ ^{79}Br and ^{81}Br ($g_n = 1.404$ and 1.513, respectively) and to ^{127}I with $I = 5/2$ ($g_n = 1.872$) [139].

Subsequent studies by Enemark and co-workers again using ESEEM but with a more rigorous experimental and analytical

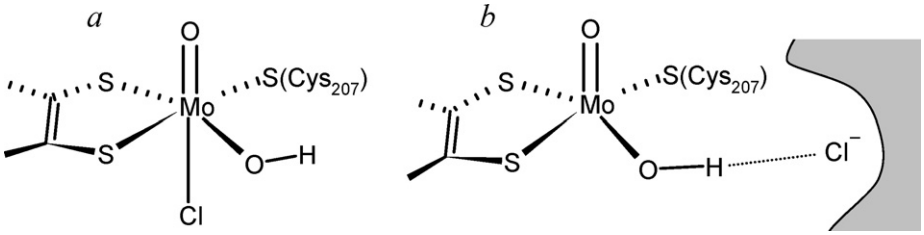

Fig. 23. Proposed structures for the low-pH/Cl^{-} Mo^{V} EPR signal. In (a) the chloride is attached to Mo in a position *trans* to the Mo=O group, in (b) the chloride is bound in the basic pocket and is hydrogen bonded to the hydrogen of the Mo–OH group.

approach, unambiguously detecting ^{35}Cl and ^{37}Cl coupling [141], and reported accurate values for both the hyperfine and quadrupole coupling for chloride. A nuclear quadrupole coupling with a value close to that expected for free chloride was obtained for the sulfite oxidase Low-pH/Cl^- signal [141]. This result would not be expected if Mo–Cl coordination was present as the proximity of Mo would give rise to a large electric field gradient at the Cl nucleus. Calculations using density functional theory (DFT) showed that the quadrupole coupling was very sensitive to structure whereas the hyperfine coupling was less sensitive to geometry [141]. Enemark and co-workers concluded that while the hyperfine coupling was within the range expected for coordinated chloride, the nuclear electric quadrupole coupling was not [141]. Thus, it now seems more likely that Cl^- is not a ligand to Mo in the low-pH species, and Enemark and co-workers propose that it is hydrogen bonded to the hydrogen of the equatorial Mo–OH group of the signal-giving species [141] (Fig. 23). Final confirmation of the nature of the signal-giving species must await EXAFS analysis of the Br^- and I^- Low-pH EPR signals – while chlorine is impossible to distinguish from sulfur by EXAFS, backscattering from heavy atoms such as bromine or iodine, if present, would be unambiguous.

We now turn to the Mo^V complex that has been called "blocked" by some workers [132,133], and referred to as a sulfite complex by others [131]. This species was first described by Bray et al. and can be generated by adding sulfite to chloride-free enzyme [131]. These workers also generated the same Mo^V EPR signal employing photoreduction with deazaflavin to first reduce oxidized enzyme, followed by anaerobic addition of sulfite to eliminate the possibility of sulfate complexes forming due to catalytic turnover [131]. These workers also unsuccessfully attempted to generate an analogous sulfate Mo^V EPR signal [131]. Bray et al. pointed out that the sulfite Mo^V EPR signal was similar to the phosphate complex [131], which we now know is one of a family of similar complexes in which the anion is coordinated via an oxygen ligand to Mo. Very similar EPR signals have been observed in *A. thaliana* SO [132] and in human SO [133]. Recently ^{33}S ESEEM has been observed using Mo^V EPR signals developed using ^{33}S-enriched sulfite [133] (Fig. 24) and this further strengthened the analogy to the phosphate and arsenate complexes. Apart from the early work of Bray et al. [131], which seemed to indicate a sulfite complex, there is little to indicate whether the signal-giving species is sulfate or sulfite. With arsenate a well-defined Mo^V EPR signal showing resolved ^{75}As hyperfine coupling ($I = 3/2$, $g_n = 0.9596$) and nuclear electric quadrupole coupling in the range expected for the nearly tetrahedral arsenate is observed [130]. If arsenite [$As(OH)_3$] is used in place of arsenate then a very similar Mo^V EPR signal to the arsenate signal is observed [142], which can be simulated with similar ^{75}As hyperfine coupling but requiring a significantly larger quadrupole coupling, consistent with the lower arsenic symmetry of arsenite [142]. Thus, if arsenite and arsenate both form viable anion complexes then it is also plausible that sulfate may bind.

We now turn to mutant sulfite oxidases. A large number of these have been characterized and we will focus primarily on those on which intensive spectroscopic work has been done.

4.1.2. The active site structure of Arg160 → Gln sulfite oxidase

Protein crystallography, EXAFS, EPR and ESEEM have also combined to clarify our understanding of an important SO clinical mutant. Arg160 → Gln (R160Q) is a lethal mutation that has been identified in a number of children worldwide. In this mutant a positively charged arginine residue that is located close to the Moco site is replaced by a neutral glutamine. This mutant SO, and the equivalent chicken R138Q mutant, have been studied by a number of techniques, including enzyme kinetics [21], crystallography [143], laser flash photolysis [144], EPR and XAS [145], and ESEEM [146]. The mutant has altered steady-state kinetic parameters [21],

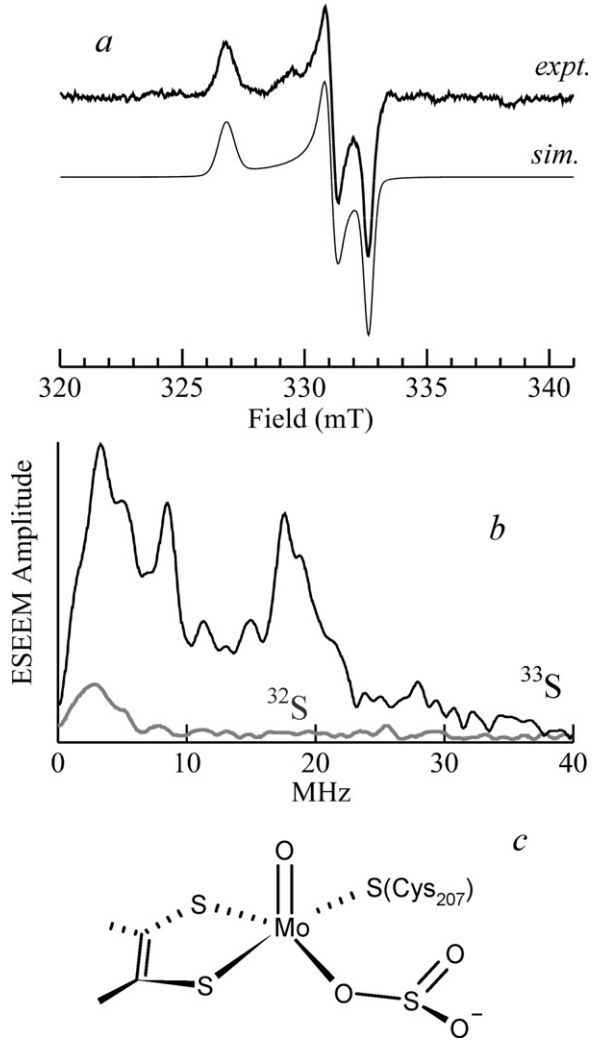

Fig. 24. Mo^V EPR (a) and ESEEM Fourier transform magnitude (b) of the human sulfite oxidase sulfite/sulfate complex. The ESEEM data in (b) are redrawn from Ref. [133] and clearly show structure due to ^{33}S hyperfine and quadrupole coupling when ^{33}S enriched sulfite is used to develop the Mo^V EPR signal. The structure of the complex is shown in (c). The postulated sulfate complex [132,133] would be very similar.

and shows remarkably decreased rates of intramolecular electron transfer [144]. The greatly increased K_m for sulfite that is displayed by this mutant has led to the proposal that Arg160 functions to stabilize binding of sulfite in the active site [21].

As we have stated above, all but one of the SO crystal structures reported to date have photo-reduced Mo sites (probably Mo^{IV}) due to the large X-ray dose required for crystallographic data acquisition [63]. Protein crystallography of wild-type chicken SO shows a five coordinate molybdenum site, with Arg138 forming part of the arginine-rich binding adjacent to Mo. Protein crystallography the molybdenum domain of R138Q chicken SO reveals modification of the 5 Å pocket with both R138 and R450 affected, with the latter being displaced from its wild-type position. The structure of the molybdenum site, which once again is photo-reduced [143], is five-coordinate and very similar to that of wild-type enzyme [21]. Both the Mo site electrochemistry and the Mo^V EPR following reduction of the enzyme with sulfite are highly altered relative to the wild-type enzyme, although the High-pH signal remains quite similar to that of wild-type enzyme [145]. Two different low-pH signals were observed, neither of which had resolved proton hyperfine [145]. As pointed out by Doonan et al. [145] when the Mo site crys-

tallographic data of wild-type and R138Q are overlaid all atoms can be superimposed to better than 0.5 Å, which is close to the positional error expected for small atoms close to a large atom (*i.e.* molybdenum) at the resolution of the crystal structures. The fact that the crystal structure indicated remarkably similar active sites seemed at odds with the large differences in enzyme properties. A combined EXAFS and DFT study, employing constraints from the crystal structure, indicated that the oxidized active site contained a six-coordinate Mo with near octahedral geometry, and the sixth ligand probably being provided by the Oε of Gln138. XAS of fully reduced human R160Q human SO showed a five coordinate site [145] very similar to that of wild-type enzyme [21] and fully consistent with the crystal structure of chicken R138Q SO [143]. This result explained most of the altered properties for the mutant enzyme mentioned above [143], with the only anomaly being the lack of proton hyperfine in the Low-pH Mo^{V} signal-giving species. Doonan et al. [145] deduced from DFT that the Mo^{V} site of the mutant enzyme was likely to be six-coordinate, and considered two alternatives for the structure of the signal-giving species. In one sulfate (or excess sulfite) was bound to Mo, occupying the site that would otherwise be occupied by Mo–OH, and in the other the Mo–OH geometry was such that the proton orientation was unfavorable to strong hyperfine and that this was hidden by the EPR linewidths [145]. Of these two Doonan et al. preferred the latter [145], however a subsequent ESEEM study using both ^{17}O and ^{33}S isotopic enrichment indicated that sulfate was in fact bound to Mo via a single oxygen in the signal-giving species [146]. Moreover, this study identified a weakly coupled nearby exchangeable proton in the active site, some 3 Å from Mo [146]. Whether or not the stability of the sulfate complex in R160Q SO contributes to the pathology is uncertain.

4.1.3. *The active site structure of Cys207 → Ser sulfite oxidase*

Another mutant SO that has attracted some attention is the Cys207 → Ser mutant. Biochemical studies of this mutant were the first indication that Cys207 provided a ligand to Mo in the human SO active site [147]. This work was subsequently extended by XAS which, consistent with the lack of a sulfur donor from Cys207, indicated two rather than three sulfur ligands [148]. An unexpected finding was that there was no long Mo–O expected from a putative Ser207 oxygen ligand in place of Cys207 [148], moreover the XAS indicated a third Mo=O ligand, and George et al. suggested a novel a novel tri-oxo Mo^{VI} active site for the mutant with no ligand to the Mo from any amino acid [148]. The enzyme was also reported to be highly resistant to reduction and because of this only Mo^{VI} data were available in the initial XAS study [148]. Resonance Raman of the molybdenum domain of the mutant enzyme proved inconclusive concerning the presence of a MoO_3 site [124]. Further studies of the mutant using a combination of redox titrations Mo EPR and XAS indicated that the active site is modified under reducing conditions to a mono-oxo Mo^{IV} species with Ser207 most likely ligated to Mo [149]. This Mo^{IV} species can be re-oxidized to a mono-oxo Mo^{V} species still coordinated to Ser207, which in turn be further re-oxidized to yield the initial tri-oxo Mo^{VI} structure with loss of Ser207 ligation [149]. This complex electrochemistry is illustrated in Fig. 25. One complication that was not mentioned in this paper was that density functional theory (DFT) could not reproduce the oxidized active site, nor could it reproduce the known structure of a low-molecular weight model [150]. Recently, the analogous chicken mutant C185S together with a new mutant C185A, were studied using a combination of protein crystallography, XAS and DFT [151]. The crystallography confirmed the presence of a novel [MoO_3] core deduced from previous XAS studies [148,149], moreover the DFT employed a novel diffuse basis set for Mo which overcame the previous difficulties and was in excellent agreement with both the crystal structure and the spectroscopy. The C185A mutant had a very similar active site structure. As we have noted above, human C207S SO and chicken C185S SO are very difficult to reduce, and these crystal structures are the only crystallographic reports to date of an oxidized SO [151].

The studies described above have contributed to our understanding of the Mo and the catalytic mechanism. The enzyme is thought to function as an oxo-transferase, as shown in Fig. 26. The presence of Mo–OH_2 in fully reduced Mo^{VI} enzyme and the fact

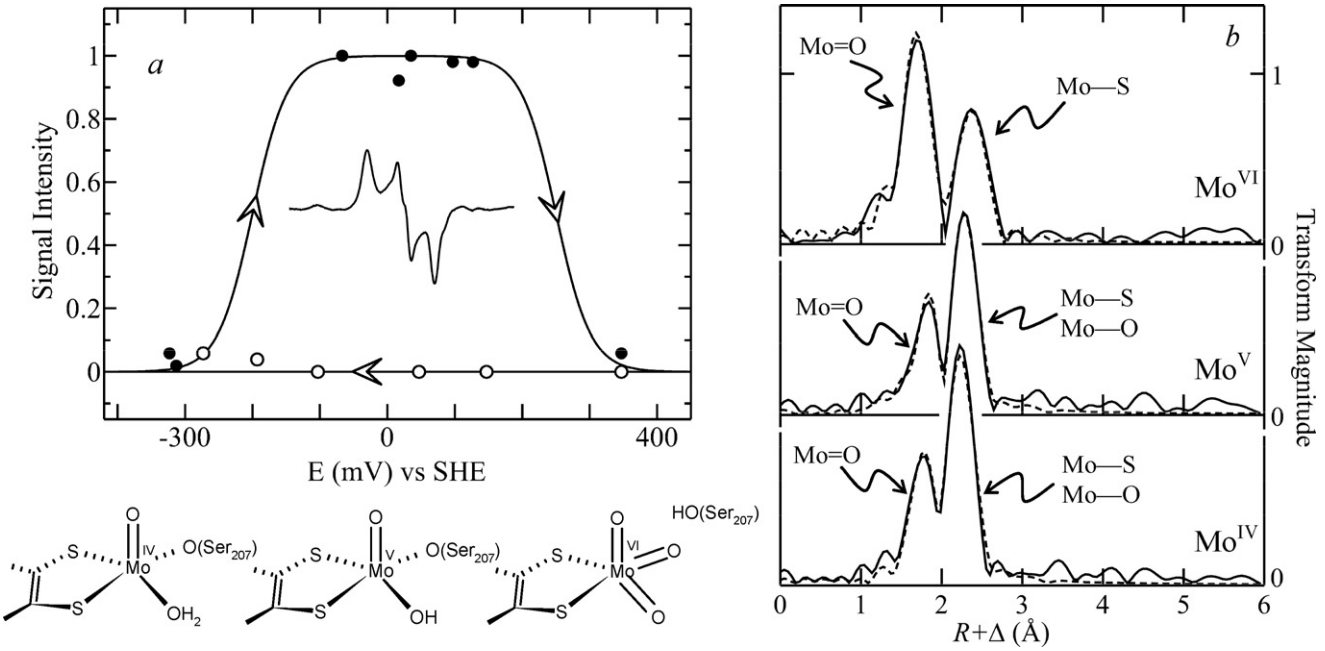

Fig. 25. Redox titration using both EXAFS and EPR of C207S human sulfite oxidase. The redox titration (a) gave Mo^{V} EPR signals only on following incubation at low potentials (<−300 mV) and subsequent oxidation. EXAFS Fourier transforms of samples redox poised at potentials corresponding to predominantly Mo^{IV}, Mo^{V} and Mo^{VI} oxidation states are shown in (b). The EXAFS curve fitting analysis indicated the following: Mo^{VI} 3 Mo=O at 1.75 Å, 2 Mo–S at 2.48 Å; Mo^{V} 1 Mo=O at 1.70 Å, 2 Mo–S at 2.37 Å, 1 Mo–O at 1.96 Å; Mo^{IV} 1 Mo=O at 1.70 Å, 2 Mo–S at 2.34 Å, and 1 Mo–O at 2.18 Å. The structures are indicated in the lower panel. Data are redrawn from Ref. [149].

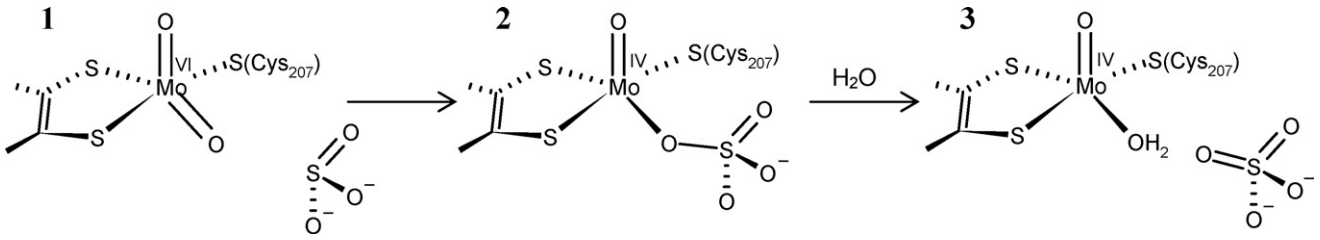

Fig. 26. Schematic of sulfite oxidase catalytic mechanism. Reaction of oxidized enzyme **1** with sulfite bound in the basic arginine-rich pocket forms an anion complex **2** from which addition of water liberates product sulfate. It has been suggested that the anion complex **2** forms the Mo^{V} species known as blocked, previously called the sulfite complex, via intramolecular electron transfer. Species 3 will loose an electron and a proton from the Mo–OH_2 via intramolecular electron transfer to form the Mo–OH of the High-pH and Low-pH signal giving species, and these in turn will loose a proton and an electron to form oxidized enzyme **1**.

that the oxidized active site is a $[MoO_2]^{2+}$ *cis*-dioxo species were both established by XAS. Despite the advanced state of our knowledge of this metabolically essential enzyme, questions concerning the nature of the sulfite oxidase active site still remain. In particular the exact structural natures of the Low-pH and High-pH EPR signal-giving species, discussed above, moreover the residue whose pK_a influences the transition between the high-pH and low-pH EPR signals remains unclear.

4.2. The active site of eukaryotic nitrate reductases

As noted above, nitrate reductase (NR) of green plants is essential for their nitrogen metabolism. Given its importance to both agriculture and in the global nitrogen cycle, it is perhaps surprising that has not been studied particularly intensively. The crystal structure of the nitrate reductase from the yeast *Pichia angusta* has been reported [26]. An active site that is very closely related to SO was observed, and indicated a similar arginine-rich anion binding pocket adjacent to Mo, but with one less arginine [26], consistent with the differing charges of the substrates $[NO_3]^-$ and $[SO_3]^{2-}$. Gutteridge et al. have investigated the Mo^{V} EPR properties of spinach (*Spinacia oleracea*) NR [152] and Barber and co-workers of *Chlorella vulgaris* NR [153]. Both enzymes show very similar spectra, specifically two different Mo^{V} EPR signals, called signal A (Fig. 27) and signal B. Signal A has one strongly coupled solvent-exchangeable proton, while signal B has two nearly equivalent exchangeable protons coupled to Mo. The XAS of *C. vulgaris* NR has been reported by Cramer et al. [154], who found that the active site strongly resembled that of sulfite oxidase. More recently the XAS of *A. thaliana* NR has been reported by George et al. [155], who found that there were intriguing differences in the oxidized Mo site induced by catalytic turnover (Fig. 27), with one long Mo–S bond prior to turnover which shortens to the same length as the other Mo–S bonds after turnover. Exactly how these results relate to catalytic mechanism is at present unclear [155].

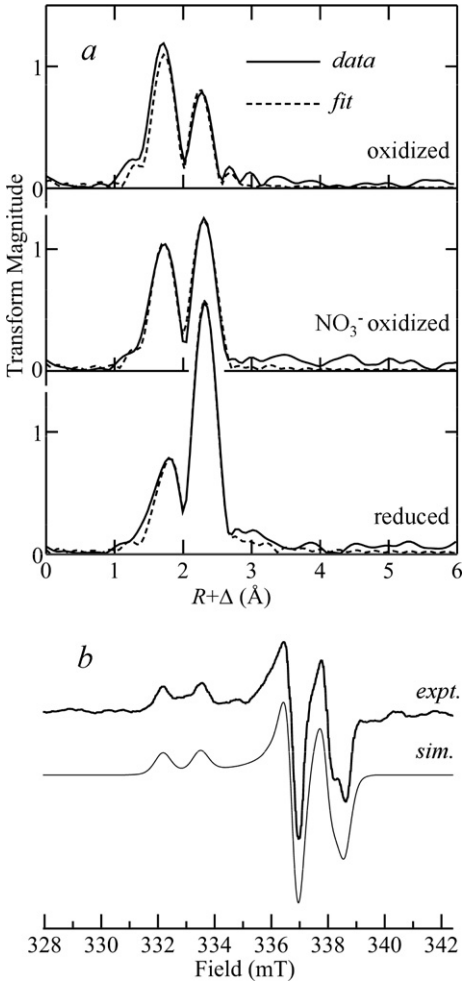

Fig. 27. Plant nitrate reductase EXAFS Fourier transforms (a) and Mo^{V} EPR (b). The EXAFS analysis indicated 2 Mo=O at 1.73 Å, 2 Mo–S at 2.40 Å, 1 Mo–S at 2.57 Å for oxidized, 2 Mo=O at 1.71 Å, 3 Mo–S at 2.40 Å for NO_3^--oxidized, and 1 Mo=O at 1.71 Å, 3 Mo–S at 2.40 Å, 1 Mo–O at 2.18 Å for reduced enzyme. The data of (a) are replotted from Ref. [155]. The EPR spectrum shown in (b) is signal A redrawn from Ref. [153] and aligned to a microwave frequency of 9.3 GHz. The simulation was calculated with g_{xyz} = ,1.967, 1.969, 1.996 and A_{xyz} = 48, 37, 39 MHz.

5. The xanthine oxidase family of molybdenum enzymes

5.1. Animal xanthine oxidases, aldehyde oxidases, and related enzymes

With some notable exceptions (discussed below) the xanthine oxidase family enzymes catalyze oxidations of organic compounds in which a C–OH bond is formed:

$$RH + H_2O \rightarrow ROH + 2H^+ + 2e^-$$

Substrates include a wide range of aldehydes, purines, alcohols and other organic compounds. The family includes the xanthine oxidases and dehydrogenases as prototypical members. The difference between xanthine oxidase and dehydrogenase is at the flavin site. Xanthine dehydrogenase can be converted to the oxidase either by proteolysis or by the formation of a disulfide [27], and the Mo sites have no significant differences. From the Mo^{V} EPR viewpoint, xanthine oxidase is easier to study as the intensity of the FAD semiquinone of the dehydrogenase is much larger and tends to partly obscure the Mo^{V} EPR spectra.

Bovine xanthine oxidase is by far the best studied member of this family, and we will therefore discuss it here at some length. The enzyme has broad substrate specificity, acting on purines, primidines, as well as various aldehydes. Purine is thought to be the physiological substrate, which is sequentially oxidized as shown in

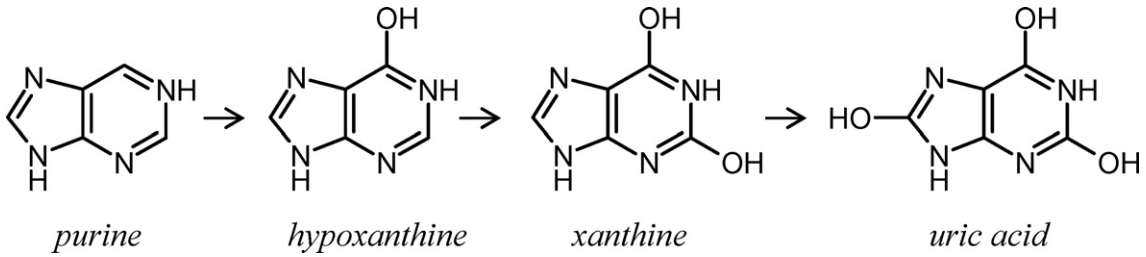

Fig. 28. Sequential oxidation of purine to uric acid by xanthine oxidase. Only the lactim tautomer of the each purine molecule is shown.

Fig. 28. Much of the research on xanthine oxidase has focused on the so-called cyanolysable sulfur. Treatment of the enzyme with cyanide results in a two-electron reduction and generation of thiocyanate, and formation of the inactive desulfo form:

$$XO(S) + CN^- + H_2O \rightarrow XO(O) + 2e^- + 2H^+SCN^-$$

The nature of the cyanolysable sulfur is a terminal sulfide group, Mo=S, in the oxidized enzyme, which is replaced by Mo=O in the inactive desulfo enzyme. Different members of the xanthine oxidase family show differing susceptibility to cyanide. For example, purine hydroxylase II from *Aspergillus nidulans* is highly resistant to cyanide, with extensive treatments being required to inactivate the enzyme [156] and develop the Slow Mo^V EPR signal [157]. Conversely, the cyanolysable sulfur of rabbit aldehyde oxidase [31] is rather more susceptible to cyanide than xanthine oxidase. Early EPR suggested [39,158,159] and subsequent EXAFS spectroscopy [160] showed that the cyanolysable sulfur was a terminal sulfide Mo=S group that was converted to Mo=O in the inactive desulfo enzyme.

Xanthine oxidase was first crystallized by Bray and co-workers in the 1950s [161] but solution of the structure remained elusive for nearly four decades. The first structure of a member of the xanthine oxidase family was that of the so-called MOP protein, an aldehyde oxidoreductase from *D. gigas* [34], and a number of structures of other family members followed, including xanthine oxidase itself.

Detailed structural information on the active site of xanthine oxidase is available from both protein crystallography and from spectroscopy. It is generally agreed that in the oxidized active enzyme the Mo atom is ligated by one short terminal sulfido unit (Mo=S), two long thiolate ligands (Mo–S) (from the cofactor dithiolene) plus one short terminal oxygen (Mo=O). Until recently, there were two major controversies about the active site structure. Firstly, the position of the Mo=S group in the molybdenum coordination sphere and secondly, the nature of the catalytically labile oxygen. With regard to the position of the Mo=S group, initial crystallographic studies of xanthine oxidase and related enzymes [34] placed this ligand in the apical position of a distorted square-pyramidal coordination geometry, with the Mo=O ligand occupying one of the equatorial positions (Fig. 29). In contrast, a detailed magnetic circular dichroism analysis of the Very Rapid Mo^V species from 2-oxo-6-methylpurine [162] clearly indicated that the Mo=O group must be apical to the ditholene ligand in at least this form of the enzyme. A high-resolution X-ray crystallographic study of the reduced Mo^{IV} enzyme complexed with a mechanism-based inhibitor also indicated a similar relative orientation of the Mo=O group, plus an equatorial Mo–SH [163], which is expected from protonation which will accompany reduction. This study clearly identified the Mo=O in the apical position, with the Mo–SH of the reduced enzyme (derived from the Mo=S) in the equatorial plane. Thus, either a large conformational change occurs on association with substrate, or the crystal structures of fully oxidized enzyme are incorrect in their assignment of the Mo=S ligation. Since this conformational change would include an inversion of symmetry at the molybdenum centre, it seems more likely that the initial assignments were incorrect. Alternatively, the enzyme preparations used for crystallography were initially predominantly in the desulfo form, and the sulfo form was regenerated using treatment with exogenous sulfide, sodium dithionite and methyl viologen [164], and it is possible that this may have sulfided a non-physiological site such as the apical oxo.

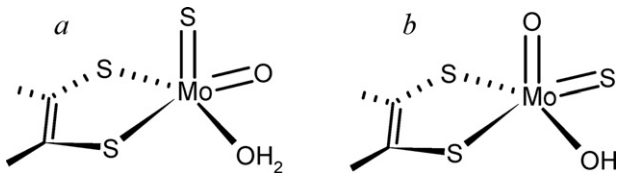

Fig. 29. Xanthine oxidase structures postulated from early crystallography (a) and from spectroscopy (b).

The nature of the catalytically labile oxygen that is transferred to the substrate during the catalytic cycle was until recently not completely clear. X-ray crystallographic analysis concluded that this is a Mo–OH_2 ligand (based upon the Mo–O distance of 2.2 Å) but determination of accurate distances for light atoms is difficult for crystallography [62] and mechanistic considerations favor a Mo–OH ligation instead, which would yield a much better nucleophile (Mo–O^-) upon base-assisted deprotonation. XAS studies showed that at high pH the enzyme has an active site with a [MoO_2(S)] core, and at low pH this becomes protonated to give a $[MoO(OH)(S)]^+$ core. Fig. 30 shows the EXAFS Fourier transforms of oxidized Mo^{VI} bovine xanthine oxidase at pH 6 and 10, together with the postulated structures of the different species [165].

Xanthine oxidase has a particularly rich Mo^V EPR spectroscopy, with different signals appearing during catalytic turnover of the enzyme and under various conditions. There are four major types of signal that are called Very Rapid, Rapid, Slow and Inhibited [166]. With many purine and pyrimidine substrates the so-called Very Rapid signal appears when the reactions are conducted at high pH shortly after mixing enzyme and substrate (*ca.* 10 ms with xanthine) [159] (Fig. 31), this is followed by the Rapid signal (*e.g.* [159]), which has hyperfine coupling from two exchangeable protons. Two types of Rapid signal are known – called type 1 and type 2 – with similar *g*-values but different proton hyperfine couplings. In the type 1 Rapid signal one proton coupling is much larger than the other, while in the type 2 signal they are more equivalent. Type 2 Rapid signals generally form in the presence of substrates or products such as xanthine [167,168], or anions such as borate [168]. The type 1 and type 2 Rapid signal-giving species probably have very similar structures. Our knowledge of the structure of the Rapid signal-giving species has benefited from the use of stable magnetic isotopes, specifically ^{17}O [169–171], ^{33}S [158,172], ^{95}Mo [39,172] and ^{97}Mo [39]. The analogous signal in prokaryotic xanthine oxidase family members has also been studied using Mo^V EPR and enrichment with stable magnetic isotopes [173]. The Slow signal is the last to develop in a time-based reduction of the enzyme [166], appearing at long times (*ca.* 20 min) with strong non-catalytic reduction agents (*e.g.* 1 mM sodium dithionite) (Fig. 31). It originates from the inactive desulfo form of the enzyme.

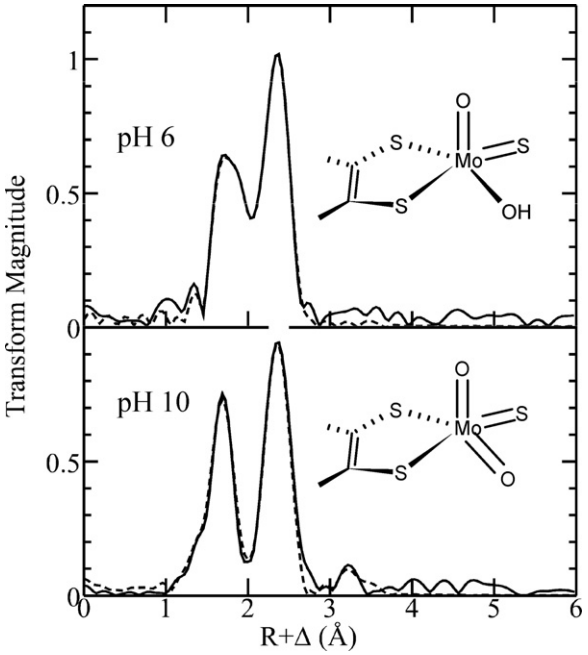

Fig. 30. Low and high pH oxidized xanthine oxidase. Solid lines show the transforms of experimental data, and broken lines those of the best fits. Structural details for pH 6 are 1 Mo=O at 1.69 Å, 1 Mo–O at 1.98 Å, 1 Mo=S at 2.15 Å, 2 Mo–S at 2.43 Å, and for pH 6 are 2 Mo=O at 1.72 Å, 1 Mo=S at 2.19 Å, 2 Mo–S at 2.47 Å. Data are re-plotted from Ref. [165].

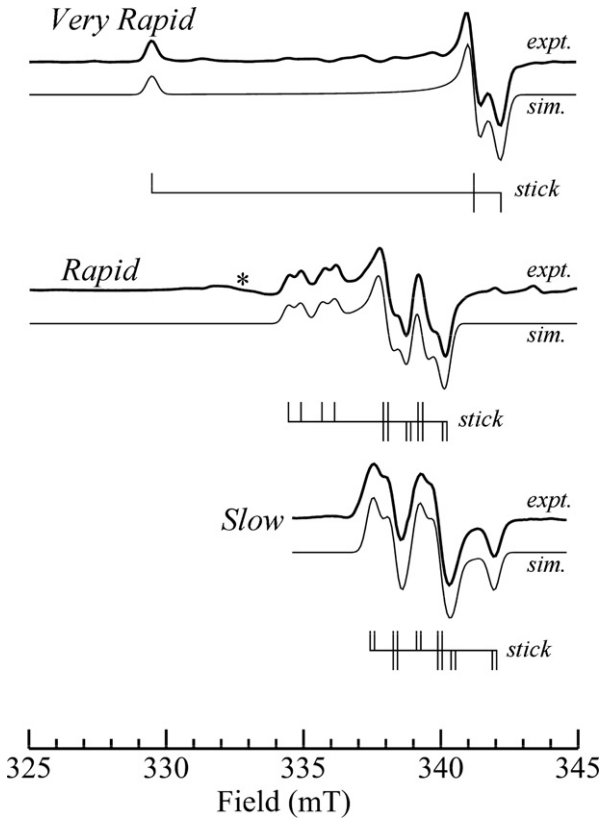

Fig. 31. Xanthine oxidase Mo^{V} EPR signals. Xanthine Very Rapid signal, the formaldehyde Rapid (a typical type 1 Rapid signal) and the Slow signal. Simulations were computed using literature values for *g*-values and for hyperfine couplings.

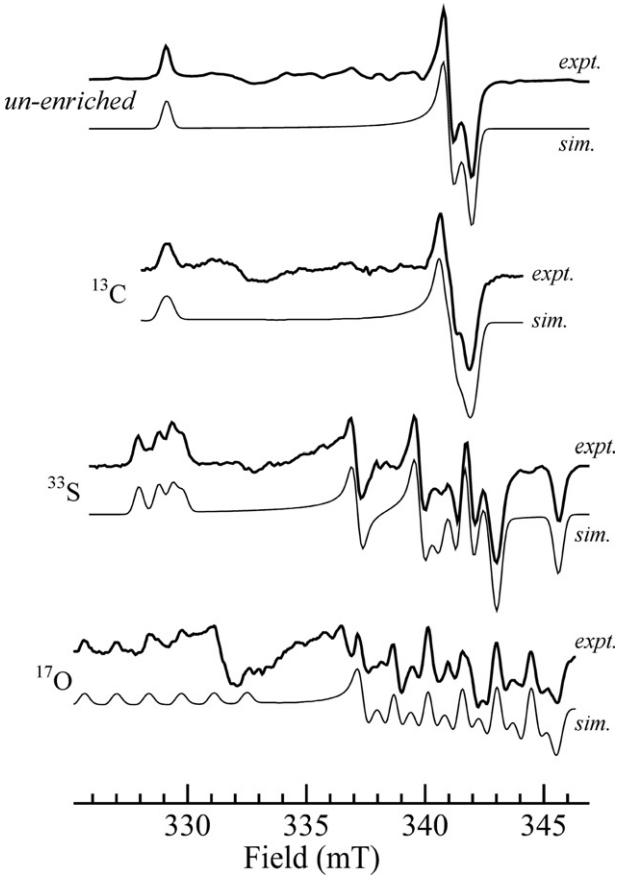

Fig. 32. Very Rapid Mo^{V} CW EPR signal developed using samples enriched with different isotopes. All traces show the xanthine Very Rapid signal, except for that for ^{13}C which is the 6-methylpurine Very Rapid. Traces are aligned to a frequency of 9.3322 GHz, redrawn from Ref. [159]. Simulations were computed using literature spin Hamiltonian parameters [159].

The structures of the signal-giving species and how they relate to catalytic mechanism has been the subject of much research. The Very Rapid EPR signal is of particular interest as ^{13}C coupling indicates that this species is covalently bound to the molybdenum. This species has been extensively studied by using EPR and ENDOR and substitution with various stable magnetic isotopes including ^{13}C, ^{17}O, ^{33}S, ^{95}Mo and ^{97}Mo (see [159] for a review of early work) and selected examples of these are shown in Fig. 32. Early EPR work using enrichment with ^{13}C and ^{17}O to detect the hyperfine coupling to these nuclei concluded that this species contained substrate bound via Mo–O–C coordination [174], where the C is the substrate carbon being oxidized, and the O is the atom being transferred to create product (Fig. 33). Subsequent studies using ^{13}C ENDOR were interpreted to suggest a side-on coordination η^2-keto system [175] with at least a partial Mo···C bond [176] but this notion was discredited by subsequent ENDOR spectroscopy which was interpreted to favor coordination similar to that originally proposed [177] (Fig. 33). Finally, recent density functional calculations support this latter assignment, giving theoretical hyperfine coupling that adequately matches experimental values [178]. When developed with enzyme containing ^{33}S in the cyanolysable sulfur, the Very Rapid signal shows unusually large and anisotropic ^{33}S hyperfine [158], which has been interpreted as indicating a Mo=S environment with extensive spin-delocalization on to sulfur, corresponding to approximately 0.3 electrons [39,158]. Moreover, the ^{97}Mo enriched enzyme is unusual among xanthine oxidase EPR signals in showing significant nuclear electric quadrupole coupling, which has been attributed to a highly asymmetric electric

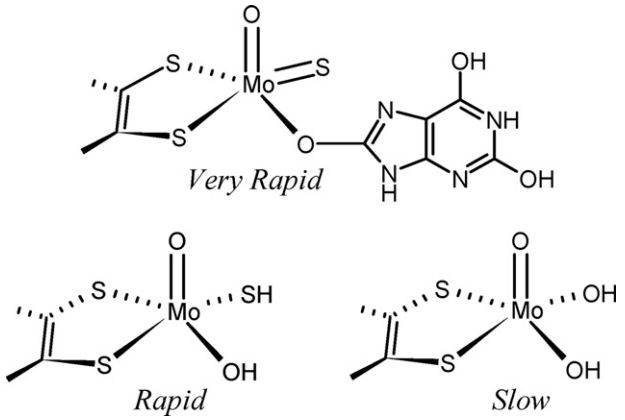

Fig. 33. Postulated structures for the Very Rapid, the Rapid and the Slow signal-giving species.

field gradient surrounding the paramagnetic ground state molecular orbital, also consistent with an equatorial Mo=S coordination [39]. Overall, the evidence that the structure of the Mo^V Very Rapid signal-giving species is that shown in Fig. 33 is compelling.

The exact relationship of the Very Rapid signal-giving species to the catalytic mechanism remains an unresolved question. The intermediate forms in quantity only at high pH, with negligible presence at the optimum pH for xanthine oxidase activity. Moreover it only forms with some substrates, in particular those with nitrogen bound to the substrate carbon atom, including formamide, NH_2CHO, the only aldehyde known to give the Very Rapid [188]. The potent inhibitor alloxanthine (Fig. 34 which has a nitrogen in the position of the carbon that would normally be oxidized by catalysis, and which is produced by enzymic oxidation of the anti-gout drug allopurinol, gives an EPR signal very similar to the Very Rapid [179]. This signal shows nearly identical *g*-values and ^{33}S coupling to the Very Rapid but differs in showing resolved hyperfine splitting from a single ^{14}N nucleus. The crystal structures of the fully reduced Mo^{IV} xanthine dehydrogenase [28] and xanthine oxidase [180] with bound alloxanthine clearly show the presence of a Mo–N bond (Fig. 34) with the carboxylate of Glu-1261 associating with the adjacent ring nitrogen [180]. EXAFS spectroscopy provides little input on this because it cannot distinguish between O and N backscatterers, although other features of the structures are confirmed [181]. Because only substrates with nitrogen in this position form the Very Rapid species (*e.g.* see [166]), it seems likely that it is indeed an intermediate of catalytic turnover, stabilized under basic conditions by association with Glu-1261.

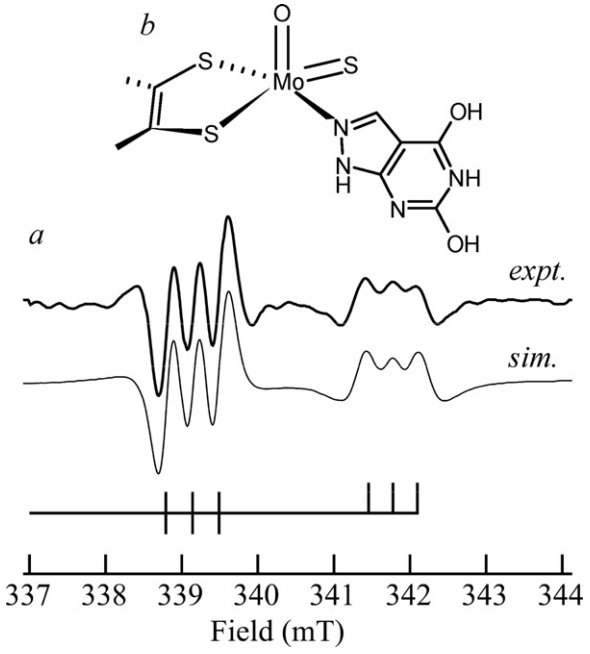

Fig. 34. Mo^V EPR signal (a) from the xanthine oxidase alloxanthine complex, showing the characteristic 3-line pattern arising from ^{14}N hyperfine coupling due to the presence of N coordination. The structure (b) shows the presumed structure of the signal-giving species, indicating the Mo–N bond to the alloxanthine ring. The spectra are re-plotted from Ref. [179] and the simulation was computed using the spin Hamiltonian parameters of Hawkes et al. [179].

The nature of the proton splitting of the xanthine oxidase Rapid signals has been studied in some depth. Here, we will restrict our discussion to the Rapid type 1 signal, which has been more extensively studied. Both the coupled protons will exchange with solvent water with different rates – the strongly coupled proton somewhat faster than the weakly coupled proton [182,183]. When oxidized enzyme exchanged into ^2H_2O buffer is reduced by exposure to 1-methylxanthine (which generates the type 1 Rapid Mo^V EPR signal) in a freeze-quench experiment, then the hydrogen from the substrate C–H position (that being catalytically converted from C–H to C–OH) appears as the strongly coupled proton in the Rapid signal [182,184]. This proton is subsequently lost by exchange with solvent ^2H_2O, slightly complicating the kinetics [182,184]. This important result implies that the group bearing the strongly coupled proton of the Rapid signal accepts the hydrogen displaced from substrate during the catalytic cycle.

With an excess of aldehyde substrates xanthine oxidase slowly loses activity, and a novel Mo^V EPR signal is observed [185], which is known as Inhibited. The aldehyde-inhibited form of xanthine oxidase spontaneously regains activity on removal of excess aldehyde. With formaldehyde H_2CO the EPR signal shows hyperfine coupling to a single resolved ^1H, which is absent when ^2H_2CO is used [185]. When ^{13}C enriched H_2CO is used and additional splitting due to ^{13}C hyperfine is observed [186]. Related species form with a range of different aldehydes (RCHO) and these have been studied by Mo^V EPR [187,188]. Apart from formaldehyde, all aldehyde-inhibited species studied to-date by Mo^V EPR lack a resolved ^1H splitting, and give *g*-values that vary systematically with the nature of the α-carbon substituent R – as R becomes more electron-withdrawing, so the value of g_{ave} increases [187]. An EXAFS study of the species indicated that the molybdenum was coordinated by one Mo=O, with no detectible Mo=S contribution, plus a number of Mo–S and Mo–O/C interactions [189], although these early data were of limited signal to noise and a repeat of these measurements is probably warranted. ENDOR studies have been used to provide more accurate hyperfine coupling [190], but the exact nature of the complex was not clear until very recently when elegant ENDOR studies of the formaldehyde-inhibited species clearly showed that both protons of the CH_2O moiety were in fact retained in the signal-giving species, with one coupling much weaker than the other and thus not observed with ordinary CW EPR, suggesting the structure shown in Fig. 35 [191]. We note that active site geometry must influence the formation of the complex, because the location for the strongly coupled proton H^A is always occupied by the substituent R when larger aldehydes RCHO are used.

Studies of other inhibited species include arsenite [31,192,193] and *p*-chloro-mercuribenzoate (PCMB) [194]. Arsenite interacts with both oxidized and reduced enzyme, and gives modified UV–vis spectra and Mo^V EPR with hyperfine and quadrupole coupling from ^{75}As [192]. PCMB, on the other hand, binds to reduced enzyme but not to oxidized, and dramatically modifies the Mo^V EPR of active but not desulfo enzyme [194]. PCMB is thought to target the Mo–SH of reduced active enzyme, and in these early studies this was used as evidence for the presence of such a group in the reduced active site [194]. The Mo^V EPR of this species is remarkable because of the

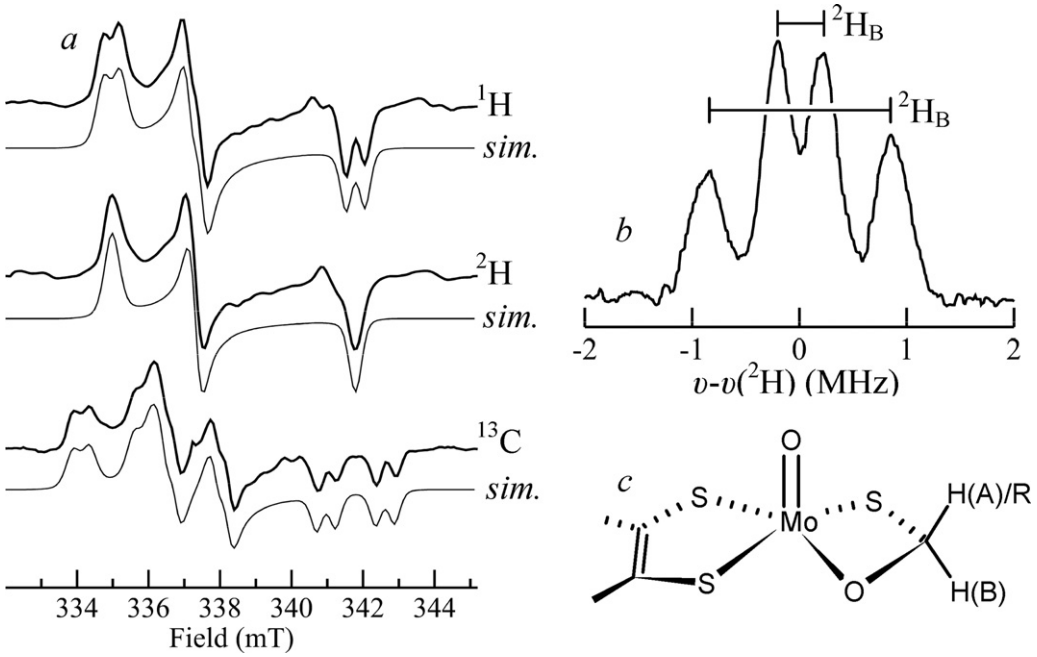

Fig. 35. EPR, ENDOR and proposed structure of the xanthine oxidase inhibited signal. The simulations were computed using the spin Hamiltonian parameters of Tanner et al. [186]. The EPR spectra are re-plotted from Refs. [185,186] and the ^{2}H ENDOR is re-plotted from Ref. [191] and clearly shows the coupling to *both* deuterons of the formaldehyde (the signal was developed with $^{2}H_2CO$). These data support the conclusion of the structure shown in (c) [191].

very large magnetic coupling to ^{199}Hg (I = 1/2) and ^{201}Hg (I = 3/2) observed by George and Bray [194]. EXAFS of the Mo^{V} PCMB complex indicates Mo–S–Hg–C coordination [195]. We note that the interaction of arsenite with a bacterial aldehyde oxidoreductase has recently been re-investigated [196] and we will discuss this in the next section.

Prokaryotes contain some novel members of the xanthine oxidase family, and these include the aldehyde oxidoreductase from *D. gigas*, on which early crystallographic studies were conducted [34]. When first discovered this enzyme lacked a known function, although its composition clearly indicated that it was related to the xanthine oxidase family [197], and subsequent studies identified it as an aldehyde oxidoreductase [198]. Recent work has shows that the enzyme activity was not affected by exposure to cyanide [199], and the authors concluded that the *active* enzyme was a dioxo species, and did not require a Mo=S group for activity [199]. However, given the known variation in susceptibility to cyanide of other family members (see above discussion) it seems much more likely that *D. gigas* aldehyde oxidoreductase is simply one of those enzymes that are resistant to cyanide. In agreement with this, the enzyme gives a Rapid Mo^{V} EPR signal when reduced with aldehyde substrates [198], a signal known to be associated with reduction of an oxo-thio core, and clearly indicating its presence in the *D. gigas* enzyme. Moreover quantitative EPR showed that the preparations showed Rapid signal integrated intensities consistent with only some 10–25% of active enzyme [198]. This low level of the active Mo=S containing enzyme would not be observed by crystallography, and this is in agreement with the crystallographic conclusions which reflect the 90–75% of desulfo enzyme present [34,199]. From these considerations is seems probable that the EPR spectroscopy represented the minor active sulfur-containing fraction, while the crystallography represented the major inactive desulfo enzyme, and that the two are not directly related. Other structural conclusions on this system concerning the structural nature of the binding of various inhibitors, such as arsenite [196] and diols [199] should be interpreted as relevant to the inactive desulfo form, and not representative of active enzyme.

Fig. 36 shows a version of the currently accepted catalytic mechanism for xanthine oxidase, showing plausible formation routes for both Very Rapid and Rapid Mo^{V} species.

5.2. Carbon monoxide dehydrogenases

Possibly the most novel members of the xanthine oxidase family are the molybdenum-containing carbon monoxide dehydrogenases. The first of these to be characterized was isolated from the aerobic bacterium *Oligotropha carboxidovorans*, and catalyzes the oxidation of CO with H_2O, yielding CO_2, two electrons, and two H^{+}. X-ray crystallography was interpreted as indicating a Mo site containing a novel *S*-selenylcysteine coordination [200] (Fig. 37) and a mechanism drawing on analogies with the chemistry of carbon oxide selenide (O=C=Se) was proposed [200]. Further X-ray crystallography studies of a related enzyme system from *Hydrogenophaga pseudoflava* were interpreted as indicating a very similar active site structure also containing *S*-selenylcysteine coordination to Mo [201]. Subsequent re-evaluation of the crystallography [32] and later EXAFS spectroscopy [202] revealed that the original crystallographic analyses had been in error, and that the enzyme did not in fact contain selenium, but instead a novel bimetallic cluster with sulfide bridging Mo and Cu Mo–S–Cu–S(Cys) (Fig. 37), with an approximately linear Cu^{I} coordination. EXAFS further indicated that the oxidized active site was a dioxo-species containing the $[MoO_2]^{2+}$ moiety [202], rather than a MoO(OH) species (Fig. 37). Crystallographic studies with the inhibitor *n*-butylisocyanide bound to the active suggested a catalytic mechanism involving a thiocarbonate-like intermediate state [32]. Reduced forms give a novel Mo^{V} EPR signal showing strong anisotropic hyperfine coupling with the $I = 3/2$ ^{63,65}Cu nuclei [32,203] and similar Cu hyperfine has recently been observed with model complexes containing a Mo–S–Cu linkage [204]. Recent EPR spectroscopy using ^{13}CO to develop the Mo^{V} EPR signal showed evidence of ^{13}C hyperfine coupling [203]. These studies suggested that CO initially binds rapidly to the enzyme, possibly at the Cu^{I} of the active site, prior to undergoing oxidation. Finally, Resonance

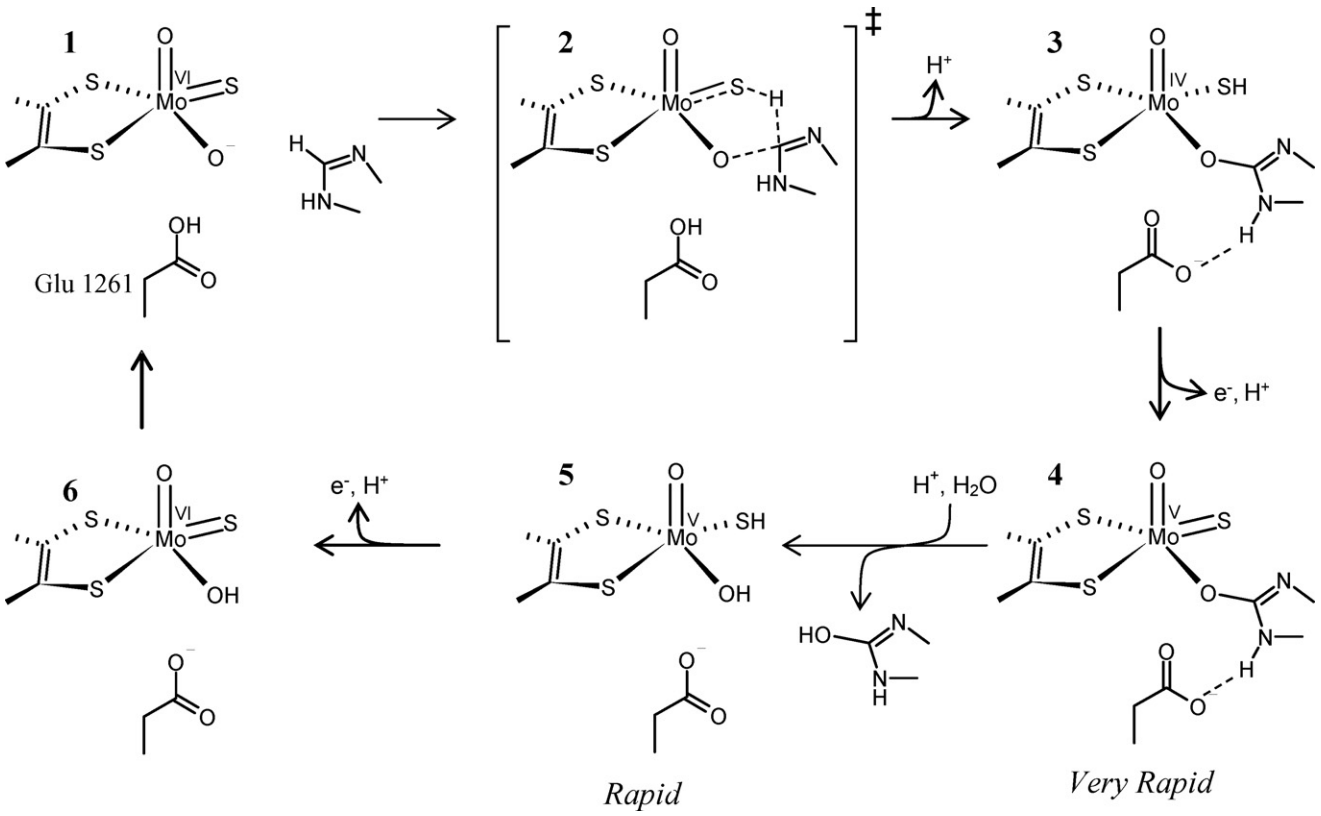

Fig. 36. Possible mechanism for xanthine oxidase showing plausible formation of both Very Rapid and Rapid Mo^{V} species (see [165,207] and references therein). A proton is abstracted from Mo–OH by Glu1261 to form a Mo–O^{-} group in **1** which attacks substrate proceeding via a transition state **2** to form a Mo^{IV} substrate bound intermediate **3**. The role of the Mo=S group is to accept the hydride from the substrate. The Mo^{V} Very Rapid **4** is then generated by intramolecular electron transfer and is stabilized by the proximity of Glu1261. The Mo^{V} Rapid **5** is then formed by subsequent hydrolysis and loss of product, and finally oxidized enzyme **6** is produced by intramolecular electron transfer. We note that loss of product may occur from the Mo^{IV} species without the formation of the Very Rapid, to form a Mo^{IV} analogue of **5**, and the Rapid could then be generated directly from this by intramolecular electron transfer.

Raman spectroscopy confirms previous conclusions of [$CuSMoO_2$] coordination in the active site [203]. This novel enzyme continues to help re-define the catalytic modes that the molybdenum enzymes can adopt.

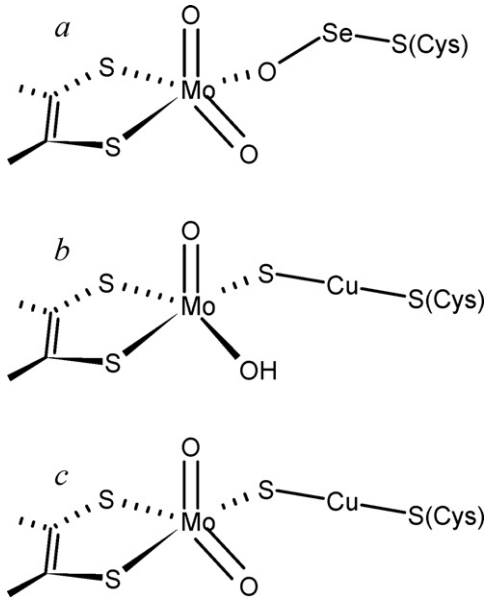

Fig. 37. Different structures postulated for the oxidized Mo^{VI} active site of CO dehydrogenase. The structure (a) shows the initial structure postulated from crystallography [200,201], (b) from the crystallographic re-evaluation [32], and (c) from EXAFS spectroscopy [202].

5.3. Selenium-containing xanthine oxidase enzymes

Despite the false alarm with CO dehydrogenase described above, the xanthine oxidase family does appear to contain some *bona fide* members that natively contain selenium. Nicotinate dehydrogenase from *Clostridium barkeri* contains selenium at the Mo active site [205]. The enzyme catalyzes the conversion of nicotinic acid to 6-hydroxynicotinic acid, with concomitant reduction of $NADP^{+}$, but possesses NADPH oxidase activity with oxygen. Substitution of the enzyme with the $I = 1/2$ stable isotope ^{77}Se results in clear splitting of the Mo^{V} due to ^{77}Se hyperfine [205]. Growth of *C. barkeri* on media containing no selenium gives a selenium-deficient enzyme which gives a Mo^{V} EPR signal that is essentially identical to the xanthine oxidase Rapid type 1 (Fig. 38). Together, these results strongly suggest that the enzyme contains a Mo=Se group analogous to the Mo=S of xanthine oxidase, although the enzyme is only slowly deactivated by cyanide, requiring an exposure of 2 mM CN^{-} for 7 days to eliminate activity [206]. Recently, this coordination has been confirmed in the nicotinate dehydrogenase of *Eubacterium barkeri* using X-ray crystallography. This study clearly indicates a xanthine oxidase-type active site with a Mo=Se group in place of the Mo=S [207]. Moreover, as expected, it unambiguously indicated that the Mo=Se group was in the equatorial plane [207]. Other selenium-dependant xanthine oxidase family members include purine hydroxylase and xanthine dehydrogenases which have been purified and characterized from *Clostridium purinolyticum* [208], and the former gave the Slow Mo^{V} EPR signal on reduction, suggesting the presence of substantial deseleno-enzyme [209]. Early work indicated that desulfo turkey xanthine dehydrogenase could be reactivated by selenide [210], which suggests that selenium

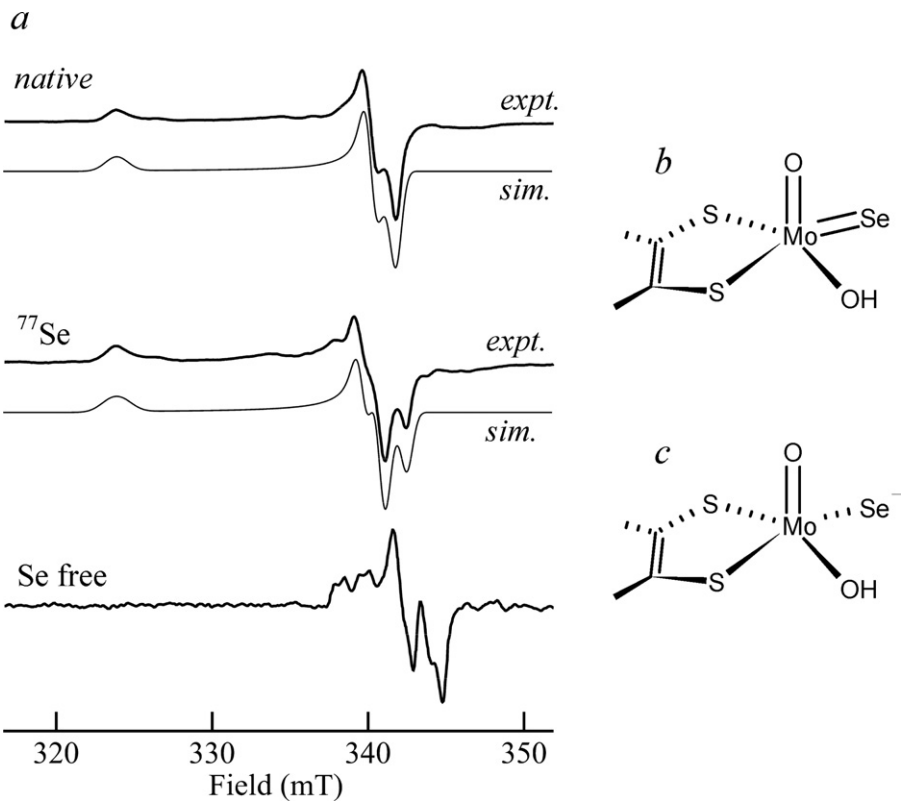

Fig. 38. Nicotinate hydroxylase Mo^{V} EPR spectra. Spectra were redrawn from Ref. [205] and simulations were computed using g_{xyz} = 1.976, 1.985, 2.085 and ^{77}Se A_{xyz} = 39, 30, 25 MHz, assuming a microwave frequency of 9.45 GHz.

might be able fill the role of sulfur in other xanthine oxidase family members.

6. Concluding remarks

Modern spectroscopic methods have been essential for developing the current state of our knowledge of the active site structures and catalytic mechanisms of the molybdenum enzymes. For X-ray absorption spectroscopy the use of high-resolution data, with extended *k*-ranges, is expected to become increasingly important in the successful use of this technique. It will also become increasingly important to obtain good quality data of acceptable signal to noise. Moreover, we anticipate that a three-way holistic view of structure will become important. This is to combine the accurate bond-lengths available from EXAFS analysis as constraints and restraints in crystallography, with density functional theory (the gold-standard in computational chemistry) to give insights into how chemically reasonable a structure being modeled actually is. Insofar as other spectroscopies are concerned, the highly sensitive techniques such as ENDOR and ESEEM in combination with conventional EPR are expected to give increasingly detailed insights into the structure and mechanism of these novel systems.

Acknowledgements

Research at the University of Saskatchewan is funded by the Natural Sciences and Engineering Research Council of Canada, the Canadian Institutes of Health Research (CIHR), the Saskatchewan Health Research Foundation (SHRF), the University of Saskatchewan, and the Canada Foundation for Innovation. GNG is supported by a Canada Research Chair award and MJP is supported by a SHRF Postdoctoral Fellowship and is also a CIHR-Training in Health Research Using Synchrotron Techniques (THRUST) fellow. The authors' research has benefited from access to the Stanford Synchrotron Radiation Lightsource (SSRL) which in the case of GNG has continued over nearly three decades. We are indebted to the SSRL staff for their continued support, without which many of the results described herein would not have been possible. SSRL is a Directorate of SLAC National Accelerator Laboratory and an Office of Science User Facility operated for the U.S. Department of Energy Office of Science by Stanford University. The SSRL Structural Molecular Biology Program is supported by the DOE Office of Biological and Environmental Research and by the National Institutes of Health, National Center for Research Resources, Biomedical Technology Program (P41RR001209).

References

[1] S.J. Lippard, J.M. Berg, Principles of Bioinorganic Chemistry, University Science Books, Mill Valley, CA, 1994.
[2] J.J.R. Fraústo da Silva, R.J.P. Williams, The Biological Chemistry of the Elements: The Inorganic Chemistry of Life, Clarendon Press, Oxford, 1991.
[3] D.C. Rees, A. Tezcan, C.A. Haynes, M.Y. Walton, S. Andrade, O. Einsle, J.B. Howard, Philos. Trans. R. Soc. A 363 (2005) 971.
[4] G.N. George, I.J. Pickering, E.Y. Yu, R.C. Prince, S.A. Bursakov, O.Y. Gavel, I. Moura, J.J.G. Moura, J. Am. Chem. Soc. 132 (2000) 8321.
[5] M.G. Rivas, M.S. Carepo, C.S. Mota, M. Korbas, M.-C. Durand, A.T. Lopes, C.D. Brondino, A.S. Pereira, G.N. George, A. Dolla, J.J.G. Moura, I. Moura, Biochemistry 48 (2009) 873.
[6] F.J. Hine, A.J. Taylor, C.D. Garner, Coord. Chem. Rev. 254 (2010) 1570.
[7] R. Hille, Chem. Rev. 96 (1996) 2757.
[8] R. Hille, Trends Biochem. Sci. 27 (2002) 360.
[9] B.M. Rosner, B. Schink, J. Bacteriol. 177 (1995) 5767.
[10] G.B. Seiffert, G.M. Ullmann, A. Messerschmidt, B. Schink, P.M.H. Kroneck, O. Einsle, Proc. Natl. Acad. Sci. U.S.A. 104 (2007) 3073.
[11] J.C. Boyington, V.N. Gladyshev, S.V. Khangulov, T.C. Stadtman, P.D. Sun, Science 275 (1997) 1305.
[12] H. Schindelin, C. Kisker, J. Hilton, K.V. Rajagppalan, D.C. Rees, Science 272 (1996) 1615.
[13] P.J. Ellis, T. Conrads, R. Hille, P. Kuhn, Structure 9 (2001) 125.
[14] G.N. George, C.M. Colangelo, J. Dong, R.A. Scott, S.V. Khangulov, V.N. Gladyshev, T.C. Stadtman, J. Am. Chem. Soc. 120 (1998) 1267.

[15] J.M. Dias, M.E. Than, A. Humm, R. Huber, G.P. Bourenkov, H. Bartunik, S. Bursakov, J. Calvete, J. Caldeira, C. Carneiro, J.J. Moura, I. Moura, M.J. Romão, Struct. Fold. Des. 7 (1999) 65.
[16] M.G. Bertero, R.A. Rothery, M. Palak, C. Hou, D. Lim, F. Blasco, J. Weiner, N.C.J. Strynadka, Nat. Struct. Biol. 10 (2003) 681.
[17] M. Jormakka, D. Richardson, B. Byrne, S. Iwata, Structure 12 (2004) 95.
[18] D.P. Kloer, C. Hagel, J. Heider, G.E. Schulz, Structure 14 (2006) 1377.
[19] H.K. Li, C. Temple, K.V. Rajagopalan, H.H. Schindelin, J. Am. Chem. Soc. 122 (2000) 7673.
[20] N.L. Creevey, A.G. McEwan, G.R. Hanson, P.V. Bernhardt, Biochemistry 47 (2008) 3770.
[21] C. Kisker, H. Schindelin, A. Pacheco, W.A. Wehbi, R.M. Garrett, K.V. Rajagopalan, J.H. Enemark, D.C. Rees, Cell 91 (1997) 973.
[22] U. Kappler, S. Bailey, J. Biol. Chem. 280 (2005) 24999.
[23] T. Eilers, G. Schwarz, H. Brinkmann, C. Witt, T. Richter, J. Nieder, B. Koch, R. Hille, R. Hänsch, R.R. Mendel, J. Biol. Chem. 276 (2001) 46989.
[24] N. Schrader, K. Fischer, K. Theis, R.R. Mendel, G. Schwartz, K. Kisker, Structure 11 (2003) 1251.
[25] A.C. Braaten, M.M. Bentley, Biochem. Genet. 31 (1993) 375.
[26] K. Fischer, G. Barbier, H.-J. Hecht, R.R. Mendel, W.H. Campbell, G. Schwarz, Plant Cell 17 (2005) 1167.
[27] C. Enroth, B.T. Eger, K. Okamoto, T. Nishino, T. Nishino, E.F. Pai, Proc. Natl. Acad. Sci. U.S.A. 97 (2000) 10723.
[28] J.J. Truglio, K. Theis, S. Leimkuhler, R. Rappa, K.V. Rajagopalan, C. Kisker, Structure 10 (2002) 115.
[29] E. Garattini, M. Fratelli, M. Terao, Cell. Mol. Life Sci. 65 (2008) 1019.
[30] R.C. Bray, G.N. George, S. Gutteridge, L. Norlander, J.G.P. Stell, C. Stubly, Biochem. J. 203 (1982) 263.
[31] N.A. Turner, W.A. Doyle, A.M. Ventom, R.C. Bray, Eur. J. Biochem. 232 (1995) 646.
[32] H. Dobbek, L. Gremer, R. Kiefersauer, R. Huber, O. Meyer, Proc. Natl. Acad. Sci. U.S.A. 99 (2002) 15971.
[33] M.K. Chan, S. Mukund, A. Kletzin, M.W.W. Adams, D.C. Rees, Science 267 (1995) 1463.
[34] M.J. Romão, M. Archer, I. Moura, J.J.G. Moura, J. LeGall, R. Engh, M. Schnieder, P. Hof, R. Huber, Science 270 (1995) 1170.
[35] G. Palmer, Biochem. Soc. Trans. 13 (1985) 548.
[36] R.C. Bray, Adv. Enzymol. Relat. Areas Mol. Biol. 51 (1980) 107.
[37] J. Weil, J.R. Bolton, Electron Paramagnetic Resonance: Elementary Theory and Practical Applications, second ed., Wiley-Interscience, 2007.
[38] R.C. Bray, L.S. Meriwhether, Nature 212 (1966) 467.
[39] G.N. George, R.C. Bray, Biochemistry 27 (1988) 3603.
[40] B.M. Hoffman, Acc. Chem. Res. 36 (2003) 522.
[41] J. Tesler (Ed.), Paramagnetic Resonance of Metallobiomolecules, ACS Symposium Series, vol. 858, 2003.
[42] J.H. Enemark, A.V. Astashkin, A.M. Raitsimring, J. Chem. Soc., Dalton Trans. (2006) 3501.
[43] T. Prisner, M. Roher, F. MacMillan, Annu. Rev. Phys. Chem. 52 (2001) 279.
[44] G.N. George, R.E. Bare, H. Jin, E.I. Stiefel, R.C. Prince, Biochem. J. 262 (1989) 349.
[45] P.E. Doan, C. Fan, B.M. Hoffman, J. Am. Chem. Soc. 116 (1994) 1033.
[46] T.G. Spiro, R.S. Czernuszewicz, Methods Enzymol. 246 (1995) 416.
[47] R.M. Badger, J. Chem. Phys. 3 (1935) 710.
[48] M.T. Green, J. Am. Chem. Soc. 128 (2006) 1902.
[49] F.W. Kutzler, C.R. Natoli, D.K. Misemer, S. Donaich, K.O. Hodgson, J. Chem. Phys. 73 (1980) 3274.
[50] F.W. Kutzler, R.A. Scott, J.M. Berg, K.O. Hodgson, S. Donaich, S.P. Cramer, C.H. Chang, J. Am. Chem. Soc. 103 (1981) 6083.
[51] G.N. George, W.E. Cleland, J.H. Enemark, B.E. Smith, C.A. Kipke, S.A. Roberts, S.P. Cramer, J. Am. Chem. Soc. 112 (1990) 2541.
[52] J.J. Rehr, J. Mustre de Leon, S.I. Zabinsky, R.C. Albers, J. Am. Chem. Soc. 113 (1991) 5135.
[53] K. Clark-Baldwin, D.L. Tierney, N. Govindaswamy, E.S. Gruff, C. Kim, J. Berg, S.A. Koch, J.E. Penner-Hahn, J. Am. Chem. Soc. 120 (1998) 2387.
[54] J.M. Berg, K.O. Hodgson, Inorg. Chem. 19 (1980) 2180.
[55] C.E. Laplaza, M.A. Johnson, J. Peters, A.L. Odom, E. Kim, C.C. Cummins, G.N. George, I.J. Pickering, J. Am. Chem. Soc. 118 (1996) 8623.
[56] G.C. Ferreira, R. Franco, A. Mangravita, G.N. George, Biochemistry 41 (2002) 4809.
[57] G.N. George, J. Hilton, C. Temple, R.C. Prince, K.V. Rajagopalan, J. Am. Chem. Soc. 121 (1999) 1256.
[58] J. Bordas, R.C. Bray, C.D. Garner, S. Gutteridge, S.S. Hasnain, Biochem. J. 191 (1980) 499.
[59] H.H. Harris, G.N. George, K.V. Rajagopalan, Inorg. Chem. 45 (2006) 493.
[60] E.A. Stern, Phys. Rev. B. 48 (1993) 9825.
[61] M. Jakolski, M. Gilski, Z. Dauter, A. Wlodawer, Biol. Cryst. D63 (2007) 611.
[62] H. Schindelin, C. Kisker, D.C. Rees, J. Biol. Inorg. Chem. 2 (1997) 773.
[63] G.N. George, I.J. Pickering, C. Kisker, Inorg. Chem. 38 (1999) 2539.
[64] C.J. Doonan, L. Zhang, C.G. Young, S.J. George, A. Deb, U. Bergmann, G.N. George, S.P. Cramer, Inorg. Chem. 44 (2005) 2579.
[65] F. Schneider, J. Löwe, R. Huber, H. Schindelin, C. Kisker, J. Knäblein, J. Mol. Biol. 263 (1996) 53.
[66] A.S. McAlpine, A.G. McEwan, A.L. Shaw, S. Bailey, J. Biol. Inorg. Chem. 2 (1997) 690.
[67] A.S. McAlpine, A.G. McEwan, S.J. Bailey, J. Mol. Biol. 275 (1998) 613.
[68] F.H. Allen, O. Kennard, D.G. Watson, Struct. Correl. 1 (1994) 71.
[69] M. Czjzek, J.P. Dos Santos, J. Pommier, G. Giordano, V. Mejean, R. Haser, J. Mol. Biol. 284 (1998) 435.
[70] G.N. George, J. Hilton, K.V. Rajagopalan, J. Am. Chem. Soc. 118 (1996) 1113.
[71] S.D. Garton, J. Hilton, O. Hiroyuki, B.R. Crouse, K.V. Rajagopalan, M.K. Johnson, J. Am. Chem. Soc. 119 (1997) 12906.
[72] P.E. Baugh, C.D. Garner, J.M. Charnock, D. Collison, E.S. Davies, A.S. McAlpine, S. Bailey, I. Lane, G.R. Hanson, A.G. McEwan, J. Biol. Inorg. Chem. 2 (1997) 634.
[73] C.A. Temple, G.N. George, J.C. Hilton, M.J. George, R.C. Prince, M.J. Barber, K.V. Rajagopalan, Biochemistry 39 (2000) 4046.
[74] B. Bennet, N. Benson, A.G. McEwan, R.C. Bray, Biochem. J. 255 (1994) 321.
[75] L. Zhang, K. Johnson Nelson, K.V. Rajagopalan, G.N. George, Inorg. Chem. 47 (2008) 1074.
[76] G.N. George, C.J. Doonan, R.A. Rothery, A. Boroumand, J.H. Weiner, Inorg. Chem. 46 (2007) 2.
[77] R.C. Bray, B. Adams, A.T. Smith, R.L. Richards, D.J. Lowe, S. Bailey, Biochemistry 40 (2001) 9810.
[78] G.N. George, K.J. Nelson, H.H. Harris, C.J. Doonan, K.V. Rajagopalan, Inorg. Chem. 46 (2007) 3097.
[79] M.G. Bertero, R.A. Rothery, M. Palak, C.C. Hou, D. Lim, F. Blasco, J.H. Weiner, N.C.J. Strynadka, Nat. Struct. Biol. 10 (2003) 681.
[80] G.N. George, R.C. Bray, F.F. Morpeth, D.H. Boxer, Biochem. J. 227 (1985) 925.
[81] C. Godfrey, C. Greenwood, A.J. Thomson, R.C. Bray, G.N. George, Biochem. J. 224 (1984) 601.
[82] G.N. George, N.A. Turner, R.C. Bray, F.F. Morpeth, D.H. Boxer, S.P. Cramer, Biochem. J. 259 (1989) 693.
[83] D.A. Sherrell, M. Solomonson, J. Weiner, R. Rothery, M.J. Pushie, G.N. George, unpublished observations.
[84] M.J. Maher, J. Santini, I.J. Pickering, R.C. Prince, J.M. Macy, G.N. George, Inorg. Chem. 43 (2004) 402.
[85] S. Najmudin, P.J. Gonzalez, J. Trincão, C. Coelho, A. Mukhopadhyay, C.C. Romão, I. Moura, J.J.G. Moura, C.D. Brondino, M.J. Romão, J. Biol. Inorg. Chem. 13 (2008) 737.
[86] P. Arnoux, M. Sabaty, J. Alric, B. Frangioni, B. Guigliarelli, J.-M. Adriano, D. Pignol, Nat. Struct. Biol. 10 (2003) 928.
[87] B.J.N. Jepson, S. Mohan, T.A. Clarke, A.J. Gates, J.A. Cole, C.S. Butler, J.N. Butt, A.M. Hemmings, D.J. Richardson, J. Biol. Chem. 282 (2007) 6425.
[88] C. Coelho, P.J. Gonzalez, J. Trincao, A.L. Carvalho, S. Najmudin, T. Hettman, S. Dieckman, J.J.G. Moura, I. Moura, M.J. Romão, Acta Cryst. Sect. F 63 (2007) 516.
[89] B. Bennet, B.C. Berks, S.J. Ferguson, A.J. Thomson, D.J. Richardson, Eur. J. Biochem. 226 (1994) 789.
[90] C.S. Butler, S.A. Fairhurst, S.J. Ferguson, A.J. Thomson, B.C. Berks, D.J. Richardson, D.J. Lowe, Biochem. J. 363 (2002) 817.
[91] C.S. Butler, J.M. Charnock, B. Bennett, H.J. Sears, A.J. Reilly, S.J. Ferguson, C.D. Garner, D.J. Lowe, A.J. Thomson, B.C. Berks, D.J. Richardson, Biochemistry 38 (1999) 9000.
[92] R. Gangeswaran, D.J. Lowe, R.R. Eady, Biochem. J. 289 (1993) 335.
[93] B.J.N. Jepson, L.J. Anderson, L.M. Rubio, C.J. Taylor, C.S. Butler, E. Flores, A. Herrero, J.N. Butt, D.J. Richardson, J. Biol. Chem. 279 (2004) 32212.
[94] F. Zinoni, A. Birkmann, T.C. Stadtman, A. Bock, Proc. Natl. Acad. Sci. U.S.A. 83 (1986) 4650.
[95] V.N. Gladyshev, S.V. Khangulov, M.J. Axley, T.C. Stadtman, Proc. Natl. Acad. Sci. U.S.A. 91 (1994) 7708.
[96] S.V. Khangulov, V.N. Gladyshev, G.C. Dismukes, T.C. Stadtman, Biochemistry 37 (1998) 3518.
[97] M. Jormakka, S. Törnroth, B. Byrne, S. Iwata, Science 275 (2002) 1863.
[98] G.N. George, C. Costa, J.J.G. Moura, I. Moura, J. Am. Chem. Soc. 121 (1999) 2625.
[99] H. Raaijmakers, S. Macieira, J.M. Dias, S. Teixeira, S. Bursakov, R. Huber, J.J. Moura, I. Moura, M.J. Romão, Structure 10 (2002) 1261.
[100] H. Raaijmakers, M.J. Romão, J. Biol. Inorg. Chem. 11 (2006) 849.
[101] G.R. Hanson, G.L. Wilson, T.D. Bailey, J.R. Pilbrow, A.G. Wedd, J. Am. Chem. Soc. 109 (1987) 2609.
[102] M.J. Romão, J. Chem. Soc., Dalton Trans. (2009) 4053.
[103] T. Conrads, C. Hemann, G.N. George, I.J. Pickering, R.C. Prince, R. Hille, J. Am. Chem. Soc. 124 (2002) 11276.
[104] K.R. Hoke, N. Cobb, F.A. Armstrong, R. Hille, Biochemistry 43 (2004) 1667.
[105] A.K. Rappe, W.A. Goddard III, J. Am. Chem. Soc. 104 (1982) 448.
[106] A.K. Rappe, W.A. Goddard III, J. Am. Chem. Soc. 104 (1982) 3287.
[107] T. Lane, M.A. Saito, G.N. George, I.J. Pickering, R.C. Prince, F.F.M. Morel, Nature 435 (2005) 42.
[108] J.R. Andreesen, L.G. Ljungdahl, J. Bacteriol. 116 (1973) 867.
[109] A.M. Sevcenco, M.W.H. Pinkse, E. Bol, G.C. Krijger, H.T. Wolterbeek, P. Verhaert, P.L. Hagedoorn, W.R. Hagen, Metallomics 1 (2009) 395.
[110] S. Mukund, M.W.W. Adams, J. Biol. Chem. 265 (1990) 11508.
[111] G.N. George, R.C. Prince, S. Mukund, M.W.W. Adams, J. Am. Chem. Soc. 114 (1992) 3521.
[112] B.P. Koehler, S. Mukund, R.C. Conover, I.K. Dhawan, R. Roy, M.W.W. Adams, M.K. Johnson, J. Am. Chem. Soc. 118 (1996) 12391.
[113] Y. Hu, S. Faham, R. Roy, M.W.W. Adams, D.C. Rees, J. Mol. Biol. 286 (1999) 899.
[114] S. Mukund, M.W.W. Adams, J. Biol. Chem. 270 (1995) 8389.
[115] J. van der Oost, G. Schut, S.W.M. Kengen, W.R. Hagen, M. Thomm, W.M. de Vos, J. Biol. Chem. 273 (1998) 28149.
[116] S. de Vries, M. Momcilovic, M.J.F. Strampraad, J.P. Whitelegge, A. Baghai, I. Schröder, Biochemistry 49 (2010) 9911.
[117] K.V. Rajagopalan, in: M.P. Coughlan (Ed.), Molybdenum and Molybdenum-Containing Enzymes, Pergamon Press, Oxford, UK, 1980, p. 243.

[118] R. Hänsch, R. Mendel, Photosynth. Res. 86 (2005) 337.
[119] J.L. Johnson, K.V. Rajagopalan, J. Biol. Chem. 252 (1977) 2017.
[120] J.L. Johnson, K.E. Coyne, R.M. Garrett, M.-T. Zabot, C. Dorche, C. Kisker, K.V. Rajagopalan, Hum. Mutat. 20 (2002) 74.
[121] M.C. Edwards, J.L. Johnson, B. Marriage, T.N. Graf, K.E. Coyne, K.V. Rajagopalan, I.M. MacDonald, Ophthalmology 106 (1999) 1957.
[122] K.K. Steinberg, M.V. Relling, M.L. Gallagher, C.N. Greene, C.S. Rubin, D. French, A.K. Holmes, W.L. Carroll, D.A. Koontz, E.J. Sampson, G.A. Satten, Environ. Health Perspect. 115 (2007) 158.
[123] G.N. George, C.A. Kipke, R.C. Prince, R.A. Sunde, J.H. Enemark, S.P. Cramer, Biochemistry 28 (1989) 5075.
[124] S.D. Garton, R.M. Garrett, K.V. Rajagopalan, M.K. Johnson, J. Am. Chem. Soc. 119 (1997) 2590.
[125] C. Hemann, B.L. Hood, M. Fulton, R. Hänsch, G. Schwarz, R.R. Mendel, M.L. Kirk, R. Hille, J. Am. Chem. Soc. 127 (2005) 16567.
[126] R.C. Bray, S. Gutteridge, M.T. Lamy, T. Wilkinson, Biochem. J. 211 (1983) 227.
[127] M.T. Lamy, S. Gutteridge, R.C. Bray, Biochem. J. 185 (1980) 397.
[128] G.N. George, R.C. Prince, C.A. Kipke, R.A. Sunde, J.H. Enemark, Biochem. J. 256 (1988) 307.
[129] A. Pacheco, P. Basu, P. Borbat, A.M. Raitsimring, J.H. Enemark, Inorg. Chem. 35 (1996) 7001.
[130] G.N. George, R.M. Garrett, T. Graf, R.C. Prince, K.V. Rajagopalan, J. Am. Chem. Soc. 120 (1998) 4522.
[131] R.C. Bray, M.T. Lamy, S. Gutteridge, T. Wilkinson, Biochem. J. 201 (1982) 241.
[132] A.V. Astashkin, B.L. Hood, C. Feng, R. Hille, R.R. Mendel, A.M. Raitsimring, J.H. Enemark, Biochemistry 44 (2005) 13274.
[133] A. Rajapakshe, K. Johnson-Winters, A.R. Nordstrom, K.T. Meyers, S. Emesh, A.V. Atashkin, J.H. Enemark, Biochemistry 49 (2010) 5154.
[134] G.N. George, J. Magn. Reson. 64 (1985) 384.
[135] A.M. Raitsimring, A. Pacheco, J.H. Enemark, J. Am. Chem. Soc. 120 (1998) 11263.
[136] A.V. Astashkin, M.L. Mader, A. Pacheco, J.H. Enemark, A.M. Raitsimring, J. Am. Chem. Soc. 122 (2000) 5294.
[137] C.J. Doonan, U. Kappler, G.N. George, Inorg. Chem. 45 (2006) 7488.
[138] G.N. George, H.L. Wilson, R.C. Prince, K.V. Rajagopalan, unpublished work.
[139] C.J. Doonan, H.L. Wilson, B. Bennett, R.C. Prince, K.V. Rajagopalan, G.N. George, Inorg. Chem. 47 (2008) 2033.
[140] A.V. Astashkin, E.L. Klein, J.H. Enemark, J. Inorg. Biochem. 101 (2007) 1623.
[141] E.L. Klein, A.V. Astashkin, D. Ganyushin, C. Riplinger, K. Johnson-Winters, F. Neese, J.H. Enemark, Inorg. Chem. 48 (2009) 4743.
[142] G.N. George, C.J. Doonan, H.L. Wilson, R.C. Prince, K.V. Rajagopalan, unpublished work.
[143] E. Karakas, H.L. Wilson, T.N. Graf, S. Xiang, S. Jaramillo-Busquets, K.V. Rajagopalan, C. Kisker, J. Biol. Chem. 280 (2005) 33506.
[144] C. Feng, H.L. Wilson, J.K. Hurley, J.T. Hazzard, G. Tollin, K.V. Rajagopalan, J.H. Enemark, Biochemistry 42 (2003) 12235.
[145] C.J. Doonan, H.L. Wilson, R.M. Garrett, B. Bennet, R.C. Prince, K.V. Rajagopalan, G.N. George, J. Am. Chem. Soc. 129 (2007) 9421.
[146] A.V. Astashkin, K. Johnson-Winters, E.L. Klein, C. Feng, H.L. Wilson, K.V. Rajagopalan, A.M. Raitsimring, J.H. Enemark, J. Am. Chem. Soc. 130 (2008) 8471.
[147] R.M. Garrett, K.V. Rajagopalan, J. Biol. Chem. 271 (1996) 7387.
[148] G.N. George, R.M. Garrett, R.C. Prince, K.V. Rajagopalan, J. Am. Chem. Soc. 118 (1996) 8588.
[149] G.N. George, R.M. Garrett, R.C. Prince, K.V. Rajagopalan, Inorg. Chem. 43 (2004) 8456.
[150] D.V. Partyka, R.H. Holm, Inorg. Chem. 43 (2004) 8609.
[151] J.A. Qiu, H.L. Wilson, M.J. Pushie, C. Kisker, G.N. George, K.V. Rajagopalan, Biochemistry 49 (2010) 3989.
[152] S. Gutteridge, R.C. Bray, B.A. Notton, R.J. Fido, E.J. Hewitt, Biochem. J. 213 (1983) 137.
[153] C.J. Kay, M.J. Barber, Biochemistry 28 (1989) 5750.
[154] S.P. Cramer, L.P. Solmonson, M.W.W. Adams, L.E. Mortenson, J. Am. Chem. Soc. 106 (1984) 1467.
[155] G.N. George, J.A. Mertens, W.H. Campbell, J. Am. Chem. Soc. 121 (1999) 9730.
[156] R.K. Mehra, M.P. Coughlan, Arch. Biochem. Biophys. 229 (1984) 585.
[157] M.P. Coughlan, R.K. Mehra, M.J. Barber, L.M. Siegel, Arch. Biochem. Biophys. 229 (1984) 596.
[158] J.P.G. Malthouse, G.N. George, D.J. Lowe, R.C. Bray, Biochem. J. 199 (1981) 629.
[159] R.C. Bray, G.N. George, Biochem. Soc. Trans. 31 (1985) 559.
[160] S.P. Cramer, R. Wahl, K.V. Rajagopalan, J. Am. Chem. Soc. 103 (1981) 7721.
[161] F. Bergel, R.C. Bray, Biochem. J. 73 (1959) 182.
[162] R.M. Jones, F.E. Inscore, R. Hille, M.L. Kirk, Inorg. Chem. 38 (1999) 4963.
[163] K. Okamato, K. Matsamuto, R. Hille, B.T. Eger, E.F. Pai, T. Nishino, Proc. Natl. Acad. Sci. U.S.A. 101 (2004) 7931.
[164] R. Wahl, K.V. Rajagopalan, J. Biol. Chem. 257 (1982) 1354.
[165] C.J. Doonan, A. Stockert, R. Hille, G.N. George, J. Am. Chem. Soc. 127 (2005) 4518.
[166] R.C. Bray, Q. Rev. Biophys. 21 (1988) 299.
[167] R.C. Bray, M.J. Barber, D.J. Lowe, Biochem. J. 171 (1978) 653.
[168] J.P.G. Malthouse, S. Gutteridge, R.C. Bray, Biochem. J. 185 (1980) 767.
[169] R.C. Bray, S. Gutteridge, Biochemistry 21 (1982) 5992.
[170] G.L. Wilson, M. Kony, E.R.T. Tiekink, J.R. Pilbrow, J.T. Spence, A.G. Wedd, J. Am. Chem. Soc. 110 (1988) 6923.
[171] R.J. Greenwood, G.L. Wilson, J.R. Pilbrow, A.G. Wedd, J. Am. Chem. Soc. 115 (1993) 5385.
[172] G.L. Wilson, R.J. Greenwood, J.R. Pilbrow, J.T. Spence, A.G. Wedd, J. Am. Chem. Soc. 113 (1991) 6803.
[173] C. Canne, I. Stephan, J. Finsterbusch, F. Lingens, R. Kappl, S. Fetzner, J. Hüttermann, Biochemistry 36 (1997) 9780.
[174] S. Gutteridge, R.C. Bray, Biochem. J. 189 (1980) 615.
[175] B.D. Howes, R.C. Bray, R.L. Richards, N.A. Turner, B. Bennett, D.J. Lowe, Biochemistry 35 (1996) 1432.
[176] D.J. Lowe, R.L. Richards, R.C. Bray, J. Biol. Inorg. Chem. 3 (1998) 557.
[177] P. Manikandan, E.-Y. Choi, R. Hille, B.M. Hoffman, J. Am. Chem. Soc. 123 (2001) 2658.
[178] C.A. Bayse, Inorg. Chem. 45 (2006) 2199.
[179] T.R. Hawkes, G.N. George, R.C. Bray, Biochem. J. 218 (1984) 961.
[180] K. Okamoto, T.B. Eger, T. Nishino, E.F. Pai, T. Nishino, Nucleos. Nucleot. Nucl. 27 (2008) 888.
[181] R. Hille, G.N. George, M.K. Eidsness, S.P. Cramer, Inorg. Chem. 28 (1989) 4018.
[182] S. Gutteridge, S.J. Tanner, R.C. Bray, Biochem. J. 175 (1978) 869.
[183] S. Gutteridge, S.J. Tanner, R.C. Bray, Biochem. J. 175 (1978) 887.
[184] R.C. Bray, P.F. Knowles, Proc. R. Soc. Lond. Ser. 302 (1968) 351.
[185] F.M. Pick, M.A. McGartoll, R.C. Bray, Eur. J. Biochem. 18 (1971) 65.
[186] S.J. Tanner, R.C. Bray, F. Bergmann, Biochem. Soc. Trans. 6 (1978) 1328.
[187] F.F. Morpeth, R.C. Bray, Biochemistry 23 (1984) 1332.
[188] F.F. Morpeth, G.N. George, R.C. Bray, Biochem. J. 220 (1984) 235.
[189] N.A. Turner, R.C. Bray, G.P. Diakun, Biochem. J. 260 (1989) 563.
[190] B.D. Howes, B. Bennett, R.C. Bray, R.L. Richards, D.J. Lowe, J. Am. Chem. Soc. 116 (1994) 11624.
[191] M. Shanmugam, B. Zhang, R.L. McNaughton, R.A. Kinney, R. Hille, B.M. Hoffman, J. Am. Chem. Soc. 132 (2010) 14015.
[192] G.N. George, R.C. Bray, Biochemistry 22 (1983) 1013.
[193] S.P. Cramer, R. Hille, J. Am. Chem. Soc. 107 (1985) 8164.
[194] G.N. George, R.C. Bray, Biochemistry 22 (1983) 5443.
[195] G.N. George, R.C. Bray, S.P. Cramer, unpublished observation.
[196] D.R. Boer, A. Thapper, C.D. Brondino, M.J. Romão, J.J.G. Moura, J. Am. Chem. Soc. 126 (2004) 8614.
[197] J.J.G. Moura, A.V. Xavier, M. Bruschi, J. Legall, J.M.P. Cabral, J. Less-Common Met. 52 (1977) 555.
[198] N. Turner, B. Barata, R.C. Bray, J. Deistung, J. Le Gall, J.J. Moura, Biochem. J. 243 (1987) 755.
[199] T. Santos-Silva, F. Ferroni, A. Thapper, J. Marangon, P.J. Gonzalez, A.C. Rizzi, I. Moura, J.J.G. Moura, M.J. Romão, C.D. Brondino, J. Am. Chem. Soc. 131 (2009) 7990.
[200] H. Dobbek, L. Gremer, O. Meyer, R. Huber, Proc. Natl. Acad. Sci. U.S.A. 96 (1999) 8884.
[201] P. Hanzelmann, H. Dobbek, L. Gremer, R. Huber, O. Meyer, J. Mol. Biol. 301 (2000) 1221.
[202] M. Gnida, R. Ferner, L. Gremer, O. Meyer, W. Meyer-Klaucke, Biochemistry 42 (2003) 222.
[203] B. Zhang, C.F. Hemann, R. Hille, J. Biol. Chem. 285 (2010) 12571.
[204] C. Gourlay, D.J. Nielsen, J.M. White, S.Z. Knottenbelt, M.L. Kirk, C.G. Young, J. Am. Chem. Soc. 128 (2006) 2164.
[205] V.N. Gladyshev, S.V. Khangulov, T.C. Stadtman, Proc. Natl. Acad. Sci. U.S.A. 91 (1994) 232.
[206] V.N. Gladyshev, S.V. Khangulov, T.C. Stadtman, Biochemistry 35 (1996) 212.
[207] N. Wagener, A.J. Pierik, A. Ibdah, R. Hille, H. Dobbek, Proc. Natl. Acad. Sci. U.S.A. 106 (2009) 11055.
[208] W.T. Self, T.C. Stadtman, Proc. Natl. Acad. Sci. U.S.A. 97 (2000) 7208.
[209] W.T. Self, M.D. Wolfe, T.C. Stadtman, Biochemistry 42 (2003) 11382.
[210] W.F. Cleere, M.P. Coughlan, Biochem. J. 143 (1974) 331.